Carbonate Petrography and Geochemistry of BIF of the Transvaal Supergroup: evaluating the potential of Iron Carbonates as proxies for Palaeoproterozoic Ocean Chemistry

A thesis submitted in Fulfilment of the requirements for the degree of

MAGISTER SCIENTAE IN GEOLOGY

at

RHODES UNIVERSITY, SOUTH AFRICA

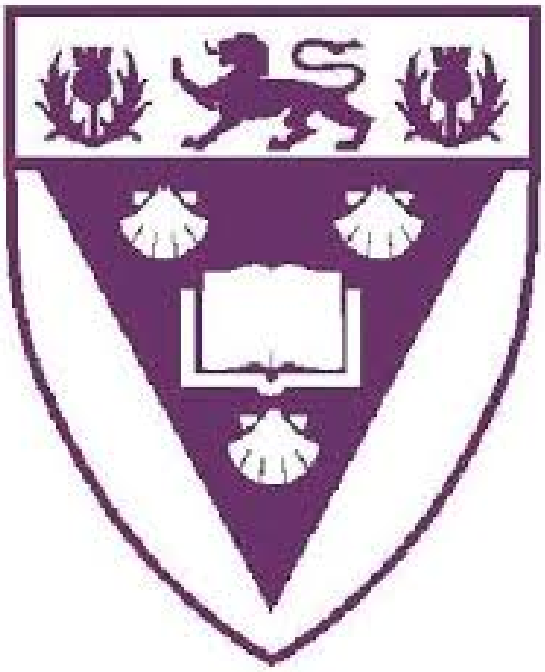

Author: Sipesihle ('Sihle') Rafuza

Supervisor: Prof Harilaos Tsikos

Date: February 2015

DECLARATION

All work in this thesis is the original work of the author, except where specific acknowledgement is made to the work of others.

SIGNED

_____

FEBRUARY 2015

GEOLOGY DEPARTMENT

RHODES UNIVERSITY
GRAHAMSTOWN – SOUTH AFRICA

No geologist worth anything is permanently bound to a desk or laboratory, but the charming notion that true science can only be based on unbiased observation of nature in the raw is mythology. Creative work, in geology and anywhere else, is interaction and synthesis: half-baked ideas from a bar room, rocks in the field, chains of thought from lonely walks, numbers squeezed from rocks in a laboratory, numbers from a calculator riveted to a desk, fancy equipment usually malfunctioning on expensive ships, cheap equipment in the human cranium, arguments before a road cut.

Stephen Jay Gould,

An Urchin in the storm: Essays about books and Ideas

ACKNOWLEDGEMENTS

There's a plethora of people that this thesis has benefited enormously from. These include the more colossal impacts that made all this come to fruition i.e. financial, supervisorial, and surrogated lab work to the more humane factors including recreational, inspirational, and self-growth impacts. First and foremost, I would like to ineffably express my gratitude towards Rhodes University Levenstein Prestigious/Henderson Master's Scholarship, National Research Foundation (NRF) and the GSSA REI research fund for giving me the financial opportunity to partake in this research. Without their monetary generosity, none of this would even be remotely possible. I owe them my life. I'd also like to extend in the same vein my deep regard and gratitude to the Rhodes University Unit on Postgraduate Research in Iron-Manganese Ore Resources (PRIMOR) that I had the privilege and opportunity to become an intricate member of. Their weekly rendezvous and discussions were crucial in establishing a much clearer understanding of the topic at hand.

I am greatly indebted to my supervisor Prof. Hari Tsikos for a myriad of things of which I'd write a whole book on given the chance. It is time spent with the mentioned that I've come to realise the truthfulness of the quote: "to teach an academic subject is not easy, but compared to coaching, it is". We can say 'two plus two is four' to every kid and be sure that we are right, but coaching, we have to literally get to the soul of the people we are dealing with. His leadership and supervision towards this thesis is unassailably unparalleled. Thanks for considering me at all for this study, for being a male figure, for the trips to the Northern Cape and Cape Town --never been--, for the experiences there, for the anecdotes and laughs, for the life lessons, for the good times, for the snoring ☺—but most of all, for being a friend. What I've learnt from you the past years since undergraduate will forever be treasured and held dear.

Furthermore, I would like to express my gratitude to all that contributed experimentally in this body of work. Prof Tim Lyons's contribution from Riverside, California, in terms of the impeccable carbonate-oxide-sulphide speciation and bulk carbonate isotope data that he and Mr Steve Bates produced in their Biogeochemistry Lab. Also for taking his time and having seat-down discussions with me and sharing his vast unsurpassed knowledge when it comes to ancient-modern geochemistry, oceanography and biogeochemistry. Prof Chris

Harris from the University of Cape Town (UCT) is greatly acknowledged for producing sequential $\delta^{13}C$ carbonate isotopic analysis for both ankerite and siderite. Prof Adrian Boyce and his lab from SUERC in Scotland, are thanked for producing bulk carbonate carbon isotope analysis. Christel Tinguely and Nicholas Laider (UCT) are thanked for their hospitality during my stay in Cape Town and for graciously letting me – and helping me – use their EPMA and XRD facilities for analysis of my samples. John Hepple and associates Chris and Thulani are thanked for the sample cutting, thin section production and polishing. Vlassis Papadopoulos is thanked for his input with regard to help create the water column genetic model. His hand in it is greatly appreciated. Lastly, I extend my gratitude to BHP Billiton Hotazel Mine for letting me utilise their facilities, laying down and allowing me to sample their ERIN core.

Key words: Kuruman, Griquatown, Iron Formation, ankerite, siderite, $\delta^{13}C$ isotopes, manganese, iron, water column model

This thesis is dedicated to my family: mother, brother and little sister, Nontle, Piwo and Bunono Rafuza. My pillars of strength, my inspiration, my everything. Without them, none of this would be possible.

ABSTRACT

The subject of BIF genesis, particularly their environmental conditions and ocean chemistry at the time of deposition and their evolution through time, has been a subject of much contentiousness, generating a wealth of proposed genetic models and constant refinements thereof over the years. The prevailing paradigm within the various schools of thought, is the widespread and generally agreed upon depositional and diagenetic model(s) which advocate for BIF deposition under anoxic marine conditions. According to the prevailing models, the primary depositional environment would have involved a seawater column whereby soluble Fe^{2+} expelled by hydrothermal activity mixed with free O_2 from the shallow photic zone produced by eukaryotes, forming a high valence iron oxy-hydroxide precursor such as FeOOH or $Fe(OH)_3$. An alternative biological mechanism producing similar ferric precursors would have been in the form of photo-ferrotrophy, whereby oxidation of ferrous iron to the ferric form took place in the absence of biological O_2 production. Irrespective of the exact mode of primary iron precipitation (which remains contentious to date), the precipitated ferric oxy-hydroxide precursor would have reacted with co-precipitated organic matter, thus acting as a suitable electron acceptor for organic carbon remineralisation through Dissimilatory Iron Reduction (DIR), as also observed in many modern anoxic diagenetic environments. DIR-dominated diagenetic models imply a predominantly diagenetic influence in BIF mineralogy and genesis, and use as key evidence the low $\delta^{13}C$ values relative to the seawater bicarbonate value of ~0 ‰, which is also thought to have been the dissolved bicarbonate isotope composition in the early Precambrian oceans. The carbon for diagenetic carbonate formation would thus have been sourced through a combination of two end-member sources: pore-fluid bicarbonate at ~0 ‰ and particulate organic carbon at *circa* -28 ‰, resulting in the intermediate $\delta^{13}C$ values observed in BIFs today.

This study targets 65 drillcore samples of the upper Kuruman and Griquatown BIF from the lower Transvaal Supergroup in the Hotazel area, Northern Cape, South Africa, and sets out to explore key aspects in BIF carbonate petrography and geochemistry that are pertinent to current debates surrounding their interpretation with regard to primary *versus* diagenetic processes. The focus here rests on applications of carbonate (mainly siderite and ankerite)

petrography, mineral chemistry, bulk and mineral-specific carbon isotopes and speciation analyses, with a view to obtaining valuable new insights into BIF carbonates as potential records of ocean chemistry for their bulk carbonate-carbon isotope signature. Evaluation of the present results is done in light of pre-existing, widely accepted diagenetic models against a proposed water-column model for the origin of the carbonate species in BIF. The latter utilises a combination of geochemical attributes of the studied carbonates, including the conspicuous Mn enrichment and stratigraphic variability in Mn/Fe ratio of the Griquatown BIF recorded solely in the carbonate fraction of the rocks. Additionally, the carbon isotope signatures of the Griquatown BIF samples are brought into the discussion and provide insights into the potential causes and mechanisms that may have controlled these signatures in a diagenetic *versus* primary sedimentary environment. Ultimately, implications of the combined observations, findings and arguments presented in this thesis are presented and discussed with particular respect to the redox evolution and carbon cycle of the ocean system prior to the Great Oxidation Event (GOE). A crucial conclusion reached is that, by contrast to previously-proposed models, diagenesis cannot singularly be the major contributing factor in BIF genesis at least with respect to the carbonate fraction in BIF, as it does not readily explain the carbon isotope and mineral-chemical signatures of carbonates in the Griquatown and uppermost Kuruman BIFs. It is proposed instead that these signatures may well record water-column processes of carbon, manganese and iron cycling, and that carbonate formation in the water column and its subsequent transfer to the precursor BIF sediment constitutes a faithful record of such processes. Corollary to that interpretation is the suggestion that the evidently increasing Mn abundance in the carbonate fraction of the Griquatown BIF up-section would point to a chemically evolving depositional basin with time, from being mainly ferruginous as expressed by Mn-poor BIFs in the lower stratigraphic sections (i.e. Kuruman BF) to more manganiferous as recorded in the upper Griquatown BIF, culminating in the deposition of the abnormally enriched in Mn Hotazel BIF at the stratigraphic top of the Transvaal Supergroup. The Paleoproterozoic ocean must therefore have been characterised by long-term active cycling of organic carbon in the water column in the form of an ancient biological pump, albeit with Fe(III) and subsequently Mn(III,IV) oxy-hydroxides being the key electron acceptors within the water column. The highly reproducible stratigraphic isotope profiles for bulk $\delta^{13}C$ from similar sections further afield over distances up to 20 km, further corroborate unabatedly that bulk

carbonate carbon isotope signatures record water column carbon cycling processes rather than widely-proposed anaerobic diagenetic processes.

Table of Contents

Page

Table OF Figures

List of Tables

Chapter 1: Introduction

1.1. Definition(s)

The term Banded Iron formation (BIF) as the term itself suggests, applies to deposits which are epitomised by high Fe content. The term is widely used in geological literature to describe thinly laminated or bedded formations that, arbitrarily assigned first by James (1954), contain Fe of no less than 15wt% in order for them to qualify and be bracketed under this classification of geological deposits. Texturally, the quintessential feature of these deposits is their conspicuous compositional interlayering of Fe-rich bands alternating rhythmically with Fe-poor chert layers containing Fe-silicates ± carbonates on a variety of vertical scales and thicknesses. This layering is expressed in different scales in a given outcrop from fine sub-millimetre varve-like laminae to metre-thick bands in some instances. The continuity of the latter can be traced on outcrop scale for hundreds of kilometres in lateral extension. Magnetite and/or haematite often dominate the iron-rich layers, accompanied by only minor other metal-oxides and sulphides such as pyrite. Chert and carbonate minerals that include ankerite and siderite (and calcite in some instances) dominate the Fe-poor, light-coloured bands. This latter state of layering persists throughout the entire lateral distribution and stratigraphic section of any given BIF outcrop exposure, even on a microscopic scale, with the transition between these often abrupt and clear.

1.2. BIF classification

The very first author to ever propose a working classification scheme for BIFs was H. James in 1954 on the basis of mineralogical composition. This marked the beginning of a new era in the research of these enigmatic rock formations. Throughout the decades, this initial classification scheme has undergone revision with later scholars classifying BIFs in terms of their proposed tectonic settings (Gross, 1965), and depositional environment (Kimberley, 1978; Simonson, 1985). Thereafter, numerous papers based on the mineralogy, geochemistry, sedimentology and origin of these rocks were brought to print. The variety of classification schemes proposed is undoubtedly a reflection of our limited understanding of these still contentious rocks. James (1954) initial classification envisaged these deposits as characterised by having four mineralogical facies namely: oxide, carbonate, and silicate

facies and a – later revised as epigenetic – sulphide facies (Phillips et al., 1984; Groves et al., 1987).

Oxide facies-rich BIFs typically consists mainly of sub- to euhedral magnetite [Fe^{2+} Fe_2^{3+} O_4], often along with some fine grained red hematite [Fe_2^{3+} O_3]. When the dominant iron oxide is mainly magnetite (which is in the vast majority of cases), Fe-carbonates and Fe-silicates are most commonly also associated with this facies (James 1966). Sulphide-rich BIFs are rare, and are commonly associated with either carbonaceous shales or volcanic increments formed under anaerobic conditions. These contain pyrite [FeS_2] and/or pyrrhotite [Fe_{1-x} S] which were initially thought to be syngenetic (Fripp, 1976) but were later revised to be of an epigenetic replacement rather than primary sedimentary origin.

Silicate-rich facies BIFs are characterised by abundant iron-silicate minerals including greenalite, minnesotaite and stilpnomelane, variously associated with magnetite, siderite and chert. Greenalite [(Fe^{2+}, $Mg)_6$ Si_4 O_{10} $(OH)_8$] and minnesotaite [(Fe^{2+}, $Mg)_3$ Si_4 O_{10} $(OH)_2$] are ferrous analogues of antigorite and talc respectively, while stilpnomelane [$K_{0.6}$ (Mg, Fe^{2+}, $Fe^{3+})_6$ Si_8 $Al(O, OH)_{27}.2\text{-}4H_2O$] is a complex phyllosilicate (James, 1954). Primary Fe-silicate precipitates are envisaged to be probably greenalite chamosite and glauconite. The varied primary mineralogy of hydrous iron silicates, carbonates and cherts in silicate-facies BIFs is particularly prone to metamorphic recrystallization.

Carbonate-facies rich BIFs are comprised of mainly ankerite [Ca Fe^{2+} $(CO_3)_2$] and siderite (Fe^{2+} CO3) (James, 1954). Both of these may display variable mineral-chemical compositions. The siderite is often subhedral or rounded and finer grained, associated with Fe-silicates and/or cogenetic with ankerite occurring in lesser abundances. Ankerite typically displays euhedral, neomorphic (equant) coarser grains, typically floating in a matrix of microcrystalline chert. The overall mineralogy of carbonate-facies BIF *sensu-stricto* is simple, with approximately equal proportions of both chert and ankerite (and/or siderite) expressed as thinly bedded or laminated alternating layers.

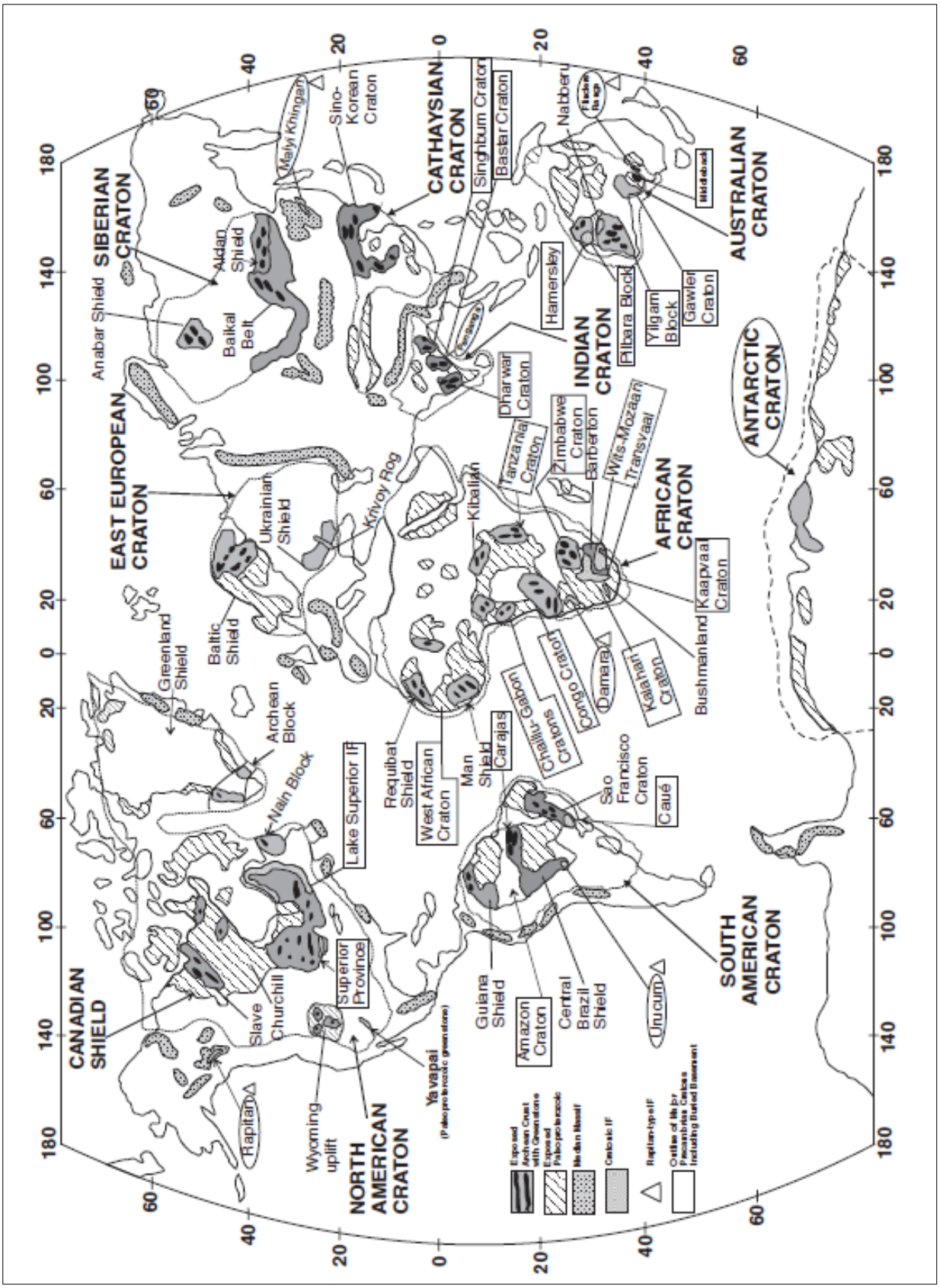

Figure 1. Global distribution of Precambrian Cratons and contained iron formations. Note the occurrence of the Transvaal BIFs in the Kaapvaal Craton in Northern Cape, South Africa. Adapted from Beukes and Gutzmer (2008)

1.3. Distribution in space and time

The very well constrained distribution of iron formation spatially and temporally, has puzzled BIF enthusiasts for decades and has been a subject of insatiable scientific investigation. BIFs are found amongst the oldest rock records on Earth's history. Contrary to earlier proposition by Cloud (1973), there exists a considerable age-spread among Precambrian BIFs, in as much as 90% of all iron formations were deposited between 3.8 and 1.6 Ga. Algoma-type tectonic settings are inferred for old (early- and mid- Archean BIFs) which are majorly hosted in greenstone-belts (Gross 1965). Late Archean to early Proterozoic BIFs are typically thicker and more laterally extensive than the Algoma type (Klein and Beukes, 1992, Klein, 2005). It is now well constrained that a vast majority of iron formation were deposited in the late Archean-Palaeoproterozoic age, between 2.7 to 1.9 Ga ago. BIFs that occur between the latter ages are designated as Superior-type BIFs.

Superior-type BIFs are found in several regions of the world, including the Hamersely group, Transvaal Supergroup, Krivoy-Rog Basin, Labrador Trough and Minas Supergroup (Klein, 2005). They display striking petrographic and geochemical similarity. Superior type iron formations are volumetrically large deposits, with total primary iron content exceeding several billions of tons that extend over hundreds of km^2 (James and Trendall, 1982). They are also practically devoid of clastic material and are associated instead with other sedimentary rock-types, typically grading into carbonate rocks or black shales, and vice versa. Deposition is envisaged to have occurred in relatively shallow marine conditions under transgressional oceans (Trendall, 1968; Beukes, 1983; Simonson, 1985; Simonson and Hassler, 1996). Gross (1965) on the other hand, advocates for deposition on continental shelves of passive tectonic margins.

The majority of Precambrian iron formation occurrences typically found in Archean greenstone terranes and Neoproterozoic glaciomarine sedimentary successions belong to the Algoma and Rapitan-type classes respectively (Gross and McLeod 1980, Klein and Beukes 1993). Gross (1965) infers a tectonic setting on the basis of BIF size and lithologic associations. Algoma-type iron formations are relatively small with total primary iron content rarely exceeding 1 billion tons, lateral extents usually under $10km^2$, thickness ranging from 10-100m (James and Trendall, 1983 Goodwin, 1973; Appel, 1980; Condie,

1981) and association with volcanogenic rocks. Favoured depositional environments for this type of BIF include island arc/back arc basins and intracratonic rift zones (Gross, 1983).

It is beyond the scope of this study to refine or discuss the ongoing issues of BIF nomenclature and/or establish new terminologies. Excellent reviews of such can be found in papers by Beukes (1980b), Trendall (1983), and Kimberley (1978, 1989a)

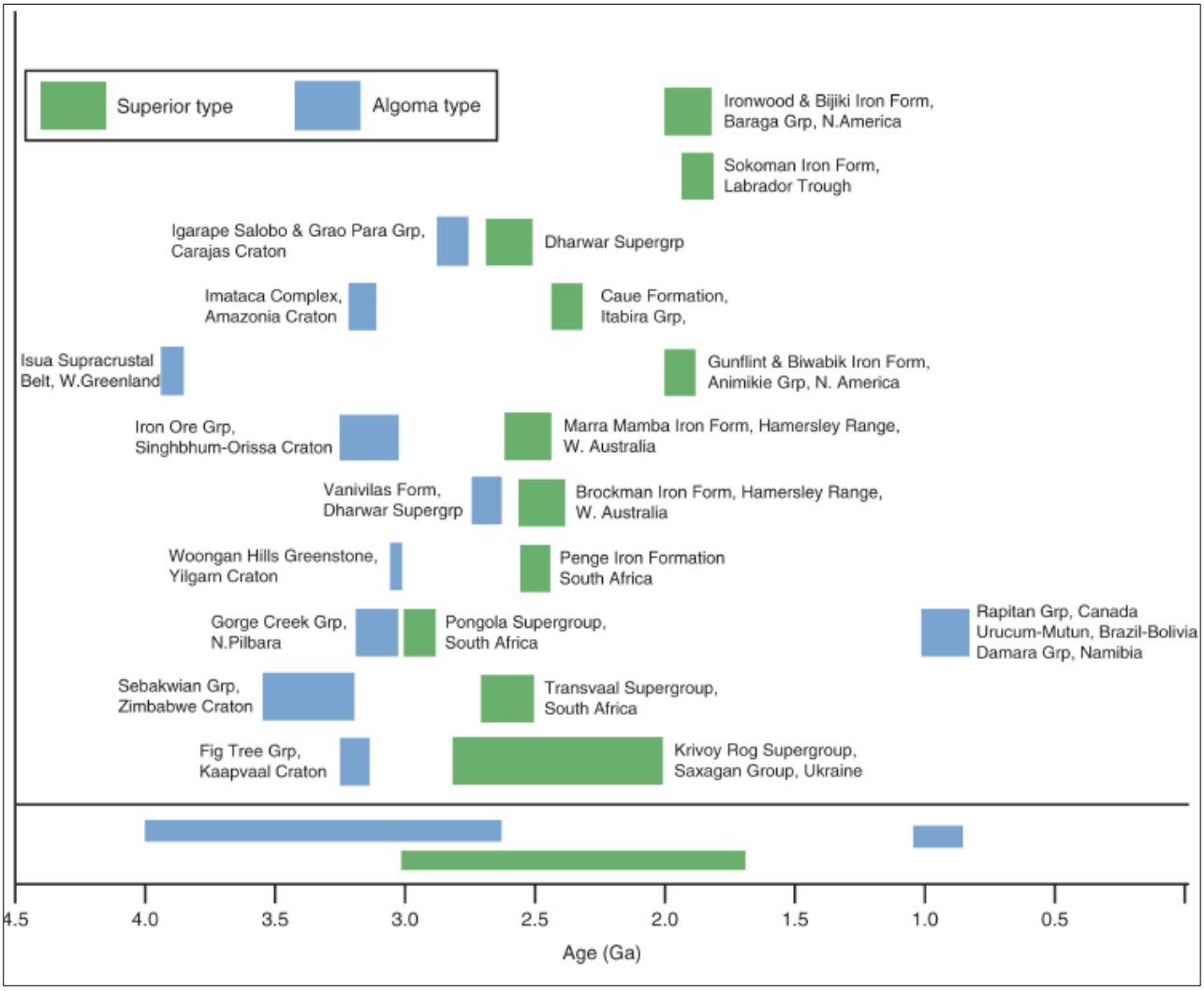

Figure 2. Appearance of BIFs in the geological record marked as Algoma & Superior types. The Algoma type occur from 3.9 to 2.6 Ga and then again from 1.0 to 0.85 Ga. The Superior type commonly occur between 1.7 and 3.0 Ga. Modified after Koehler et al., (2010)

1.4. Previous work

The geology of the Transvaal Supergroup has received considerable attention and resultant publications from scholars throughout the decades, since as far back as the 1960s (Engelbrecht 1962, Trendall 1965, La Berge 1966, Hanekom 1966, Fockema 1967). However, the history and documentation of the Transvaal depository and its contained iron formations can be traced back to as early as 1812, when early pioneers in the field first mentioned rocks belonging to the Transvaal Supergroup with notable mention of the economic crocidolite asbestos beds associated and intercalated with the iron formations in Griqualand West (Burchell 1822, Stromeyer and Hausmann 1831, Moffat 1858) and Transvaal sequence (Mauch 1870, Harger 1934, Rogers 1937). Naming of the rock units of the Griqualand West (Stow 1874, Homes 1904a) and Transvaal (Cohen 1874, Penning 1885, Gibson 1892, Francke 1897) became a frequent customary topic and publication among scholars in the subsequent years. The formation and establishment of the Geological Survey of South Africa (GSSA) in 1912 resulted in the extensive mapping of the depository and resultant description of the stratigraphy and general geology of the Griqualand West (Rogers 1960a, 1907, 1908, Rogers and Du Toit 1909a, Nel 1929, Visser 1944 1958, Hanekom 1966, De Villiers 1960) and Transvaal sequences (Hall 190-1910-1911, Holmes 1905, Humphrey 1908, Hall & Humphrey 1910).

First detailed descriptions and account of the stratigraphy, mineralogy and economic potential of the iron formations themselves dates back to as early as Du Toit (1945) with later much more rigorous work done by follow-up scholars including Cilliers (1963), Engelbrecht (1962), Harrington (1962) Harrington and Cilliers (1963), Cullen (1963), Von Backstrom (1963), La Berge (1966), Hanekom (1966) and Malherbe (1970). The period from 1973 onwards saw the first detailed description and rapid development in the sedimentology of the iron formations mainly by accounts described by Beukes (1973, 1978, 1980a) and later Button (1976b) and Klemm (1979).

In his 1984 publication, Beukes utilised his previously proposed nomenclature and classification of iron formations published in 1980(b) as modified from the principle that iron formations display many physical features very similar to those of carbonate rocks (Dimroth and Chauvel, 1973). According to this nomenclature, components of Iron Formations are allochems, femicrite and chert. Allochems are subdivided into gravel-sized

fragments - pisoliths, discs (angular flat chert pebbles), chip- and finer grit-sand-silt sized particles including intraclastic shards pellets and ooids. Femicrite refers to a facies of microcrystalline iron minerals within BIFs. These can be felutite or ferhythmites. The latter term simply refers to any microbanded iron formation while the former refers to very fine grained iron formations lacking distinct banded texture. Allochemical BIFs thus refers to clastic-textured iron formations composed of all allochems such as pebbles and grains whereas orthochemical BIFs consists of felutite (very fine grained sediment). Chert most predominantly constitute mesobands which may be either massive or microbanded but can be present as disseminated particles (cement and matrix) in felutite, constitute microbands in ferhythmites or may be present as cementing allochems. Microbanded chert mesobands are almost invariably associated with ferhythmite. By contrast, massive chert is invariably associated with felutite.

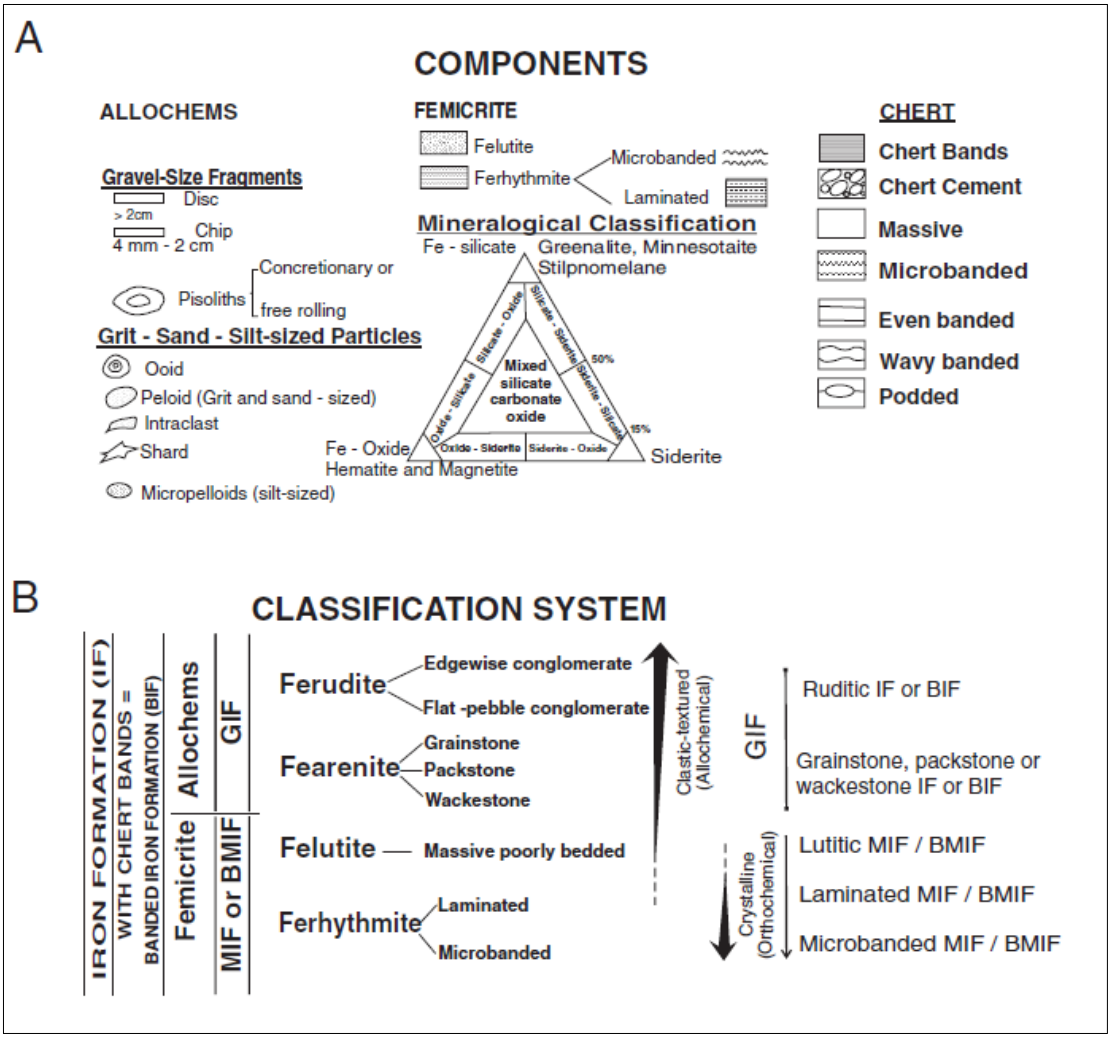

Figure 3. Components, classification and nomenclature of iron formation as described by Beukes (1990). Image adapted from a recently modified version in Beukes and Gutzmer (2008)

A mesoband (>10mm thickness) can be of even thickness along strike, pinch and swell and be lenticular. These textures are termed ribbons, waves and pods respectively. Thicker chert mesobands displaying similar morphology are refered to as bands, billows and pillows respectively. Both textural and structural components can be accounted for in the naming of these rocks by using collective names through a combination of chert and mesoband names e.g. bandlutites and podrhythmites.

Later work by Beukes and Klein (1990) focused on using trace element geochemistry, carbon and oxygen stable isotopes and petrography on the Kuruman and Griquatown transition. They came to the conclusion that the BIFs were deposited in a shallow water submerged platform with the only terrigenous material reaching the depository being episodic volcanic increment expressed as stilpnomelane rich beds running the transition between the Bretby and Alphen zone, the so-called “Stilpnomelane bearing horizon”.

For all intent and purposes, the above nomenclature will be used to describe BIFs in this study (see petrographic section) unless otherwise stated.

1.5. Thesis Outline and Objectives

The present study is a new and original contribution to an ongoing research trend on the Transvaal BIFs and adjacent rocks by several groups over the past few decades. Early work of these rocks have been mainly focused on nomenclature and classification. Subsequent work by Beukes& Klein (1990) sampled the transition (60m of core) between the Kuruman and Griquatown BIFs to obtain valuable knowledge pertaining the stratigraphy, petrography, bulk geochemical and stable isotope geochemistry of these rocks. Recent unpublished studies have sampled the lower Kuruman BIFs as well as Griquatown BIFs at relatively low sampling resolution and have analysed them for their bulk rock geochemistry and metal (Fe, Mn) speciation (Fryer, 2015), with the goal of obtaining valuable insights into the genesis of these rocks and the environments in which they have formed.

This study samples the Asbeusheuwels BIFs on a diamond drillcore named ERIN, which became available to the author from the company BHP-BILLITON-HMM in Hotazel, Northern Cape, South Africa. The said drillcore intersects the Transvaal stratigraphy and captures a large portion of the BIFs under investigation. Sampling was carried out at a moderate resolution of one sample per 5m on average, straddling ca. 300m of continuous stratigraphic

section in the uppermost Asbestos Hills Subgroup (upper Kuruman & Griquatown BIFs). The chosen analytical approach included the application of Fe and Mn speciation coupled with petrographic and microprobe analyses of carbonate species in BIF, specifically ankerite, siderite and occasionally calcite too. Carbonates were selectively targeted due to them being the key Mn host, as evidenced in previous unpublished studies (Fryer, 2015), and in view of recent models that link the Asbesheuwels BIFs with the Mn rich Hotazel formation under a single and chemically evolving paleodepository (Tsikos et al., 2010). The high Mn signal recorded in the carbonate fraction of the upper Griquatown BIF and its significance is in itself a key factor underpinning the current study. However, as the Mn is directly associated with the carbonate fraction of the Griquatown BIF, the focus is transferred to the broader theme of the origin of carbonate minerals in BIF, i.e. which of their chemical signatures are related to diagenesis only and which are carried mainly from primary water-column processes, and constrain how Mn is encapsulated in this broad framework of processes.

In the following sections, this study is subdivided into four main parts. The first part follows the introductory chapters and pertains to the petrographic and mineralogical make-up of the Kuruman-Griquatown iron formations as it appears stratigraphically. It introduces the chapter by delving into descriptions of the different mineralogical and major lithological facies of these rock as they appear in thin section and core-logs i.e. the silicate-, oxide- and carbonate-facies, with the main emphasis in describing the textural association(s) and/or occurrence of the carbonate minerals i.e. ankerite and siderite with respect to the various facies in which they occur. Relative abundances of ankerite relative to siderite will be explored, and much rarely the occurrence of calcite will be considered as well.

The second part of this study focuses on the mineral-specific and speciation geochemistry of the BIFs. Data on the major oxide compositions of the carbonates and how they vary stratigraphically is presented and evaluated. Emphasis is placed on the relative Mn enrichment and stratigraphic variability in Mn/Fe ratio of the Kuruman-Griquatown BIF. Fe and Mn speciation data are also presented to corroborate EPMA-determined major oxide concentrations of the carbonates. Plots of element-element relationships, elemental ratio relationships as they appear (particularly those of Mn and Fe) stratigraphically are presented to further elucidate the behaviour of these rocks geochemically.

The third part pertinently focuses on the stable isotope geochemistry. Here, a presentation of the ERIN core $\delta^{13}C$ isotope profile is presented bringing into focus the carbon isotope signatures recorded in the Kuruman-Griquatown samples. The latter is then juxtaposed next to the $\delta^{13}C$isotope profiles of additional drillcores not examined here, namely GAS1, HEX5 and ARPAN, and to the CORETSI intersection of Beukes & Klein (1990), which samples a 60m transitional zone between the Kuruman and Griquatown BIFs. These drillcores occur up to 20 Kms apart from each other. A comparison between the five profiles is done to further provide insights into the potential causes and mechanisms that may have controlled $\delta^{13}C$ signatures in the diagenetic versus the primary depositional environments of the BIFs.

The last part concludes with a detailed discussion based on the data obtained from this study including the potential implications of the combined findings and conclusions with respect to the redox evolution and carbon cycle of the ocean/atmosphere system of the time. Suggestions with regard to the significance of variable Mn/Fe in BIF stratigraphically is undertaken with the aim to first evaluate it in light of the prevailing diagenetic models against the proposed water column model. We corroborate this by discussing the constraints acquired from carbonate-carbon isotopes and draw conclusions on which is the most likely palatable model to explain accurately such observed and analysed geochemical signatures.

Chapter 2: Regional Geology

2.1. Introduction

The Neoarchearn to Palaeoproterozoic (2.7 – 2.1 Ga) Transvaal Supergroup in Southern Africa occupies an area of some 250,000 km^2, and develops in two major successions in the north-eastern and western basinal segments of the Kaapvaal Craton named in accordance with the two geographical areas they occupy, namely: Transvaal and Griqualand West Supergroup (Beukes 1983, Tsikos, 1999, Moore et al, 2001). The former basin circumscribes the Bushveld Complex towards the east, whilst the latter basin is situated at the western Kaapvaal margin and extends into southern Botswana beneath Kalahari cover as the Kanye Basin (Moore et al 2001). The two basins are isolated from each other by a broad basement high, the so-called 'Vryburg Arch' (Moore et al 2001). Rocks of the Transvaal sequence rest on a crystalline basement (>3.0Ga) of either Archean gneisses, granites and/or greenstone belts (Cheney et al 1988), Ventersdorp volcanics, and later sedimentary rocks of the Witwatersrand Supergroup (Tsikos, 1994).

Gross stratigraphic subdivisions between the two basins are comparable, consisting of a basal mixed chemical-volcanic-siliciclastic rock unit conformably overlain by a mixed chemical sedimentary unit, which is in turn uncomformably overlain by a mixed chemical-volcanic-siliciclastic rock unit (Beukes, 1983). With respect to Iron formations, they are better developed in the Griqualand West Basin relative to the Transvaal one, with seven recognised iron formation units (although 10 beds or members are present) from the base of the lower Ghaap Group to near the top of the overlying Postmasburg group (Beukes, 1983). The lower Asbeusheuwals subgroup iron formation consists of the lower Kuruman microbanded BIF, which is conformably overlain by the more clastic-textured Griquatown BIF. These collective can reach up to 1000m in thickness in some areas and are the thickest preserved iron formation across the two basins. The only known iron formation from the Transvaal basin,, is the Asbeusheuwals subgroup-equivalent Penge Iron Formation, although a less conspicuous and very thin unit of BIF of restricted lateral extent has also been described from near the base of the Pretoria group.

Lithostratigraphic similarities, particularly those of the Griqualand West succession of the Kaapvaal Province and the Brockman Iron Formation of the Hamersley Group in the Pilbara Province have long been appreciated (Trendall, 1968; Button, 1976; Beukes, 1984) and have led scholars to purport that the Kaapvaal province was once part of and conjoined with the Pilbara province, in the form of a massive supercontinent variously designated as *Vaalbara* (Cheney 1995). This is mainly founded on the notion that the former and latter provinces correlate laterally across three out of four major unconformity bounded units spanning the age range 2.7 to 2.1 Ga (Cheney 1995). This chapter – and the thesis by extension – will only be concerned with mainly the palaeoenvironmental setting and stratigraphy of the Transvaal Supergroup in the Northern Cape Province, and specifically its lower part that contains the ~2.46 – 2.43Ga Kuruman-Griquatown iron formations of the Asbesheuwel subgroup (Cornell et al 1996, Summer and Bowring 1996, Moore et al 2012).

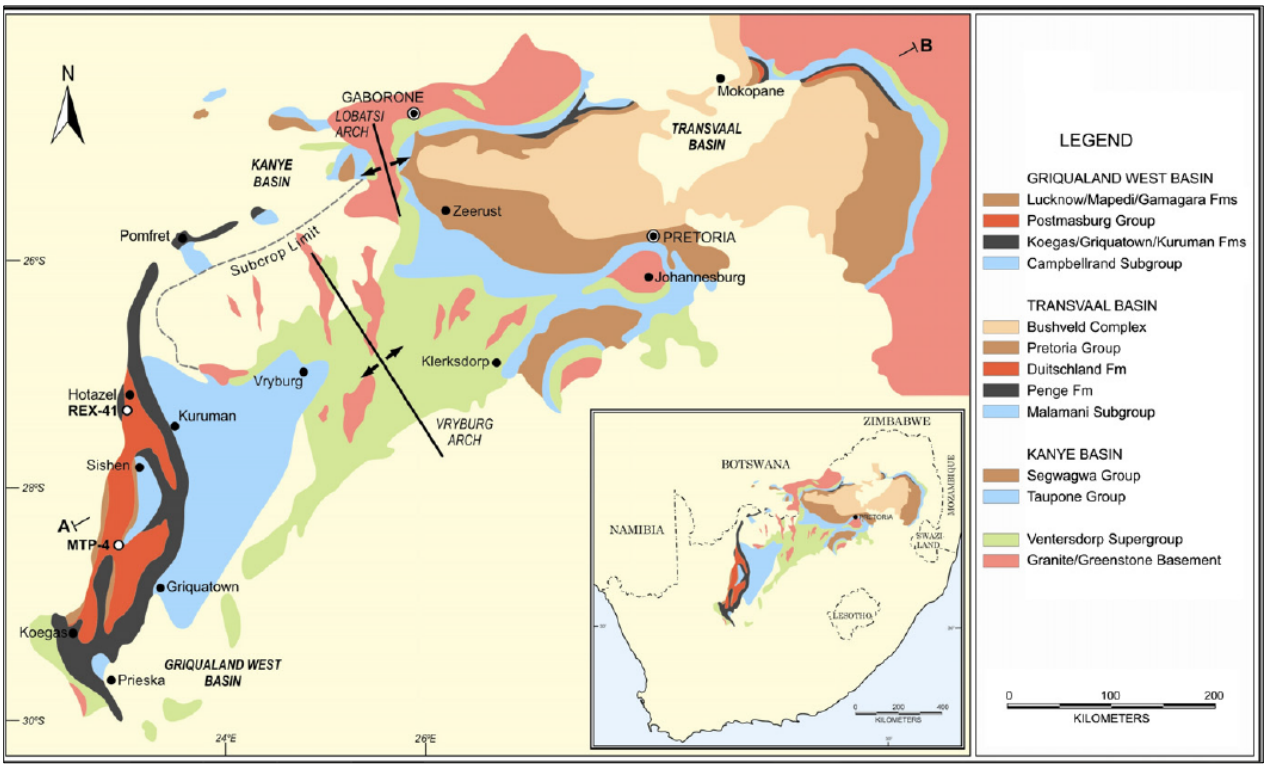

Figure 4. Regional geological map of exposures of the Transvaal Supergroup and adjacent basement. These include the Transvaal, Griqualand West and Kanye Basins with the former two separated by the Vryburg Arch. Adapted from (Moore et al., 2012).

2.2. Transvaal Supergroup in Griqualand West

The subdivisions of both Transvaal basins show striking lithostratigraphic similarity. They consist of a basal succession of mixed siliciclastic and volcanic units, followed conformably by a chemical sedimentary unit, which in itself is in turn unconformably overlain by a mixed chemical-volcanic-siliciclastic rock unit (Moore et al., 2001). As indicated earlier, only the stratigraphic sequence of the Griqualand West will be dealt with in detail here.

The Griqualand west sequence can be divided into two major groups namely: the basal Ghaap group and the top Postmasburg group (see table 1 below). The latter comprises a mixed volcanic-glacial-chemical rock unit (Beukes 1986a) while the former is made up of a relatively pure chemical sedimentary succession with the exception of siliciclastic material found in the Koegas subgroup (itself not developed regionally within the basin), and in the basal Schmidtsdrit subgroup.

2.2.1. The Ghaap Group

The Ghaap group is developed on top of either crystalline basement rocks of Archaean age, or on acid to mafic volcanic rocks of the Late Archean Ventersdorp Group (Moore et al., 2001). It comprises a 1500 – 1700m thick succession of carbonate rocks belonging to the Campbellrand Subgroup, overlain by chemical iron formation of the Asbesheuwels subgroup (refer to table 1 below). The latter is divided into two texturally different iron formations, namely, the lower, microbanded 150 – 750m thick Kuruman iron formation, and the clastic-textured, orthochemical and allochemical 200-300m thick Griquatown iron formation. Mixed sequences of siliclastic-carbonate-volcanic rocks of the Schmidstrift Subgroup and Koegas Subgroup are developed at the base and top of the chemical sedimentary succession (Beukes 1983, 1968).

2.2.1.1. The Schmidtsdrif subgroup

The Schmidtsdrif subgroup forms the basal unit of the Ghaap group in the Griqualand West basin. It unconformably overlies the 2.7Ga volcanic rocks of the Ventersdorp subgroup and is divided into three formations, namely: Vryburg, Boomplaas and Lokammona. The basal Vryburg formation is dated at 2642±3Ma and 2650±8Ma by Walraven & Martini (1995) and Gutzmer and Beukes (1998) respectively, is a 100m-thick sequence interpreted by Beukes (1986) to represent fluvial to marginally marine deposits consisting of shales, siltstones,

quartzites, carbonates and basaltic to andesitic amygdaloidal lavas (Altermann & Siegfried, 1997). The central Boomplaas formation consists of platformal carbonates with well-preserved oolitic and stromatolitic textures (Beukes 1979, 1983). Altermann & Siegfried (1997) advocate for a deeper subtidal depositional environment for the deposition of the oolitic textures, despite the latter being absent in the basinal facies of the Prieska area. The Lokammona formation is composed of banded siderite lutites overlying tuffaceous siltstones, carbonate oolite and stromatolitic reef deposits, and is interpreted by Alterman and Seigfield (1997) to represent a marine regressive cycle over the underlying deeper-water Boomplaas formation.

2.2.1.2. The Campbellrand Subgroup

The Campbellrand subgroup follows via the widespread carbonate accumulation that develops conformably on the underlying Lokammona formation of the Schmidtsrif subgroup. Following the earlier work by Beukes (1980, 1983, 1984), this subgroup is subdivided into two main facies, namely the basinal and platformal facies, also known as Prieska and Ghaap Plateau respectively. The latter platform facies is further subdivided into 8 formations, namely: the basal Monteville followed by Reivilo, Fairfield, Klipfonteinhewel, Papkuil, Klippan, Kogelbeen and upper Gamohaan formations (Altermann & Wotherspoon, 1995, Eriksson and Altermann, 1998). These platform facies extend laterally into the basinal facies, deeper-water carbonates of the Nauga and Naragas formations (Altermann & Nelson,1998) and they are composed of laminated, clastic textured dolostones and pyritic carbonaceous shales (Beukes 1983). The overlying Kamden Member iron formation that extends from the basinal to platform facies,is a few metres thick and has been interpreted by Beukes (1978) as reflecting a distinct marine transgression in the depositional palaeoenvironment. Rare mafic tuff beds occurring within the Prieska facies are overlain by ankerite-banded cherts which are further capped by finely laminated black shale of the Klein-Naute Member, representing depositional conditions below storm-wave base (Altermann & Nelson, 1998). The latter shale essentially forms the footwall of the Kuruman iron formation of the overlying Asbeusheuwels subgroup, which together with the Griquatown iron formation will be the focus of this study.

Table 1: Stratigraphy of the Griqualand West Transvaal Sequence. Models ages after (Cornell et al 1996, Summer and Bowring 1996, and Moore et al (2012). Modified after Tsikos (1999) and Beukes and Smith (1987)

Supergroup	Group	Subgroup	Formation	Lithology	Approx. thickness (m)	Age (Ga)
Transvaal	Postmasburg	Voelwater	Mooidraai	Carbonate+ /- Chert	250	2.394
			Hotazel	BIF + Mn Ore		
			Ongeluk	Andesite	500	2.222
			Makganyene	Diamcitite	50-150	2.436
	Ghaap	Koegas	Nelani	Siliciclastic, BIF + Mn Ore	240-600	
			Rooinekke			
			Naragas			
			Kwakwas			
			Doradale			
			Pannetjie			
		Asbesheuwels	Griquatown	Clastic Textured BIF	200-300	2.431
			Kuruman	Microbanded BIF	150-750	2.460
		Campbellrand	Gamohaan	Carbonate +/- Shale	1500-1700	2.557
			Kogelbeen			
			Klippan			
			Papkuil			
			Klipfonteinheuwel			
			Fairfield			
			Reivelo			
			Monteville			
		Schmidtsdrift	Lokammona	Siliciclastic, Carbonate, Lava	10-250	2.642
			Boomplaas			
			Vryburg			

2.2.1.3. The Asbeusheuwels Subgroup

The transition from carbonate deposition represented by the underlying Campbellrand subgroup to banded iron formation represented by the conformably overlying Kuruman and Griquatown iron formations has been attributed by Beukes (1983) as marking a major marine transgression and associated sea level rise in the palaeoenvironment of deposition of these chemical sediments. The Asbesheuwels (Afrikaans for: “Äsbestos Hills”, due to its

abundant asbestiform riebeckite content) Subgroup has been a topic of major research throughout the past few decades. The stratigraphy, mineralogy and economic crocidolite asbestos deposits of the Asbesheuwels iron formations have been described in detail by previous accounts including Du Toit (1945), Engelbrecht (1962), Hanekom (1966), Fockema (1967) and others. Subsequently, Beukes and Klein (1989, 1990) concentrated on the sedimentology and stratigraphy of the iron formations, particularly their implication for a reconstruction of the Transvaal depository. For the sake for simplicity and consistency, this section will contain sedimentological and stratigraphic nomenclature as proposed by and derived from the works of the aforementioned scholars.

Beukes and Klein (1990) designate a number of major lithologic units that subdivide the transition from the predominantly microbanded Kuruman to the dominantly granular Griquatown iron formations. The former contains the Bretby and Alphen zones of the *Riries* member in its upper part, whereas the Griquatown Iron Formation, characterised by the intercalation of granular and microbanded BIF, is subdivided into the first and second upper crocidolite zones of the *Danielskuil* member. Both these are separated from each other by a granular unit draped by thin felutite displaying wavy to lenticular bedding, termed the *Ouplaas* member (Beukes 1983). Autochthonous ferhythmites of the Kuruman Iron-formation reach a maximum thickness development in the deeper part of the paleobasin near the present town of Prieska, whereas orthochemical and allochemical units of the Griquatown iron formation are relatively more abundant elsewhere in the region (Beukes 1984).

2.2.1.3.1. The Kuruman iron formation

The lower orthochemical, rhythmically banded Kuruman Iron formation is considered to have been deposited in an open-shelf marine environment (Beukes, 1983). It varies in thickness from 150m to the north of the Griqualand fault zone reaching up to 750m to the south of the same fault zone (Beukes, 1983). Ankerite-banded cherts of the Kliphuis Member forms the basal unit of the Kuruman iron-formation, consisting of chert mesobands alternating with ankeritic/ferruginous dolomitic intramicrite mesobands, interpreted to correspond to chertified and ankeritized limestone turbidites (Beukes, 1983). The *Groenwater* member overlies the ankerite banded cherts, and consists of bands of stacked

macrocycles of stilpnomelane lutite – siderite microbanded chert – siderite magnetite bandrhythmites and magnetite-hematite ribbon-rhythmites – siderite microbanded chert (Beukes, 1983). The latter macrocycles of deposition range in thickness from 1 – 10m and are rarely complete. Frequent stilpnomelane-siderite macrobands seen within the Groenwater member are thought to be of a mixed volcanic-biological origin, representing periods of sporadic addition of volcanic ash and fumarolic silica resulting in the stilpnomelane-lutite mesobands, and periods of increasingly decreasing volcanic activity resulting in biological flourish and resultant higher oxygen fugacity and deposition of siderite-hematite rich ferhythmites (Beukes, 1983).

The transition from the Kuruman to the overlying Griquatown iron formation has been comprehensively described by Beukes and Klein (1990). The said transition comprises at its base the *Riries* Member, which is a chert-poor greenalite-siderite rhythmite following on the relatively chert-rich underlying Groenwater Member. Weakly alkaline conditions prevailed in the basin at this time allowing for favourable conditions for the deposition of greenalite-siderite lutite laminae alternating with siderite microbands (Beukes, 1983). These greenalite-siderite rhytmites lack well defined chert mesobands and consist of greenalite-siderite lutite laminae alternating with siderite microbands (Beukes 1983).
The Riries member is interpreted to comprise a series of distinct lithostratigraphically zones, which from base to top include (Beukes and Klein, 1990):

- Bretby zone, characterized by the occurrence of Fe-silicate-siderite-ankerite feryhthmites. The upper Bretby zone is typified by a stilpnomelane-bearing horizon which marks the transition into the overlying Alphen Zone, and is typified by the occurrence of iron silicate-ankerite-siderite-magnetite ferhythmites interbedded with cm- to dm-thick intercalations of stilpnomelane felutite. A broad stratigraphic distribution can be seen here with minnesotaite/greenalite-rich assemblages developing at the top of the Bretby Zone, whereas the base of the Alphen zone contains relatively more abundant stilpnomelane.
- The Alphen zone is characterized by the occurrence of granular, banded magnetite-ankerite-siderite ferhythmites with virtually no other iron silicate but stilpnomelane. Very characteristic here are the granular cherts and intra-clastic felutite mesobands

interbedded with magnetite-ankerite-siderite ferhythmites, which essentially herald the first appearance of granular facies assemblages in the Asbesheuwels sequence.

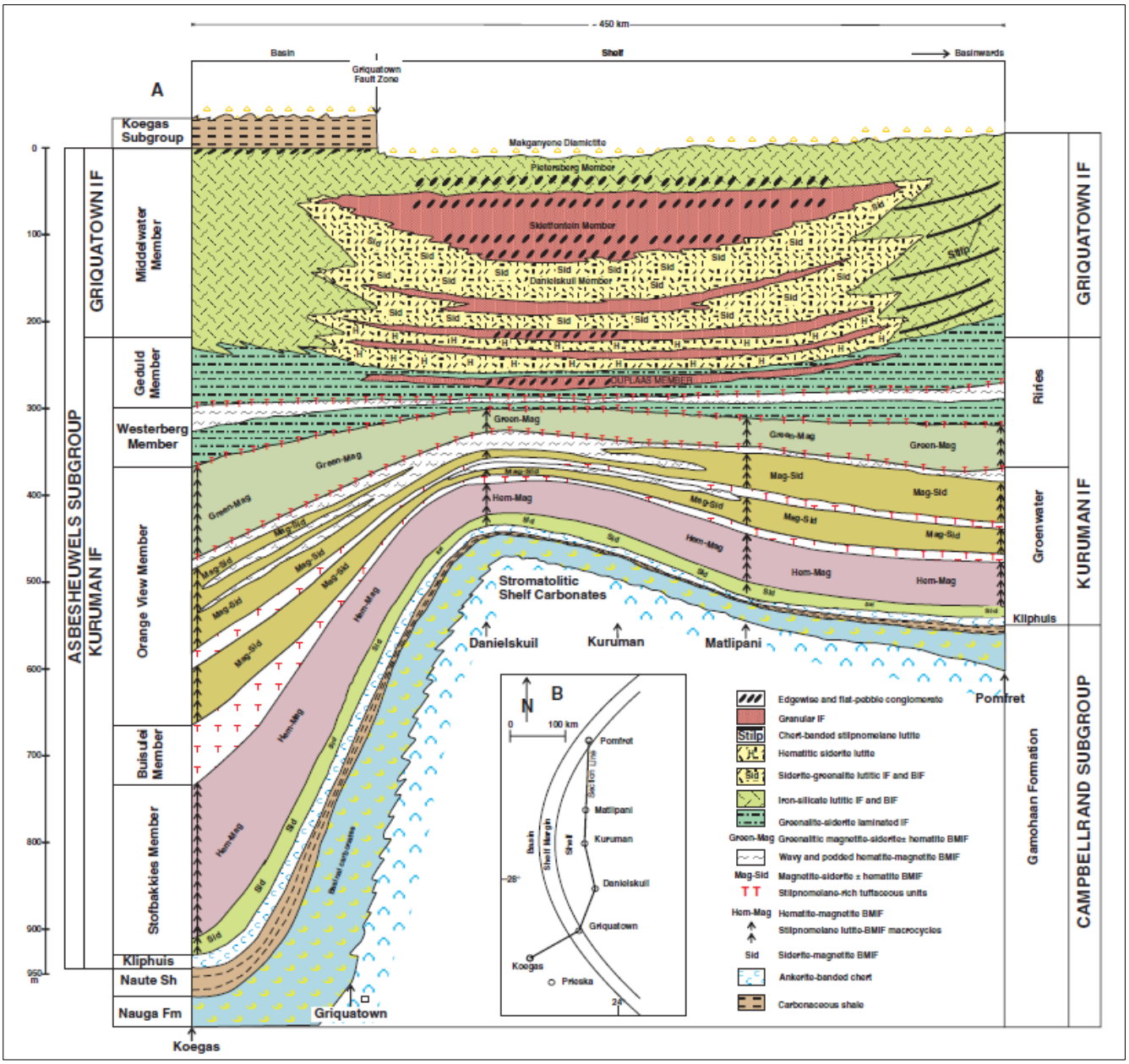

Figure 5. South-North cross section from koegas to Pomfret illustrating stratigraphic relationships, palaeodepostional environments in the Asbestos Hills Subgroup in Griqualand West. Adapted from Beukes & Gutzmer (2008)

- The *Ouplaas* member is characterized by the occurrence of granular iron formation beds draped by thin felutite or ferhythmite partings. The granular units are very chert-rich and display wavy to lenticular bedding.

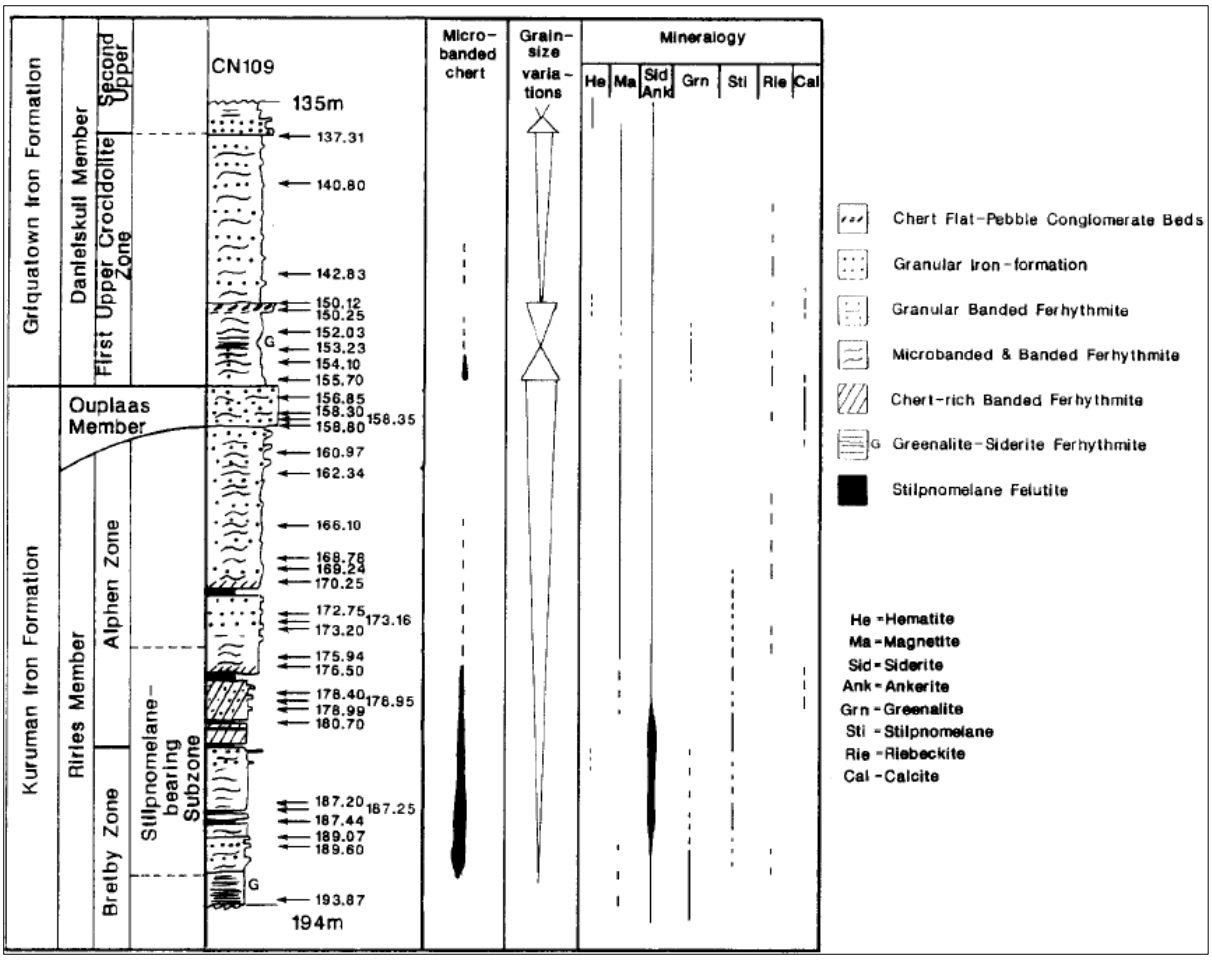

Figure 6. Stratigraphy of the Kuruman-Griquatown iron formation and their stratigraphic subdivisions and sample positions. Adapted from Beukes and Klein (1990).

2.2.1.3.2. The Griquatown Iron Formation

On the Kaapvaal platform, the Griquatown Iron formation is subdivided into the *Middlewater*, *Danielskuil* and *Pietersberg* Members. The Middlewater and Pietersberg Members are developed within the basinal facies whereas the Danielskuil member is deposited in a sub-tidal platform environment (Beukes, 1983). The *Danielskuil* member is characterised by being more clastic-textured (allochemical) relative to the immediately underlying Kuruman Iron Formation. These allochemical beds represent intermittent, high energy wave interruptions of microbanded BIF deposited in a continental epeiric sea environment (Beukes 1983, 1984, Beukes and Klein 1990). The lower, *Middlewater* member was deposited in a shallow basin below wave base, and consists of riebeckite-minnesotaite-greenalite lutites which interfinger with orthochemical-allochemical iron formation cycles of the Danielskuil member (Beukes, 1983). The upper, *Pietersberg* Member consists of banded greenalite lutites deposited in an interpreted fresh water lacustrine environment and marks

the top of the Griquatown iron formation and Asbestos Hills Subgroup by extension (Beukes, 1983).

The Danielskuil Member can be further subdivided into four discrete, second order, upward coarsening orthochemical – allochemical iron formation megacycles (Beukes 1983, 1984). These megacycles consist of zones rich in siderite lutites, sideritic grainstones/disclutites and greenalite lutite, hich are interpreted to represent respectively low energy subtidal, high energy, and calm lagoonal environments respectively (Beukes 1983, 1984). These subfacies are separated from each other by disclutite beds representing lag deposits along transgressional surfaces (Beukes 1983). The Danielskuil Member is thus interpreted to have been deposited in a generally low energy environment in the subtidal zone below normal wave base, and probably weakly alkaline as well (Beukes 1984).

2.2.1.4. The Koegas Subgroup

The Koegas Subgroup consists of terrigenous clastic-siliciclastic sediments and subordinate iron formations which conformably overlie the Griquatown iron formation (Beukes, 1983, Eriksson et al., 2006). It stratigraphically represents the top of the Ghaap group and is subdivided into five upward-coarsening iron formation-sedimentary formations, namely: *Pannetjie*, *Doradale*, *Kwakwas*, *Naragas*, and *Rooinekke*. The Doradale, Kwakwas and Rooinekke formations constitute the iron formation stratigraphic units of the Koegas, and show marked textural similaritites with the underlying Kuruman and Griquatown iron formations. The Pannetjie and Naragas formation constitute the siliciclastic portions of the Koegas Subgroup, consisting of quartz wackes and quartz-chlorite mudstones respectively. Beukes (1983) and Beukes & Smit (1987) interpret the regional contact of the Koegas Subgroup and overlying basal glacial Makganyene Formation of the Postmasburg Group, to be in the form of an angular unconformity, an interpretation, however, which is strongly disputed by Polteau *et al* (2006).

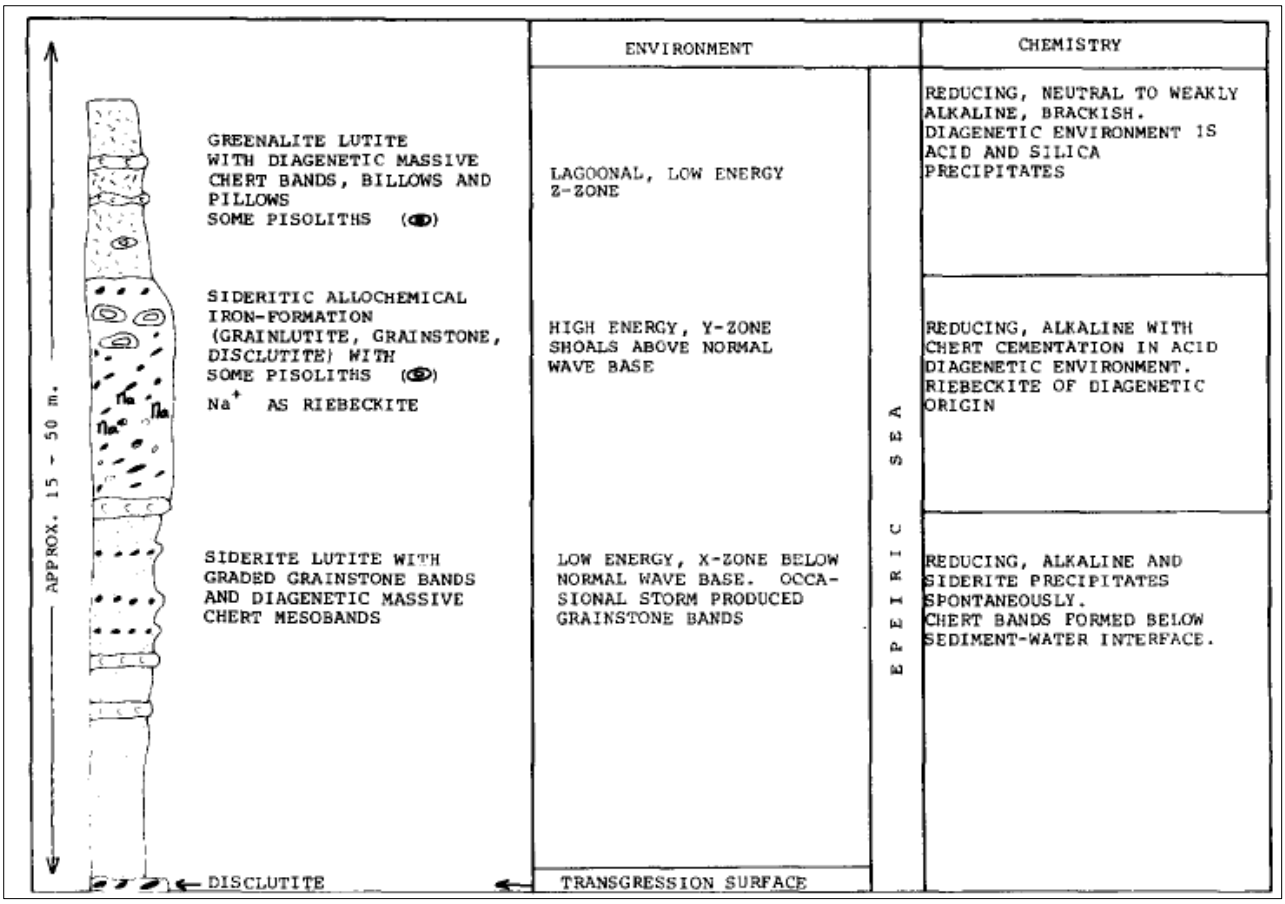

Figure 7. Orthochemical-allochemical iron-formation megacycle from the Danielskuil Member and the interpretation of its environment of deposition. Adapted from Beukes (1984).

2.3. The Postmasburg Group

The Postmasburg Group comprises a mixed volcanic-glacial-chemical rock unit (Beukes 1986a) which at the upper part of the Transvaal Supergroup in the Griqualand West Basin. It can be further subdivided into a basal glacial-volcanic interval (Makganyene and Ongeluk Formations) and an upper chemical sedimentary package (Hotazel and Mooidraai Formations). The Hotazel Formation in particular contains the giant manganese deposits of the Kalahari Manganese Field, in the form of three cycles of manganese-rich sedimentary rock interbedded with microbanded iron formation. These rocks essentially represent the youngest episode of iron-rich chemical sedimentation in the Transvaal Supergroup (Tsikos, 1999; Tsikos and Moore, 1997; Tsikos et al., 2003, 2010).

2.3.1. The Makganyene Formation

The Makganyene diamictite formation is developed as the basal part of the Postmasburg Group. Clasts contained in the diamictite consists of mainly chert, sandstone and BIF set in a fine-grained ferruginous matrix (Polteau et al., 2006). As mentioned earlier, the purported regional unconformity with the underlying Ghaap Group (e.g. Beukes and Smit, 1987) is not unanimously accepted (Polteau, 2000; Polteau et al., 2006). Polteau et al. (2006), in particular, show through systematic mapping and regional-scale field observations, that this stratigraphic relationship is not universal and that the Makganyene Formation is, in fact, conformable with underlying formations of the Koegas Subgroup in the deep southern Prieska basin, and possibly rests on an unconformity only on the shallow Ghaap platform to the north-east. The presence of dropstones in both underlying and interbedded Koegas BIFs, emphasizes the transitional nature of the basal contact in the deep basin (Polteau 2000, Polteau et al 2005).

2.3.2. Ongeluk Formation

The Ongeluk Formation conformably overlies the Makganyene diamictites and consists of a 500-900m thick succession of continental flood-type basaltic andesites (Polteau et al., 2006). Widespread pillow lavas are indicative of a sub-aqueous depositional environment (Cornell et, al., 1996). The uppermost part of the Ongeluk Formation consists of hyaloclasites, volcanic tuffs and hematitic jaspilites interbedded with the BIF of overlying Hotazel Formation (Polteau et al., 2006).

2.3.3. Hotazel Formation

The Hotazel formation represents the largest land-based manganese deposit in the world, and consists of iron-formation units interbedded with carbonate-braunite-rich manganese layers in three conspicuous sedimentary cycles (Tsikos, 1999). The lowermost manganese unit (12-45m thick) is the most economically viable due to a combination of larger reserves and marginally economic 38 wt% manganese ore grade (Tsikos, 1999). The overlying two manganese units are of no economic significance with only the upper one having been mined locally. The lithologic transitions between the BIF and Mn units are gradational,

consisting of very fine grained carbonate-rich hematite rock which is variously described as hematite lutite (Kleyenstuber, 1984).

2.3.4. Mooidraai Formation

The Mooidraai Formation represents the uppermost part of the Transvaal Supergroup in the Northern Cape region. It conformably overlies the Hotazel Formation, and is composed of microcrystalline banded Fe-bearing limestone, dolomite and subordinate chert (Tsikos et al., 2001; Fairey et al., 2013). The Hotazel and Mooidraai Formations are unconformably overlain by interbedded red and black shales and quartzites of the Mapedi Formation of the Olifanshoek Supergroup through a regional unconformity developed subsequent to mild deformation of the Transvaal Supergroup. The said deformation has led to the formation of large scale open folds such as the so-called *Maremane Dome*, where high-grade iron and manganese ores have developed through carbonate dissolution and largely *in situ* residual enrichments in iron and manganese, at the expense of BIF and carbonate-protoliths respectively.

2.4. Age of the Transvaal Supergroup

The absolute age of the Transvaal Supergroup age and encompassing lithostratigraphic correlation between the Griqualand West and Transvaal sequences, has been an area of much contentiousness particularly in earlier years, primarily due to the rarity of available datable lithologies. Beukes (1983) brackets the Transvaal strata between 2460±120 m.y. and 2100 m.y. The latter upper age constraint of the Transvaal is based on the age of the Bushveld mafic igneous rocks which is well-constrained to be around 2055±24 m.y. using Rb-Sr dating (Hamilton, 1977). The age of the basement Ventersdorp Supergroup lavas on the other hand has remained somewhat uncertain due to radiometric determinations giving out a bimodal distribution of age data: specifically, Rb-Sr dating has yielded an age cluster at around 2300 m.y. (Van Niekerk and Burger 1964, Harding et al., 1974) whereas a second set of ages using the U-Pb dating technique produced an age range from 2500-2700 m.y. (Van Niekerk and Burger 1978). Coertze et al., (1978), have also dated with the U-Pb technique pre-Transvaal acid volcanics that underlie the Transvaal strata in the eastern part of Bushveld complex, which yielded an age of around 2460±120 m.y. An age of approximately

2.7Ga for the Ventersdorp Sequence is currently regarded as the most likely, based on the single zircon U-Pb dating work on Armstrong et al (1991).

On the basis of radiometric U–Pb zircon ages obtained from interbedded volcanic tuff layers, the Campbellrand carbonate rocks are dated at 2555±19 Ma (Altermann 1997, Altermann and Nelson 1998). The conformably overlying Kuruman Formation has a SHRIMP U–Pb zircon age of 2465±5Ma (Pickard, 2003) and the Griquatown Formation has a calculated SHRIMP U–Pb zircon age of 2432±31 Ma (Trendall et al., 1990). One Pb/Pb age of 2415± 6Ma was determined for the Koegas's Rooinekke Formation (Kirschvink et al., 2000) and a 2222 Ma Rb–Sr age was determined for the Ongeluk Formation (Cornell et al., 1996). The latter remains controversial to date, as the Pb–Pb and U-Pb whole-rock age of the stratigraphically younger Mooidraai carbonate Formation, is at 2394±26 Ma from both dolomitised (Bau et al., 1999). and un-dolomitised (Fairey et al., 2013) parts of the succession. Finally, radiometric dating of the Hartley Basalt Formation that stratigraphically succeeds the basal Mapedi/Gamagara Formations of the unconformably overlying Olifantshoek Supergroup, has provided an age for the latter not lower than 1900 Ma (Cornell et al., 1996).

Chapter 3: Petrography & Mineralogy

3.1 Introduction

The first detailed accounts of the petrography and mineralogy of the Kuruman-Griquatown iron formations dates back to as early as the publication of Du Toit (1945), whose main focus at the time was the origin of the contained economic Na-amphibole asbestos deposits. Subsequently, much more detailed work on these iron formations was carried out by a number of authors including Cilliers & Genis (1964), Engelbrecht (1962), Harrington (1962) Harrington and Cilliers (1963), Cullen (1963), Von Backstrom (1963), La Berge (1966), Hanekom (1966) and Malherbe (1970). Later and much more detailed work by Beukes (1973, 1978, 1980a,c, 1984) included a proposed nomenclature and descriptions of a number of iron formation facies, on the principle that iron formations display many physical features very similar to those of carbonate rocks (Dimroth and Chauvel, 1973). This thesis will utilise greatly that specific nomenclature.

3.2 Sample Selection, methods and macroscopic observations

Detailed sedimentological work on the Kuruman-Griquatown iron formation was first undertaken by Beukes (1983, 1984) focusing mainly on the lithostratigraphic subdivisions and corresponding depositional modelling. Subsequent additional geochemical and sedimentological work was carried out by Beukes and Klein (1990), focusing mainly on a 60m transition zone between the Kuruman-Griquatown iron formations. To the knowledge of the author and his supervisor, the present study is the first of its kind to sample at moderate resolutionroughly300m of continuous drillcore intersection that straddles the upper part of the Kuruman iron formation and the entire Griquatown iron formation stratigraphically higher. The sampling was specifically done on a vertical diamond drilled core designated as ‘ERIN’ from the core-storage facility of the company BHP Billiton at the Hotazel Manganese Mine.

The first stage of the petrographic work involved careful logging and collection of fresh samples from the upper part of the BIF stratigraphy of the Asbesheuwels Subgroup, of individual lengths generally between 10-15cm and at a resolution of circa 5m (see figure 8

below for sample location and concentration). The specific objectives of the sampling and subsequent petrographic work presented here were to capture as comprehensively as possible, lithological variations across the examined section, with particular emphasis on the carbonate fraction of the samples which is known from concurrent and previous similar studies to control the distribution of Mn in the rocks (see chapter 1, this thesis, for details). Special emphasis was therefore placed on light-coloured sub-facies of BIF which were most likely to contain appreciable abundance of carbonate minerals for subsequent detailed geochemical study. For the same reason, sections of the examined drillcore proximal to two observed dolerite sills, or those overwhelmed by relatively thick monominerallic bands of fibrous riebeckite, were cautiously avoided. Hand specimen observations and a detailed log are presented in the forthcoming sections of this chapter.

3.3. Analytical Methods

Polished thin sections of the sampled material were cut from <5cm sub-portions of the collected core-sections across stratigraphy, based on macroscopic lithological variations and observations. Petrographic studies were undertaken by means of standard examination under the petrographic microscope, utilising both transmitted and reflected light. The same sections were subsequently used in the acquisition of mineral chemical data of carbonate minerals. All powdered samples were also examined by means of standard X-Ray Diffraction (XRD) analysis in order to determine the overall bulk mineralogical composition of the samples, and with specific regard to the carbonate minerals present, to obtain a broad estimate of their relative abundance where applicable. The latter was essentially done in a relatively crude sense on the basis of the relative heights of the main peaks for the two carbonate minerals of key interest, namely ankerite and siderite.

3.4. Macroscopic observations

The “ERIN” diamond drillcore straddles a large part of the Griqualand West sequence of the Transvaal Supergroup, from the basal Ongeluk lavas of the Postmasburg Group, underlying diamictitic Makganyene formation, and upper part of the Asbeusheuwels iron formations of the Ghaap group, namely the entire Griquatown and uppermost Kuruman Iron formations. The present study focuses and samples the latter iron formations across a section spanning-from approx. 370 m to 640m depth below present surface. Macroscopically, the ERIN core samples vary greatly in terms of textural relationships on all scales, from fine-grained

rhythmically mm-to-cm-scale banded lithologies to relatively coarse grained granular textures, akin to those described previously for the same rocks (e.g. Beukes and Klein, 1990). Although most of the samples collected are very fine grained and lutitic (except for the granular textured mesobands), preliminary mineral and textural identification were possible for those which show conventional properties like the strong magnetic susceptibility of magnetite, hardness of chert, rounded and angular textures of conglomerates/grainstones and breccias respectively, or granular-clastic textures of allochems and/or peloids. In some cases, the presence of very fine-grained Fe-silicates in some samples was diagnosable by conspicuous colouration i.e. green for greenalite, reddish-brown for stilpnomelane and blue for riebeckite.

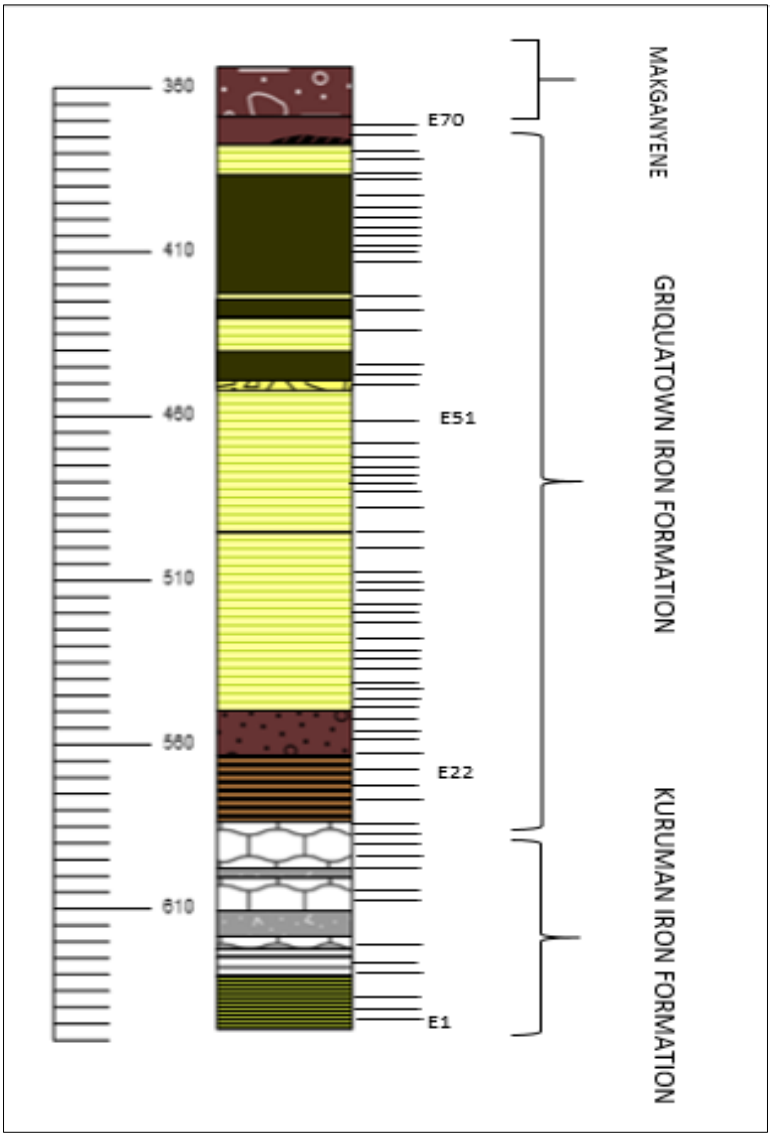

Figure 8. Sample location on the ERIN drillcore represented by the black lines towards the right. Note the relative lesser sample concentration in the Kuruman IF as compared to the conformably overlying Griquatown IF. Sample names can be correlated with those in table 8 in chapter 5.

3.3. Stratigraphy

Refer to figure 9 & 10 below for this section. Petrographic variations across stratigraphy based on non-analytical techniques such as colour and nature of banding permitted the differentiation of four different iron formation subfacies namely:

(i) Greenish grey to light-grey, well banded, carbonate-poor chert-Fe silicate (±magnetite) BIF – this is commonly developed at the basal part of the examined intersection and corresponds largely to the Kuruman iron formation, although it also occurs periodically in the Griquatown iron formation as well.

(ii) Light-coloured, fine- to granular, chert/carbonate-rich bands – these start to become prominent in place of the microbanded facies across the entire Griquatown iron formation. Ribbon- and pillow-like textures as described by Beukes (1984) are seen primarily in the mid sections, with granular textures peculiarly being associated with elevated contents of riebeckite. Abundant neomorphic grains of carbonate appear to 'float' on abundant microcrystalline chert matrix. The latter is commonly also associated with minnesotaite.

(iii) Granular allochemical/peloidal grainstone bands – these are dominant in the Griquatown iron formation at the mid to top sections of the stratigraphy, and are likely to represent reworking material by storms below wave-base (Beukes and Klein, 1990). They are normally greyish to light greenish in colour, concentrically rounded to lenticular in habit, are composed by chert and carbonate and are cemented by the same material.

(iv) Dark, fine grained, Fe silicate-rich lutites – these are mainly composed of either very fine grained greenalite and/or stilpnomelane in a matrix of chert ± Fe carbonate. Stilpnomelane-rich subfacies appears to be dominant in the Kuruman iron formation at the base of the examined section, as sporadic dark bands associated with riebeckite-rich ones, while the greenalite-rich subfacies is relatively more dominant in the upper part of the stratigraphy mostly in the 2nd Crocidolite zone of the Danielskiul member (see forthcoming section for more details).

3.3.1. Kuruman Iron Formation

The basal 9m meters of the examined ERIN drillcore intersection are characterised by thin rhythmic layering of greenish-grey chert-rich bands intercalated with thin dark metallic ones, on a 1-5mm scale. The greenish-grey bands are macroscopically taken to contain variable greenalite with associated Fe carbonate in variable amounts, whilst the intercalated metallic laminae are composed almost exclusively by magnetite (Fig. 9A). This lithology is tentatively assigned here to the Bretby zone of Beukes and Klein (1990). Occasionally, this facies exhibits disrupted banding resembling intraclastic breccia on a core-specimen scale, characterised by contorted whitish chert bands intercalated with dark Fe-rich (magnetite-dominated) ones. Fibrous riebeckite is frequently seen here in textural association with the chert bands.

The stilpnomelane-bearing horizon of Beukes and Klein (1990) is also seen to develop here as a series of no less than eight dark, stilpnomelane lutite bands (Fig. 9A), of a thickness ranging between 10-20cm.The BIF hosting the stilpnomelane-rich horizon is still thought to belong to the Bretby zone but the banding becomes gradually thicker up-section with whitish chert/carbonate bands intercalated with magnetite ones. A 7.8m thick dolerite sill intrudes at the top of this horizon (Fig. 9B & 10) with characteristic vesicular texture at its top contact with the BIF, possibly suggesting a shallow depth of intrusion.

The BIF overlying the sill (Fig. 9C) is tentatively assigned to the Alphen zone of Beukes and Klein (1990), over a vertical thickness of approximately 25 meters. Banding here is also conspicuously thicker than that in the underlying BIF of the Bretby zone, with individual chert-rich bands up to 15 cm in some instances, intercalated with magnetite-rich ones that vary greatly in thickness from 1-2 mm-thick laminae to sometimes a few cm-thick bands. The banding is also characterised by less rhythmic alternations than underlying BIF, instead being typified by well-developed, wavy “pinch & swell”, and pod- to ribbon-like structures (Fig. 9C-D). Riebeckite is very common here, especially along the edges of the thick magnetite bands. A second, approximately 4m thick sill displaying similar textural nature to the aforementioned one, intrudes this zone. The nature of the banding remains similar above the sill with the chert-carb bands displaying dominant wavy-to pod-like structures (Fig. 9D). The latter take on a faint red tint relative to the white chert bands, probably due to hematite pigmentation. As the 1st Crocidolite zone of the Griquatown iron formation is

approached, (see also relevant section below), banding becomes thinner and more rhythmic again (Fig. 9D), reminiscent of the basal microbanded facies of the Bretby zone described earlier.

The Ouplaas member is described as a stratigraphic “marker bed” by Beukes (1984), who proposes that it serves well in dividing the predominantly well-banded autochtonous Kuruman iron formation, from the clastic and granular textured Griquatown iron formation. The Ouplaas member consists of granular Fe-formation layers draped by thin felutite or feryhmite domains, and it is in this mode that it has been observed in the ERIN core. The granular units are very chert-rich, and display characteristic wavy to lenticular bedding.

3.3.2. Griquatown Iron Formation

The Griquatown Iron formation conformably overlies the Kuruman Iron formation. In the examined ERIN drillcore, the dominant iron formation facies observed is markedly dissimilar to the microbanded Kuruman iron formation, being typified instead by granular-textured, medium- to coarse-grained dm-thick mesobands. The nature of the banding in this part of the stratigraphy becomes rather monotonous up-section, displaying a complex interplay of microbanded, ferhythmitic domains intercalated in an apparently cyclic fashion with abundant, dm-thick granular chert bands. These essentially orthochemical-allochemical iron formation cycles are conspicuous throughout the rest of the core.

Two characteristic crocidolite (i.e. asbestiform riebeckite) zones occur in the lower half of the Griquatown iron formation (Fig. 9E). These are typified by the presence of riebeckite impregnations within thick, granular-chert mesobands, resulting in a conspicuously blue colouration in the field. Coarser-grained granular textures are seen progressively upwards in the section, accompanied by a gradual disappearance of the blue tone in the chert mesobands and return to a milky-white granular appearance. Characteristic feature of the riebeckite-rich zones in the Griquatown Iron formation are the conspicuous orthochemical-allochemical cycles first described in detail by Beukes (1983). Four such cycles were observed in the ERIN drillcore, characterized by chert (+carbonate)-rich granular mesobands overlain by allochemical peloidal grainstones, which are in turn overlain by fine-grained dark Fe-lutite mesobands (Fig. 9F). Beukes (1984) interprets the latter cycles to respectively record cyclic paleoenvironmental transitions from low-energy subtidal, to high energy storm-dominated environments, culminating into lagoonal settings.

Figure 9. Drill core images

Different facies and lithological classification based on Beukes and Klein (1990). Note the meter ruler on the left for scale. Each drillcore measures 1m each.

A) Typical basal Kuruman IF characterized by thin rhythmic layering of greenish-grey chert-rich bands intercalated with thin dark metallic ones. The chert-rich bands are frequently impregnated with fibrous riebeckite giving them a blue tint and crosscut by later quartz veins. These are classified as falling under the Bretby zone. Note the dark lutitic stilpnomelane bed at the center. Numerous occurrences (8 in total) of the latter were observed in the stilpnomelane bearing horizon.
B) First encountered thick dolerite sill intrusion characterized by fine grain size and vesicular texture suggesting a shallow depth of intrusion. The latter is also prone to crosscutting quartz veins. Note the BIF here (on the right) as compared to (A) has relatively thicker whitish chert/carbonate bands intercalated with magnetite ones.
C) Typical Alphen zone Kuruman IF characterized by varied thickness but thicker white chert bands (up to 15cm in some instances) with paucity of fibrous riebeckite and thicker magnetite mesobands displaying well developed diagenetic textures including pinch and swell and pod-to ribbon-like structures. A 2^{nd} dolerite sill intrusion is seem above this BIF with the same characteristics as the 1^{st} dolerite sill.
D) The thick chert-carbonate bands of the latter Alphen zone become progressively more reddish in color as a result of possible hematite pigmentation. Note the dark stilpnomelane bed with thick monominerallic quartz at its base. The banding becomes progressively thinner and more rhythmitic closer to the overlying Griquatown iron formation.
E) Typical thick granular chert-rich mesobands endowed in riebeckite denoting the start of both the 1^{st} Crocidolite zone and 2^{nd} Crocidolite zone of the Danielskuil member. The presence of blue riebeckite dissipates with distance from the base of both the crocidolite zone shown by the 'whitening' of the granular chert bands.
F) Conspicuous orthochemical-allochemical cycles observed mainly in the 2^{nd} Crocidolite zone characterized by chert (+carbonate)-rich granular mesobands overlain by allochemical peloidal grainstones, which are in turn overlain by fine-grained dark Fe-lutite mesobands (left)

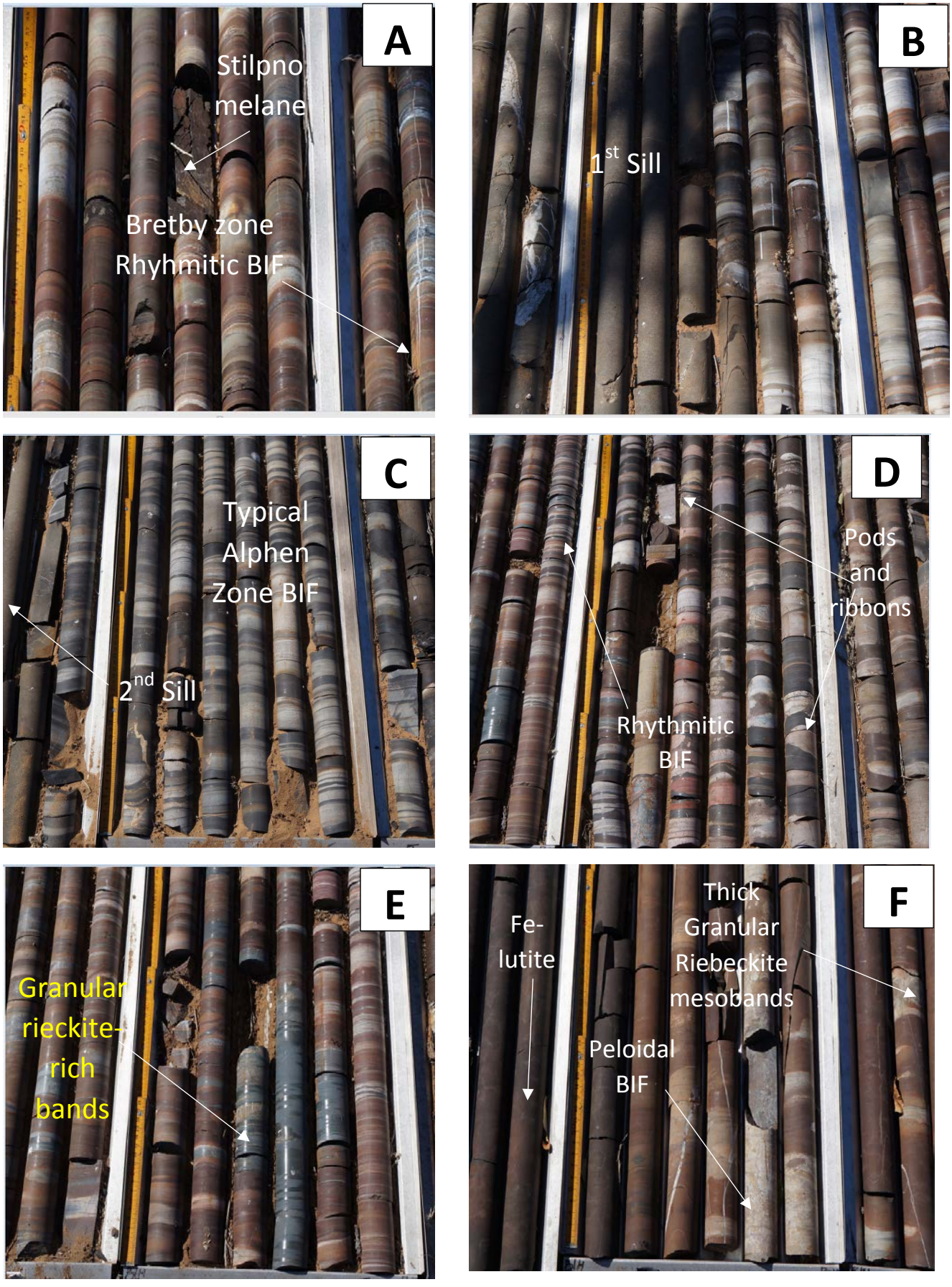
A
Stilpno melane
Bretby zone Rhyhmitic BIF
B
1st Sill
C
Typical Alphen Zone BIF
2nd Sill
D
Pods and ribbons
Rhythmitic BIF
E
Granular rieckite-rich bands
F
Fe-lutite
Thick Granular Riebeckite mesobands
Peloidal BIF

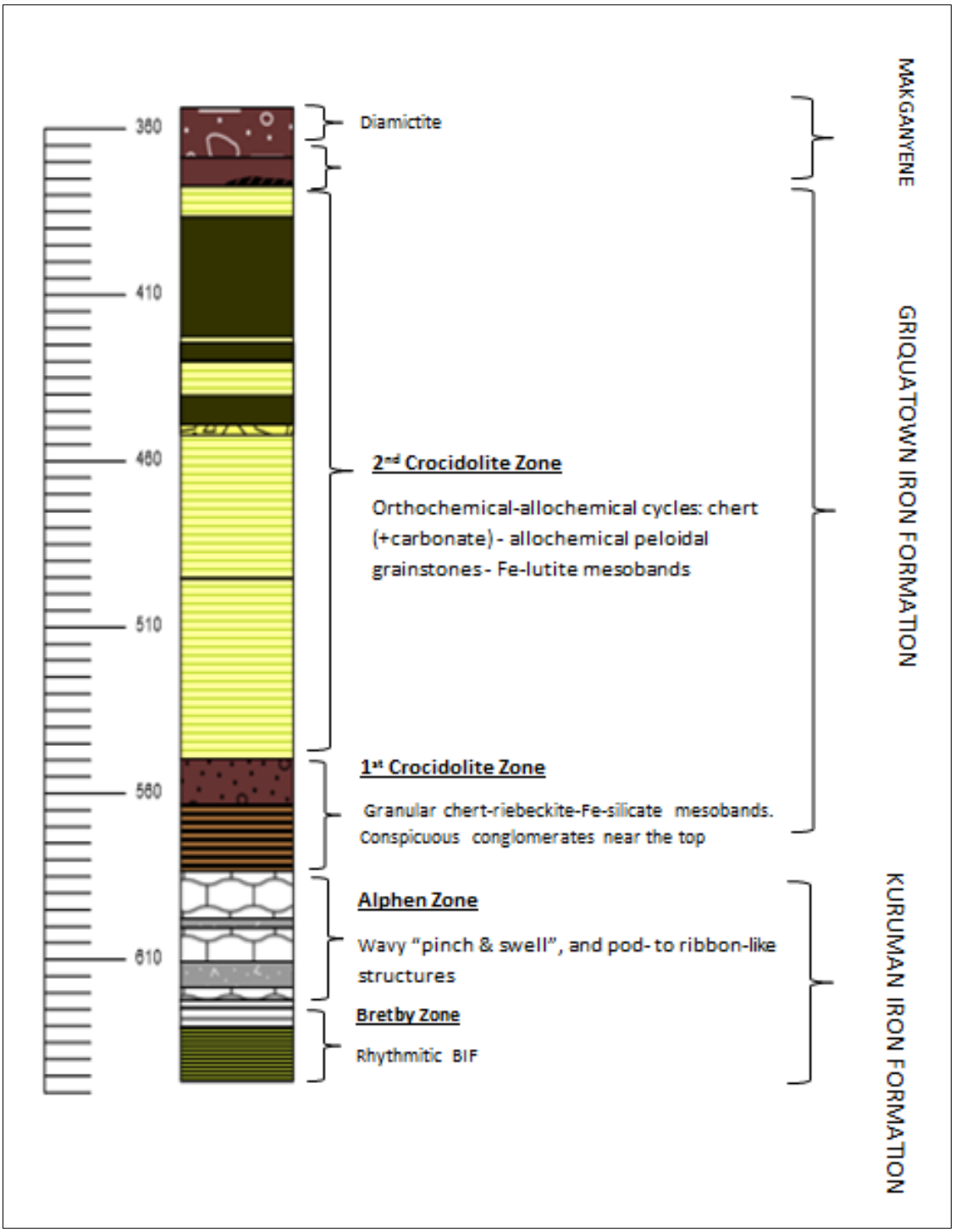

Figure 10. ERIN core showing the occurrences of the different mineralogy, textures and subdivisions observed macroscopically. The subdivisions are based on Beukes and Klein (1990).

As expected, there is no evidence whatsoever in the ERIN drillcore that the Koegas Subgroup of rocks develops in any way in this region (Figure 10 above), or that it was previously present and removed by subsequent erosion. To the contrary, microbanded- to granular facies intercalations of Griquatown iron formation appear to prevail right through

the entire studied section, up to the contact with the overlying Makganyene diamictite. Moreover, the contact between the two formations is evidently gradual and conformable, with dropstones characteristically appearing to have "sunk" into precursor BIF sediment over 2-3 meters of the uppermost Griquatown section.

3.4. Petrography

Many of the Archean-Paleoproterozoic iron formations studied through the decades, such as those of the Transvaal Supergroup and Hamersley Group of Australia, are suggested to have undergone only very low grade metamorphism. Preserved sections of BIF most commonly contain mineral assemblages typical of late (burial) diagenesis, barely entering the low grade, greenschist facies of metamorphism (Klein 1983, 2005). This is a feature which is generally deemed very favourable for the geochemical examination of BIF, and the interpretation of a variety of geochemical data in the context of the primary depositional environment of these rocks. To this end, the Kuruman and Griquatown Iron formations constitute no exception: their bulk mineralogy (Table 2) suggests that they are essentially unmetamorphosed in a strict sense, as discussed in detail for other Precambrian iron formations by a number of previous authors (James 1954, Klein 1976, 1978, 1983, Klein & Bricker 1977, French 1968, Floran and Papike 1978, Gole 1980a, 1981, Klein and Fink 1975).

Table 2. Identified mineral groups in the Asbesheuwels BIFs are presented in the table below. Relative abundances are designated below.

Mineral group	Mineral	Formula	Kuruman	Griquatown
Carbonates	Ankerite	$[Ca\ Fe^{2+}\ (CO_3)_2]$	XX	XXX
	Siderite	$(Fe^{2+}\ (CO_3)$	XX	XX
	Calcite	$CaCO_3$	X	X
Oxides	Magnetite	$[Fe^{2+}\ Fe_2{}^{3+}\ O_4]$	XXX	XX
	Hematite	$[Fe_2{}^{3+}\ O_3]$	X	X
Silicates	Greenalite	$[(Fe^{2+}, Mg)_6\ Si_4\ O_{10}\ (OH)_8]$	XXX	XX
	Minnesotaite	$(Fe^{2+},Mg)_3Si_4O_{10}(OH)_2$	XX	XX
	Stilpnomelane	$[K_{0.6}\ (Mg, Fe^{2+}, Fe^{3+})_6\ Si_8\ Al(O, OH)_{27}.2\text{-}4H_2O]$	XX	XXX
	Riebeckite	$Na_2(Fe^{2+}{}_3Fe^{3+}{}_2)Si_8O_{22}(OH)_2$	XXX	XXX
	Chert (Quartz)	$Si\ O_4$	XXX	XXX
Sulphides	Pyrite	FeS_2	X	X

Key:
XXX: Synonymous to abundant component (>20%)
XX: Common component (>5%)
X: Trace component

This chapter presents a rigorous petrographic examination of the mineral assemblages and common textural attributes as encountered in the BIF samples of his study. Although the mineral assemblages are treated holistically and reference is made to the bulk mineralogy of the rocks as the latter relates to the silicate, oxide and carbonate fraction of the studied samples, special emphasis is placed on the carbonates and on any petrographic evidence that would support a primary versus diagenetic origin for the carbonate mineral species variously encountered. Refer to figure 11 & 12 below for photomicrographs concerned in this section.

3.4.1. Silicates& oxides

Quartz is a major constituent, occurring in modal abundance of over 50% in many samples. It commonly exhibits a characteristic microcrystalline texture with sutured grain boundaries, which signifies very low grade metamorphic conditions of crystallisation (Passchier and Trouw, 1996). Besides Fe silicate minerals which commonly "impregnate" chert bands thus imparting characteristic tints of green, brown or blue in plain polarised light (for greenalite, stilpnomelane and riebeckite respectively), carbonates are also very common constituents of the chert bands. Ankerite and/or siderite may be present as fine disseminations to frequently coarser, sub- to euhedral grains seemingly 'floating' in the chert. A characteristic occurrence of chert is in the form of cores in some coarse ankerite grains, imparting a crude zonation of chert to carbonate from core to rim with carbonates growing around the cherty centre. Later coarse grained quartz veins cross-cutting the mineral assemblages also occur, albeit rarely.

Greenalite is relatively common with increased abundances in the basal part of the examined intersection (Kuruman iron formation). It is extremely fine-grained, exhibiting criss-crossed disseminated flakes commonly associated with overprinting magnetite, other silicates like minnesotaite and chert. Samples rich in greenalite exhibit a characteristic yellowish-green colour and these are particularly conspicuous in the green, well banded, carbonate poor-bands which occur in the Kuruman and to a lesser extent upper Griquatown iron formations. Greenalite is generally thought to be syngenetic or early diagenetic in origin (Jolliffe 1935, Gruner, 1936, Klein, 1983, Webb et al., 2003), forming from reactions between dissolved Fe^{2+} or and dissolved or amorphous silica (Maynard, 1982, Pecoits et al., 2009).

Stilpnomelane typically occurs in the form of micro-crystalline and highly phleochroic (yellowish brown to dark brown) sheaf-like grains, or as radiating, acicular masses or thin needle-like crystals. In the Asbeusheuwels iron formation, stilpnomelane is commonly associated with the carbonate fraction of the rock, found in close association with mainly calcite and less so ankerite. Other occurrences include as very fine-grained brown matrix, overprinted by disseminated sub- to euhedral magnetite in dark, Fe-lutite mesobands, as apparent replacement textures or overgrowths around and/or at the core of carbonate granules in allochemical, granular bands; and as very fine-grained interfingering masses with greenalite in greenalite-rich microbands. Stilpnomelane is thought to form either via early diagenetic reactions involving ferric iron and silica (Klein and Bricker, 1977; Maynard, 1982; McConchie, 1987; LaBerge et al., 1987) but has also been suggested to be a late diagenetic or metamorphic alteration product of greenalite (Gole, 1980; Krapez et al., 2003).

Minnesotaite exhibits high birefringent, fine- to medium-grained needles arranged in its classic “bow-tie” texture. It is particularly abundant in selected parts of the studied rocks, mainly in association with chert at the Kuruman-Griquatown transition. It is also present in the stilpnomelane-bearing subzone of the Kuruman iron-formation, and apparently overgrows greenalite-bearing assemblages as well. It is variously proposed that the formation of minnesotaite is a reaction product of either greenalite or siderite with chert (Gruner 1944; Klein, 1974; Klein and Bricker, 1977; Klein, 1983; Gole, 1980; LaBerge et al., 1987; Webb et al., 2003; Pecoits et al., 2009). The common cross-cutting and overprinting textural character of minnesotaite supports the notion that it is of late diagenetic origin.

Riebeckite is a rather abundant Fe silicate species in the studied rocks. It has a distinctive blue to yellow-brown phleochroism under plain polarised light. Texturally, it exhibits typical fibrous, bladed, columnar and radiating crystal habits with the fibrous form commercially known as *crocidolite asbestos*. The distribution of riebeckite is not restricted to any part of the examined section, but tends to be associated primarily with light granular carbonate-rich mesobands at the base of the aptly-named crocidolite-rich zones of the Griquatown Iron formation. Its concentration reaches a maximum at the start of each of these crocidolite zones and gradually dissipates with stratigraphic height. The common cross-cutting and/or overprinting nature of riebeckite has been widely used to support a late diagenetic, metamorphic and even hydrothermal origin for the mineral (Klein, 2005).

Magnetite Is to all intents and purposes the only oxide mineral present in the examined iron formations and one of the most common minerals in general. It occurs in distinctive, essentially monominerallic and well-defined laminae and bands, and/or as disseminated grains in Fe-silicate/carbonate/chert assemblages. The magnetite bands are exceptionally well-developed and conspicuous in the Kuruman iron formation. Disseminations of fine-grained magnetite are also very common in the Griquatown iron formation and specifically in granular chert (+carbonate)-rich mesobands, imparting a "speckled" texture to the latter. Aggregates of magnetite also appear to replace stilpnomelane that envelopes aggregates of ankerite-rich chert. Carbonates such as ankerite are also commonly seen to be cross-cut by magnetite grains, suggesting that magnetite may well be one of the last minerals to crystallize in the paragenetic sequence. The late diagenetic origin of magnetite is supported by a number of authors in the relevant literature (La Berge 1964, Garrel et al 1973, Gross 1972, Dimroth & Chauvel 1973, Perry & Tan 1973, Klein 1974, Mel'nik 1982).

Hematite occurs in negligible amounts in the Asbeusheuwels iron formation, as faint red impregnations in granular carbonate-rich bands at the base of the Griquatown iron formation, or as occasional minute bright red grains associated with magnetite laminae.

Pyrite is all but absent from the examined iron formation stratigraphy.

3.4.2. Carbonates

The Griquatown and to a somewhat lesser extent Kuruman iron formations, are well-endowed with respect to carbonate mineralogy. Carbonates are common constituents in essentially unmetamorphosed iron formations, having being reported for major iron formations all across the globe such as the Marra Mamba and Brockman iron formations of Western Australia (Ewers and Morris 1981, Klein & Gole 1981, Gole & Klein 1981a, Trendall & Blockey, 1970); Sokoman and Gunflint iron formations of Canada (Klein & Fink 1976, Lesher 1978, Floran & Papike 1978,); and Biwabik iron formation, US (French 1968 1973, Morey 2003, Mcswiggen & Morey 2007) amongst others. Samples of the iron formation intersection examined here contain three varieties of carbonate species, namely members of the dolomite-ankerite series, siderite, and calcite. The latter is a relatively lesser constituent by comparison to the other two. Ankerite and siderite make up the very bulk of the carbonate fraction of the examined samples. From a textural viewpoint, although

siderite is much finer grained relative to ankerite, the identity of the two could only be confirmed through mineral-chemical analyses.

3.4.2.1. Dolomite-ankerite series

Carbonates of the dolomite-ankerite series are arguably the most common carbonate phase in the Griquatown and Kuruman iron formations. They occur as well-crystallised, distinctively sub- to euhedral, medium- to coarse-grained rhombohedral grains that are normally associated (and thus coexist) with either siderite or quartz or both. Although end-member dolomite as such [$CaMg(CO_3)_2$] is practically absent in the studied rocks, ankerite [$Ca(Mg,Fe)(CO_3)_2$] is abundant and well-distributed throughout the stratigraphy of both the Kuruman and Griquatown iron formations.

Ankerite typically occurs as medium- to coarse-grained rhombohedra that can be conspicuously zoned. When zoned, they appear petrographically as forming clear margins with rather cloudy cores/interiors. The ankerite grains are typically associated with light-coloured chert bands seemingly 'floating' on the microcrystalline chert (±minnesotaite) matrix. They can also be found as well-crystallised grains forming – along with siderite – the cement around allochemical particles in granular/peloidal grainstone bands of the Griquatown Iron-formation. Ankerite aggregates in packstone bands are also found in the mid-section of the stratigraphy, surrounded by domains rich in stilpnomelane which is itself typically overprinted by euhedral aggregates of magnetite. Finally, it is seen as aggregates of abundant carbonate enveloped by thin, Fe-silicate-rich rhythmites, like the micro-granular pods seen in the transitional Ouplaas Member (figure 11F). Microprobe analyses of the zoned ankerite grains reveal similar mineralogical composition for both the clear margins and for the interior core, although analyses of the latter was often problematic due to the abundance of chert in the interior of the grains.

3.4.2.2. Siderite

Siderite (Fe^{2+} (CO_3) is the chemically simplest Fe^{2+}-bearing carbonate in the studied rocks. It is very fine-grained relative to other carbonate counterparts and virtually impossible to discern its exact identity microscopically without employing mineral-chemical work. The difficulty in distinguishing between siderite and ankerite under the microscope invariably hampers estimations of their relative (modal) abundance, and this was a key problem in the present study as well. French (1973) recognised the common association of siderite with

chert-greenalite-hematite mineral assemblages in conjunction with its fine grained nature, and purported that siderite might be one of the most primitive mineral phases in iron formations. Siderite in iron formation is typically present as granules, microspheres and intraclastic patchy concentrations, with recrystallized secondary versions of it being relatively rare (French 1973, Klein 1974, Floran & Papike 1975, Ewers and Morris 1981). The petrographic study of siderite in the studied iron formation was particularly problematic due to its very fine-grained nature; to this end, the combination of XRD and microprobe analyses was decisive in permitting a proper determination of its occurrence and abundance relative to other carbonate species.

Siderite in the Griquatown and Kuruman iron formations occurs as very fine-grained, sub-to euhedral, largely equant but often sub-rounded rhombohedral grains typically associated with comparatively much coarser-grained ankerite. The latter is dark in backscattered electron images whereas siderite occurs as very bright grains because of its higher iron content relative to ankerite (see Fig. 12 A,B,D). Siderite grains are in some instances found occurring in the interior of larger ankerite host grains, in the form of apparent inclusions. However, they are also found in abundance outside such ankerite hosts as well. In those instances, microprobe analyses of the siderite grains hosted in the interior of ankerite grains reveal similar chemical major oxide compositions with those on the exterior.

3.4.2.3. Calcite

Calcite is an uncommon constituent of the Griquatown and Kuruman iron formations, forming primarily on the margins of magnetite-rich laminae along with stilpnomelane needles. It typically develops very fine-grained masses and exhibits polysynthethic twinning when grains are sufficiently coarse. It is especially common in the mid-section areas of the stratigraphy just above the lower well banded rhythmitic iron formations of the Kuruman IF, and is also associated with minnesotaite-bearing chert bands in proximity to stilpnomelane-bearing mesobands. Selected back-scattered images show apparent replacement of ankerite by calcite (figure 12 E & F) near the intruding sills suggesting a possible replacement process linked to contact (thermal) effects (see also Dasgupta, 1965).

Photomicrographs

Figure 11. Mineral occurrences, textures and lithologies of the Asbeshewels iron formation. All photomicrographs were taken under transmitted light. Scale at the top.

A) Typically well banded, greenalite-rich, carbonate poor mesobands. The green laminae are composed of very fine grained greenalite and the light bands are composed of carbonate (mostly siderite in this area) and chert phases. These are dominant at the basal Kuruman iron formation.
B) Typical granular sideritic allochemical/peloidal grainstone bands. The allochems are well rounded +/- lenticular in shape typically zoned and cemented by either chert and/or carbonate material or both. Note the replacement stilpnomelane brown needles replacing the carbonate material on the allochems and the much later overprinting blue riebeckite needles and euhedral disseminated magnetite grains.
C) A typical grainstone (grain supported) composed of finer grained allochems and coarser grained rounded-angular clasts. These are present in the Griquatown iron formation and are completely absent in the underlying Kuruman. Scale similar to latter i.e. 0.2mm
D) Typical siderite+/-silicate lutite represented by two different bands. The bottom is a typical carbonate-chert rich band and the top is the finer grained brown (stilpnomelane) lutitic band. Note the abundance and or preference of banded magnetite for the latter relative to the former and the sharp boundary between the two bands.
E) Typical chert bands with coarse zoned ankerite rhombohedrals with a cloudy interior composed of microcrystalline chert. These ankerite seemingly 'float' on a matrix composed of chert (microcrystalline quartz). Note the late origin overprinting fibres of blue crocidolite.
F) Pods / pinch and swell structures completely made up of amalgamated carbonate grains and/or chert enveloped by thin ferhythmites of Fe-silicates. This is typically a diagenetic texture with blobs of carbonate flowing during early diagenesis. Note the

preference of overprinting magnetite grains for the enveloping thin Fe-silicate ferhythmites.

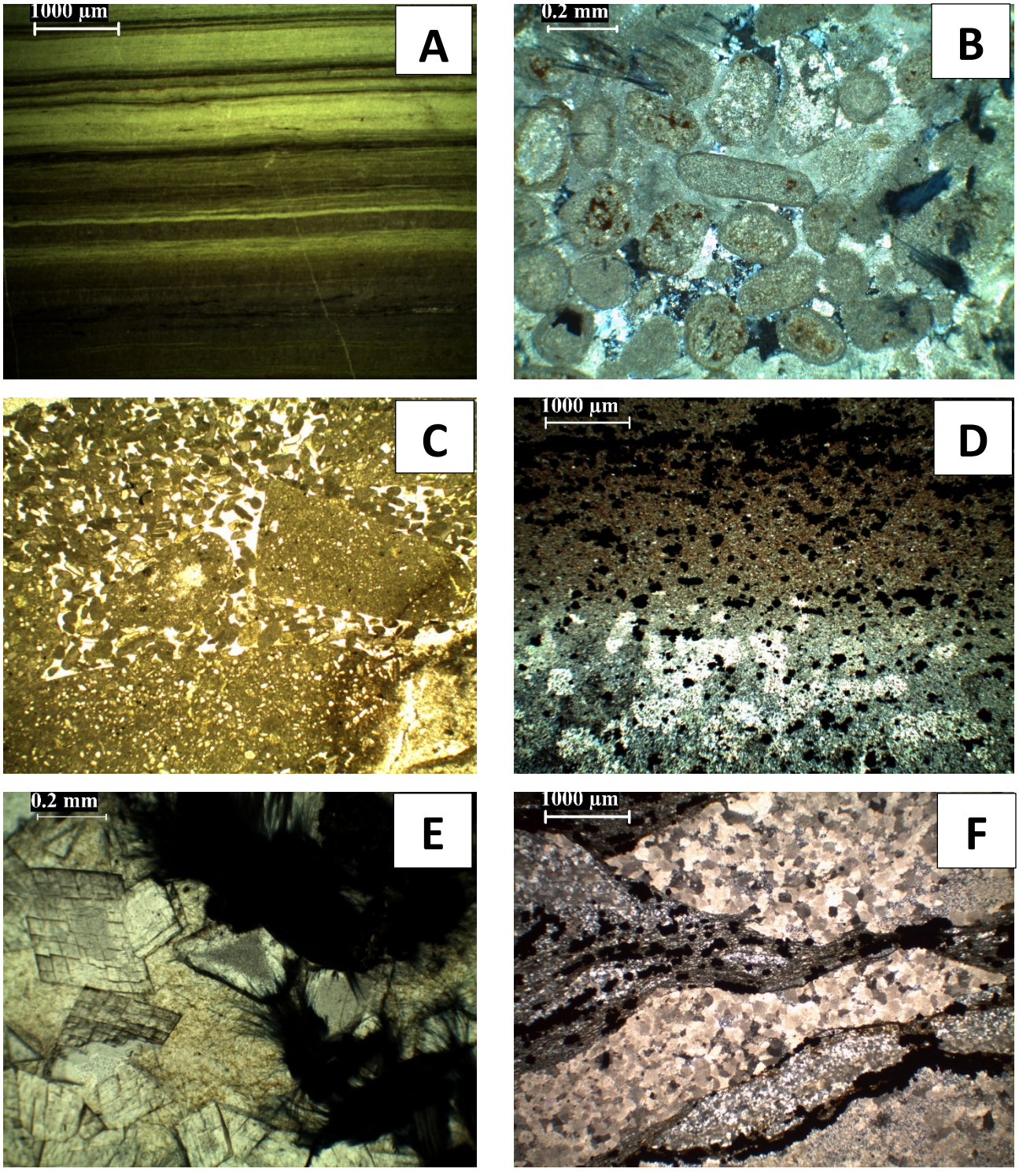
1000 µm
A
0.2 mm
B
C
1000 µm
D
0.2 mm
E
1000 µm
F

Backscattered images

Figure 12. Mineral occurrences, textural relationships of the Asbeshewels iron formation. Scale at the bottom.

A) Siderite (bright grains) and ankerite (darker grains) embedded in a matrix of microcrystalline chert. Note the close association of these two carbonates with siderite occurring on the exterior and interior of the host ankerite grains giving the impression of replacement of primary siderite by coarser grained recrystallizing ankerite during early diagenesis.
B) Thinly zoned coarse grained ankerite rhombohedra with a finer grained siderite grain hosted within the middle ankerite grain embedded in a microcrystalline chert groundmass.
C) Rounded zoned allochemical grains composed of an interior carbonate material (mostly sideritic) and a cherty silica rim cemented by carbonate material of mostly ankerite composition (dark) and siderite composition (bright)
D) Fine grained siderite grains embedded in a greenalite matrix. These siderite grains are typically found in the lower part of the stratigraphy in these well banded greenalite-rich bands with rare or absence of ankerite grains.
E) Close association displayed in an anhedral grain with both ankerite (dark) and siderite (bright) embedded in a matrix of minnesotaite-chert.
F) Coarser Mn-rich anhedral ankerite grains associated with finer subhedral siderite grains. Texturally, minnesotaite is seen overprinting the carbonates thus proposed to be of later origin. Bright aggregates overprinting all other mineral assemblages are fine magnetite grains.

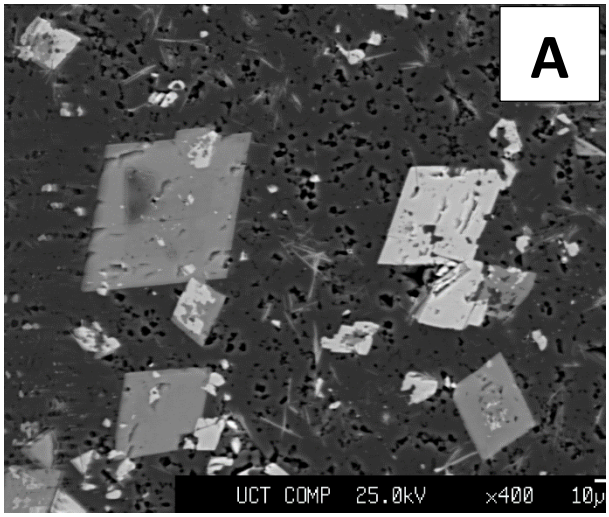
A
UCT COMP 25.0kV x400 10µ

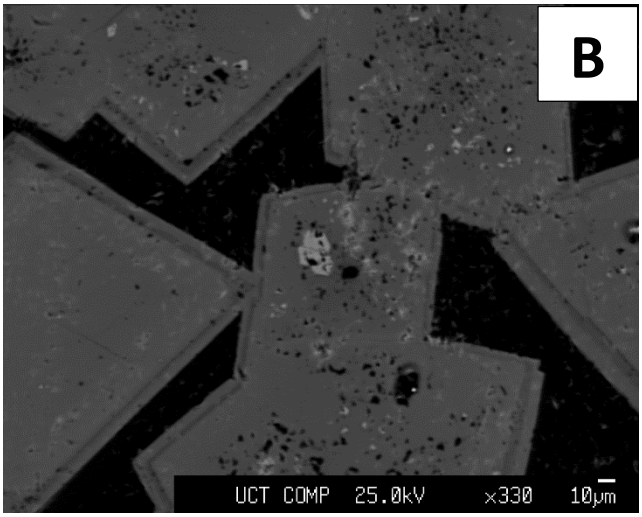
B
UCT COMP 25.0kV x330 10µm

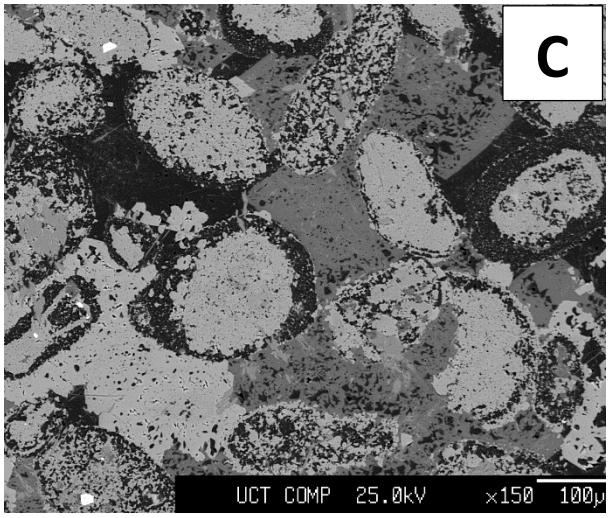
C
UCT COMP 25.0kV x150 100µ

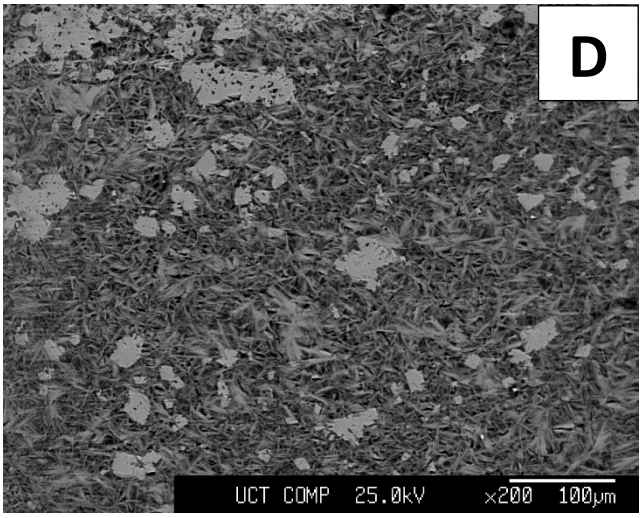
D
UCT COMP 25.0kV x200 100µm

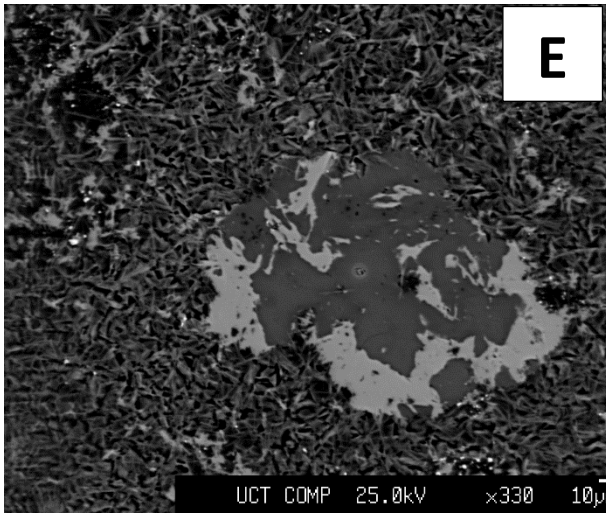
E
UCT COMP 25.0kV x330 10µ

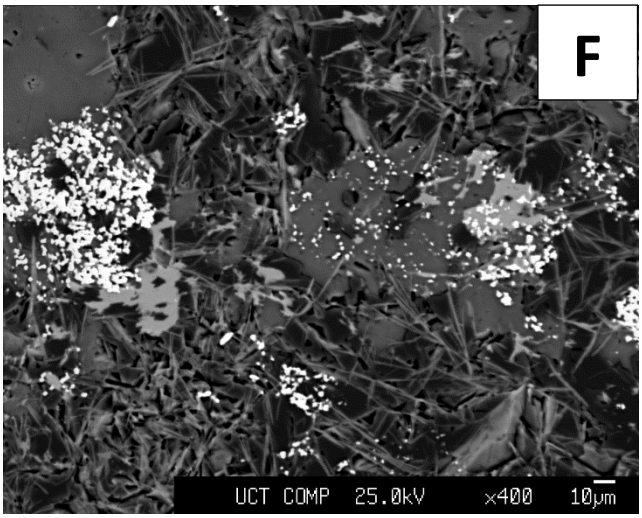
F
UCT COMP 25.0kV x400 10µm

3.5. Constraints on diagenesis and/or metamorphism

Klein (1983) compiled relevant mineralogical data (table 3 below) from various iron formations worldwide which experienced various degrees of metamorphism and juxtaposed them in a paragenetic scheme corresponding to increasing grades of metamorphism. Iron silicates are particularly useful indicators of metamorphic grade, as opposed to Fe-oxides and carbonates. The abundance of greenalite-stilpnomelane-minnesotaite iron silicate mineral assemblages that characterise the Asbesheuwels iron formation as discussed in the foregoing sections, supports the idea that these iron formations experienced little to no metamorphism, with the highest envisaged grade affecting these samples being late diagenesis to very low greenschist facies. The apparent textural overprinting of minerals such as magnetite and riebeckite against many of the characteristic mineral assemblages observed in the section, supports a late diagenetic origin for at least those two mineral species.

On the basis of textural observations presented here, features like the occurrence of recrystallized sutured quartz, calcite mosaics, rhombohedral ankerite crystals associated with quartz-minnesotaite-magnetite banded assemblages, and various other sedimentary features such as carbonate-rich pods and pillows, point to a complex diagenetic history of the examined rocks at least with regard to the physical manifestation of the said assemblages. Pod- and pillow-type structures could also be explained by early silica cementation preventing their burial compaction. By contrast, compaction of more than 80% may have taken place in uncemented, microbanded sedimentary material that surrounds such structures (Beukes, 1984).

Concerning the carbonate fraction of the rocks, the textures variously observed cannot be absolutely conclusive of the exact mode of origin of the carbonate minerals present. The very fine-grained nature of siderite may well record direct precipitation out of seawater, by reaction between dissolved aqueous Fe and bicarbonate, as also suggested by previous authors (Ewers and Morris, 1981; Klein and Beukes, 1989; Morris, 1993; Webb et al., 2003; Pecoits et al., 2009). By contrast, ferroan dolomite/ankerite almost invariably shows evidence for growth during diagenesis.

Table 3: Grade of metamorphism and expected BIF mineral assemblages expected for the respective metamorphic grades. Modified after Klein (1983)

<table>
<tr><td colspan="5">Grade Of Metamorphism</td></tr>
<tr><td colspan="2">Low</td><td colspan="2">Medium</td><td colspan="2">High</td></tr>
<tr><td colspan="2">Diagenetic
Early | Late</td><td>Biotite zone</td><td>Garnet zone</td><td>Staurolite-kyanite and kyanite zone</td><td>Sillimanite zone</td></tr>
<tr><td colspan="2">Chert→quartz
Greenalite
Stilpnomelane</td><td rowspan="3"></td><td rowspan="8"></td><td rowspan="9"></td><td rowspan="9"></td></tr>
<tr><td colspan="2">Ferri</td><td rowspan="2">annite
minnesotaite</td></tr>
<tr><td colspan="2">Talc</td></tr>
<tr><td colspan="2">Siderite
Ankerite
Calcite
Riebeckite</td><td rowspan="4"></td></tr>
<tr><td colspan="2"></td><td>Cummingtonite</td><td>Grunerite
Tremolite
(hornblende)</td></tr>
<tr><td colspan="4" rowspan="2"></td><td>Almandine
Orthopyroxene
Clinopyroxene</td></tr>
<tr><td></td><td>Fayalite</td></tr>
</table>

It is however, considered inopportune to ascertain the timing of growth of these carbonates on the basis of textures alone, because both minerals often showcase recrystallization textures (Krapez et al., 2003). This process may involve the precipitation of primary carbonate in very fine-grained form, i.e. as minute particles out of the primary water column, and irrespective of their exact chemical and isotopic composition each time. These particles then would carry the very chemical (including isotopic) signature of the water

column into the sediment. Once in the sediment, they can (partly) dissolve and recrystallize *in situ* into larger particles with neomorphic textural form, thus suggesting clear diagenetic growth but potential preservation of the primary chemical signals.

The abundance of fine-grained, subhedral to anhedral siderite grains across stratigraphy closely associated and/or occurring in the interior or exterior of coarser grained ankerite grains, are features that collectively point to a relatively earlier origin for the siderite. Dissolution of such siderite precursors during diagenesis, along with incorporation of Ca and Mg from pore-fluid, may lead to the formation of ankerite thereafter. Indeed, ankerite texturally appears to be recrystallizing during burial in an aqueous environment. If the process of dissolution and re-precipitation of carbonate happens in situ or is confined to a very small scale, i.e. within a single band or around pre-existing mineral particles, some of the primary chemical signatures –such as the carbon isotope ratio of the precursor carbonate particles – may be quantitatively preserved. This would be especially so if the pore fluid involved contains volumetrically little dissolved bicarbonate, and/or the latter is isotopically indistinguishable from the carbon-dioxide in the carbonate particle itself. These aspects will be discussed and illuminated further in the forthcoming chapters.

Chapter 4: Geochemistry

4.1. Introduction

An appreciable number of researchers have tried in the past to elucidate the origin and palaeoenvironmental significance of Precambrian banded iron formation (BIF), through the application of a wide variety of geochemical applications, such as REE geochemistry (Fryer 1977a,b, 1983; Appel, 1983; Jacobsen & Pimentel-Klose, 1988; Dymek & Klein, 1988; Klein & Beukes, 1989; Beukes & Klein, 1990a,b; Bau et al., 1997; Beukes & Klein 1996, amongst others) and light stable isotope geochemistry (Becker & Clayton, 1972, 1976; Perry & Tan, 1973; Perry et al., 1973; Dimroth & Kimberley; 1976 Kaufman et al., 1990; Beukes et al., 1990a,b; amongst others). In recent years, the application of more novel techniques such as iron isotope geochemistry (e.g. Johnson et al., 2008), have helped understand further some of the more enigmatic aspects of BIF deposition and diagenetic modification. Nevertheless, a number of aspects surrounding the genesis of BIF remain elusive to date, such as the primary oxidative mechanism/s for Fe precipitation and particularly the relative roles of biological *versus* abiotic oxidation mechanisms (e.g. Konhauser et al., 2002); as well as the possible controls and/or forcings that dictated the development of the characteristic banding typically observed in these rocks worldwide (Li, 2014).

The Hotazel BIF in the uppermost part of the Transvaal Supergroup represents a rather atypical occurrence, as it happens to host the largest land-based sedimentary Mn deposit in the world, namely the Kalahari Manganese Field (Tsikos et al., 2003, 2010). The Hotazel BIF is typically microbanded, and encloses three discrete braunite/Mn carbonate-rich layers of a collective stratigraphic thickness up to 70m in places. This is a feature which is not encountered whatsoever in other BIF of similar age and sedimentological character worldwide. Tsikos et al. (2010) have interpreted the anomalous occurrence of thick manganese deposits in the Hotazel BIF, as a result of long-term, Rayleigh-type Mn enrichment in solution in an evolving Palaeoproterozoic marine basin, wherein very large volumes of Mn-lean BIF had previously been deposited. Suitable candidates for such BIF in the lower Transvaal Supergroup are understandably the Kuruman and Griquatown BIFs in the Griqualand West Basin as well as their lateral correlative Penge BIF in the Transvaal

basin. By implication, Tsikos et al (2010) suggested that these older BIFs may in fact record a progressive enrichment in contained Mn as a precursor signal to the major Mn anomaly in the Hotazel strata.

Although the age of the Hotazel Formation in relation to the GOE remains elusive to date (Fairey et al., 2013) the suggestion of Tsikos et al. (2010) can be simply tested and then further elucidated. To this end, Fryer (2015) carried out a preliminary study of Mn abundances in the Kuruman and Griquatown BIF from drillcore intersections similar to the ERIN core studied here. The results show that there is indeed a Mn enrichment recorded in the upper Griquatown BIF, albeit with Mn hosted entirely in the carbonate fraction of the rock. The present study is effectively an attempt to understand further the significance of that signal, in light of prevailing models that interpret BIF carbonates as entirely diagenetic in origin. For that reason, the majority of samples examined petrographically in Chapter 3 were also analysed geochemically via two methods, namely microprobe analyses of carbonate species (at the University of Cape Town) and specifically ankerite, siderite and much more occasionally calcite; and speciation analyses of bulk-rock sample powders (at the University of California at Riverside, USA), based on the analytical protocol of Poulton and Canfield (2005) and with special focus on the carbonate fraction of the rocks. In conjunction with petrographic and mineralogical information discussed in the previous chapter, interpretation(s) will be drawn focusing on key mineral-specific elemental oxide abundances and their distribution across stratigraphy. The ensuing conclusions and preliminary interpretations will then be transferred to the next chapter dealing with the carbon isotope geochemistry of the same carbonates, where further data interpretation and discussion on the origin of the carbonate fraction in the studied rocks will be made.

4.2. Sample selection and analytical methods

A total of 42 carbon-coated thin sections, chosen solely on the basis of capturing variable lithologies and corresponding occurrences of – coexisting where possible – carbonate minerals, were used for mineral-chemical investigations using EPMA analysis. Preceding petrographic work as well as x-ray diffraction (XRD) acted as a basis to determine the suitability of the samples chosen for microprobe work. Due to the difficulty in determining the exact mineralogical make-up of the carbonate fraction in most samples under the microscope, a combination of EPMA data and accompanying back-scattered images was

used to illuminate the exact chemical nature of coexisting carbonates. Considering the findings of Fryer (2015) indicated earlier, the main objective of this exercise was to capture and interrogate any stratigraphic signal in manganese distribution with respect to ankerite, siderite and/or both (calcite was rare in the section and was therefore hardly considered further). Common obstacles to achieving optimum data towards the above objective were:

- occasionally substandard polishing and coating of some samples;
- the very fine-grained nature of the carbonate grains, especially with regards to siderite;
- mixed analytical data, particularly through the detection of Si related to the groundmass surrounding carbonate grains; and finally:
- the occurrence only of a single carbonate (specifically ankerite) in many sections.

The mineral-specific measurements were coupled with speciation analyses of corresponding bulk-rock powders of the same samples, in order to reveal broad trends in manganese distribution across stratigraphy for the different fractions analysed, in keeping with earlier similar results on lower resolution (Fryer, 2015). The speciation results were therefore used in conjunction with and support of the EPMA data, in order to establish in as much detail as possible the stratigraphic and mineral-specific behaviour of manganese and other carbonate-associated components (CaO, MgO and FeO) in the examined drillcore section. The same data also constitute the benchmark for the carbon isotope applications that follow in chapter 5 later, before all results are collectively assessed and interpreted in the "Discussion" and concluding sections of this thesis.

4.3. Results

4.3.1. Speciation analyses

The paper of Poulton and Canfield (2005) comprehensively presents the speciation methodology as used for the purposes of this study. Emphasis, however, was placed here essentially only on the acetate-soluble fraction which targets specifically the carbonate component of the BIF samples examined. This was done on evidence from recent studies (Fryer 2015) suggesting a strict mineralogical association of manganese with the carbonate fraction. Table 4 provides major element concentrations (as oxides) for the acetate-soluble fraction (bulk carbonate) as extracted during the sequential acetate-dithionite-oxalate

dissolution steps of Poulton and Canfield (2005). Analytical measurements on resultant solutions were performed via ICP techniques at the University of California at Riverside. It should be noted that the acetate reaction was done over 48 hours at 50^{o}C temperature, in order to dissolve the otherwise resilient Fe carbonates (ankerite and particularly siderite) as efficiently as possible. The Tables of Appendix II contain all speciation data, including those for the dithionite and oxalate steps, for reference. Geochemical variations of the four carbonate-hosted elemental oxides (i.e. CaO, MgO, FeO and MnO) across the examined upper Kuruman-Griquatown BIF stratigraphy are illustrated on the variation plots of Figure 13.

It is evident from the plots of Figure 13 that the MgO, FeO and MnO show an overall increase upwards in the stratigraphy. MnO values range from 0.01-2.11 wt% with an average of 0.58wt%. MnO specifically shows relatively low values at the base of the examined section (around 0.2wt% on average) and appears to increase gradually up-section, reaching values of up to 2wt% near the top of it. However, a distinct spike of high MnO is also present at *circa* 470m depth below surface, pointing to a two-prong excursion towards high MnO separated by a plateau of lower values. This pattern is also faithfully reproduced in the examined sections of Fryer (2015).

The acetate-fraction MgO values range from 0.15-3.44wt%, with an average of 1.61wt%. The stratigraphic profile shows a characteristic “zig-zag” pattern of sharply fluctuating values over short stratigraphic intervals, with distinct MgO minima towards the base of the examined section (partial average at ~0.8wt%). It does, however, also appear to record a broad and discernible increase in MgO stratigraphically upwards, in concert with the MnO profile. Highest MgO (3.4wt%) is recorded at the top of the stratigraphy. FeO also exhibits a similar profile to MgO with a gradual increase up stratigraphy, starting from low values at the base ranging from 1.6-18wt% and increasing to maximum FeO values as high as 33.8wt% at the top. CaO on the other hand varies throughout the stratigraphy showing no obvious stratigraphic trend, except for a peak around mid-section where CaO is as high as 24.24wt%. This part of the stratigraphy corresponds to samples where abundant calcite was identified petrographically. Overall, the stratigraphic patterns of increasing MgO, FeO and MnO seen in Figure 13 below seem to suggest a broad modal increase in carbonate component up-

section, which in itself would account for the increased manganese in the rocks. This signal is interrogated further in the sections that follow.

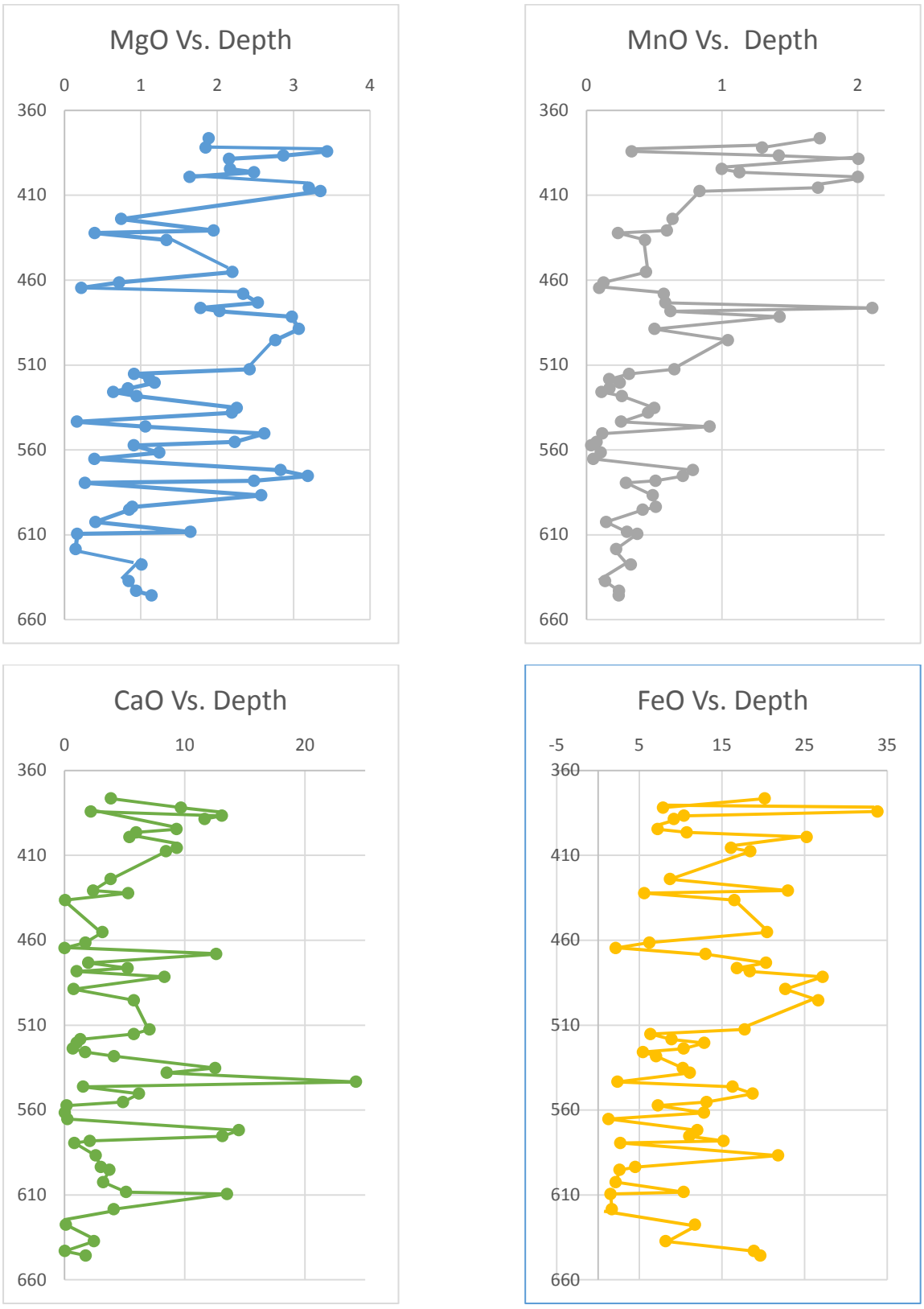

Figure 13. Major oxide (MnO, MgO, CaO, FeO) compositional variations against stratigraphy for the acetate-soluble fraction of the collected BIF samples (see text for details).

Table 4. Major element oxide concentrations obtained for the carbonate (acetate-soluble) fraction of the collected samples from ERIN drillcore, according to the step-wise sequential extraction procedure of Poulton and Canfield (2005).

	Mg(wt%)	Ca(wt%)	Mn(wt%)	Fe(wt%)	Depth(m)
E71	1,698	2,699	0,414	12,938	**372.5**
E70	1,180	2,263	0,970	11,362	376,5
E69	1,156	5,656	0,731	4,433	381,9
E68	2,150	1,282	0,188	19,038	384,2
E67	1,792	7,634	0,800	5,850	386,7
E66	1,348	6,806	1,131	5,178	388,6
E64	1,356	5,445	0,562	4,070	394,6
E63	1,551	3,483	0,636	6,048	396,5
E62	1,024	3,158	1,129	14,206	399,2
L3	2,001	5,449	0,963	9,056	405,6
E60	2,095	4,931	0,471	10,371	407,6
E59	0,465	2,248	0,358	4,904	424
E58	1,220	1,395	0,335	12,928	430,8
E57	0,248	3,094	0,132	3,159	432,3
E56	0,835	0,035	0,244	9,287	436,4
E53	1,375	1,847	0,248	11,516	455,3
E51	0,449	1,019	0,071	3,495	461,4
E50	0,139	0,005	0,053	1,200	464,6
E48	1,464	7,368	0,322	7,333	468,2
E47	1,583	1,159	0,328	11,441	473,3
E46	1,113	3,065	1,189	9,470	476,4
E45	1,270	0,600	0,349	10,339	478,3
E44	1,860	4,857	0,803	15,297	481,6
E42	1,918	0,442	0,283	12,755	488,8
E40	1,726	3,370	0,588	15,009	495,4
E39	0,668	3,577	0,186	4,235	**499.8**
E38	1,012	4,318	0,279	5,113	**504.3**
E36	1,517	4,130	0,365	9,990	512,5
E35	0,571	3,362	0,177	3,575	515,3
E34	0,696	0,767	0,095	5,003	518,4
E33	0,738	0,590	0,138	7,240	520,5
E32	0,520	0,415	0,096	5,831	523,8
E31	0,400	1,003	0,063	3,058	525,9
E30	0,591	2,410	0,147	3,967	528,3
E29	1,411	7,313	0,282	5,779	535,3
E28	1,372	4,971	0,257	6,252	538,1
E27	0,103	14,139	0,144	1,322	543,4
E26	0,664	0,908	0,512	9,168	546,3
E25	1,637	3,621	0,066	10,536	550,4
E24	1,394	2,848	0,042	7,396	555,3
E23	0,569	0,112	0,020	4,081	557,4
E22	0,776	0,025	0,060	7,223	561,6
E21	0,246	0,150	0,028	0,720	565,3
E19	1,768	8,464	0,443	6,766	571,9
E18	1,992	7,663	0,401	6,212	575,4
E17	1,551	1,232	0,287	8,545	578,2
E16	0,167	0,485	0,165	1,525	579,4
E14	1,610	1,514	0,276	12,268	586,8
E13	0,555	1,772	0,289	2,533	593,6
E12	0,530	2,177	0,234	1,477	595,3
E10	0,254	1,879	0,082	1,211	602,5
E9	1,032	2,997	0,169	5,839	608,3
E8	0,106	7,890	0,212	0,866	609,5
E7	0,092	2,397	0,124	0,941	618,4
E6	0,159	0,178	0,016	1,711	**621.4**
E5	0,631	0,077	0,185	6,602	627,5
E4	0,188	0,013	0,008	0,905	**630.5**
E3	0,526	1,435	0,077	4,605	637,3
E2	0,588	0,021	0,136	10,622	643,1
E1	0,713	1,028	0,134	11,056	645,7

4.3.2. EPMA data

In addition to the speciation data presented in the foregoing section, individual ankerite and siderite grains were targeted with respect to their mineral chemistry across stratigraphy, in order to establish any distinct geochemical patterns which, in conjunction with the preceding speciation data and the petrography, may help elucidate the possible cogenetic origin of the carbonates and their specific environment of formation. In this chapter, ankerite will be dealt with first as it is the relatively more abundant carbonate in the examined rocks, whilst siderite will follow. With regard to the data used in the mineral-chemical considerations, all relatively impure analyses (i.e. those with SiO_2 >1wt %) were excluded from any further consideration for each sample, and the remaining analyses were averaged for each elemental oxide considered. In very few instances, only a single analyses for a given section is used, due to the inability to obtain good data for more than one carbonate grains. These samples are highlighted on the relevant tables as appropriate.

4.3.2.1. Ankerite

Ankerite microprobe data are shown in Table 5. Values for MgO display significant variability throughout the stratigraphy, ranging from 5.69 – 9.23wt%, with an average value at 6.86wt%. CaO, on the other hand, ranges from 26.01 – 29.36wt%, with an average value of 27.52wt%. With respect to FeO, it exhibits a profile with variable but generally higher values over most part of the section, and an evident lowering thereof at the stratigraphic top. The FeO content specifically ranges from 19.90 – 22.74wt% over most part of the section, but drops to as low as 17.1 wt% at the stratigraphically uppermost part.

By comparison to all other oxide components, MnO in ankerite reveals a relatively contrasting profile of generally increasing values with stratigraphic height. In absolute terms, the MnO content of ankerite ranges substantially, from 0.17 – 4.65 wt% with an average of 1.74wt%. Along with that increasing upward trend, however, is a pronounced MnO maximum in ankerite near the base of the examined section. This suggests that ankerite does not become progressively richer up-section but also occasionally records high values even at stratigraphically lower levels. Such high Mn “spikes”, however, may be masked in bulk-rock or speciation geochemical data (see by comparison the speciation profile for Mn in the previous section) if the modal abundance of such ankerite in respective samples is relatively low.

4.3.2.2. Siderite

Microprobe data for individual siderite grains are presented in Table 6 and plotted in Figure 14, just like with the preceding ankerite data. Data represent averages of multiple analyses of siderite grains in a given sample, unless otherwise stated. It should be noted upfront that the profiles for siderite are not as densely populated with data as those for ankerite, as siderite is evidently less abundant in the rocks and is also substantially finer-grained in most samples. Therefore, obtaining a richer population of data for siderite was not practically possible.

Major oxide stratigraphic variations for siderite chemistry are effectively similar to those presented for ankerite in the previous section. Values for CaO and MgO portray similarly variable stratigraphic pattern as for ankerite, although it may be argued that the siderite in the examined section does become distinctly more calcic up-section. In absolute terms, MgO ranges from 4.98 – 8.53wt%, averaging at 6.86wt%; CaO ranges from 0.32-1.90wt% and averages at 0.91wt%.

FeO and MnO are no exception either: the former exhibits a profile with relatively high values at the base and mid sections of the stratigraphy and gradual lowering thereof at the top. FeO content specifically ranges from 46.44 – 53.12wt% with an average value of 49.52wt%. MnO on the other hand, shows a characteristic gradual increase with stratigraphic height, just like ankerite does. With respect to the lower part of the section, the lack of measurable siderite grains does not resolve a high MnO peak as correspondingly seen for ankerite, though there is a hint of elevated MnO in stratigraphically adjacent samples (i.e. sample E18 at 575m). Absolute MnO values for siderite record a significant range from 0.20 – 5.44wt% with an average of 2.07wt%.

Table 5. Ankerite major-oxide concentrations with stratigraphic height for the collected ERIN drillcore samples analysed with EPMA. Totals are calculated by the sum of major element concentrations excluding CO_2. Presence of small amounts of SiO_2 in some samples indicate minor contribution by silica adjacent to analysed carbonate grains. Highlighted samples are those with singular point data.

		Major-oxide concentrations (wt%)						
Sample	Height(m)	MgO	MnO	FeO	CaO	SiO_2	Totals	# Averaged samples
E1	645,7	7,73	0,62	20,35	28,08	1,53	58,30	2
E3	637,3	7,00	0,55	22,16	27,30	0,95	57,95	4
E13	593,6	7,62	4,65	16,90	27,17	1,58	57,91	9
E14	586,8	6,27	1,71	21,20	27,06	1,05	57,28	6
E18	575,4	7,10	1,90	18,73	27,87	2,11	57,71	5
E19	571,9	9,23	0,61	19,85	27,35	0,44	57,47	4
E21	565,3	7,60	1,79	19,66	28,24	0,09	57,38	1
E24	555,3	8,45	0,17	19,12	26,01	4,84	58,57	3
E25	550,4	8,74	0,30	19,97	27,30	1,00	57,31	4
E27	543,4	5,69	1,44	22,74	27,57	0,37	57,81	10
E29	535,3	7,05	1,20	20,84	27,82	0,39	57,30	3
E30	528,3	7,99	1,15	20,80	26,28	1,00	57,22	3
E31	525,9	8,69	0,68	19,31	26,30	3,24	58,22	3
E32	523,8	7,89	0,70	20,41	26,83	0,88	56,72	3
E36	512,3	8,45	0,80	17,98	29,36	0,67	57,26	3
E38	504,3	7,75	1,54	19,10	27,61	0,97	56,97	13
E39	499,8	7,21	1,46	20,78	27,61	0,31	57,37	1
E44	481,6	7,63	1,93	19,63	26,53	3,61	59,33	1
E50	464,6	6,02	1,37	22,43	27,09	1,33	58,24	3
E52	458,9	6,64	2,71	19,25	28,59	0,37	57,57	3
E54	452,2	6,18	1,56	19,97	29,03	0,10	56,84	4
E57	432,3	6,11	1,91	21,36	27,35	1,14	57,86	9
E59	424	6,22	2,92	18,85	29,02	0,84	57,85	5
E60	407,6	8,93	1,26	19,15	26,87	0,63	56,83	4
E61	405,2	8,26	1,33	17,66	28,24	0,93	56,43	9
E64	394,6	8,78	3,06	17,40	26,71	1,94	57,89	7
E66	388,6	6,93	4,57	17,08	27,60	0,08	56,26	9
E69	381,9	6,95	3,90	18,62	27,88	0,06	57,41	6
E70	376,5	6,15	2,73	19,70	27,41	1,82	57,80	3

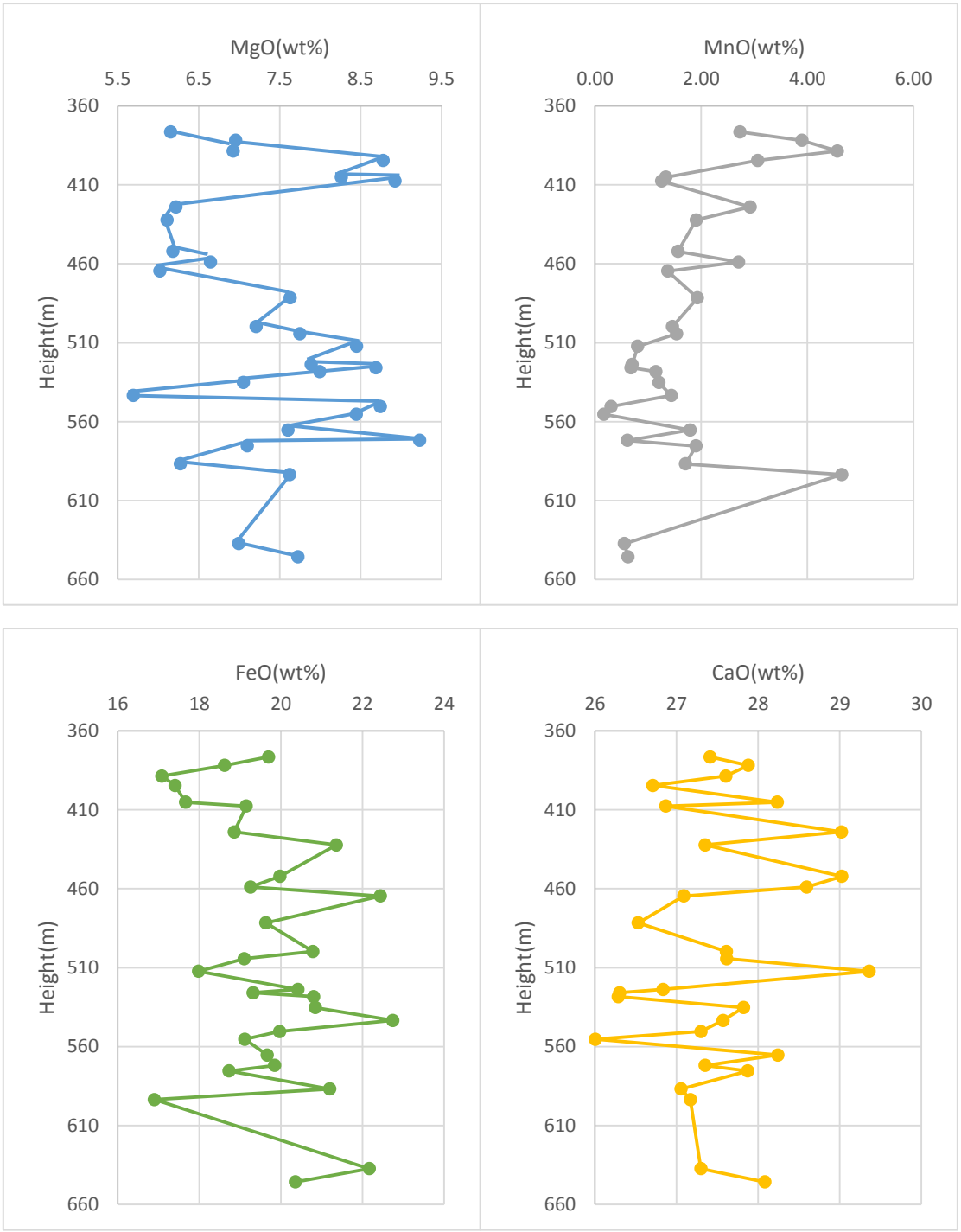

Figure 14. EPMA major oxide (MnO, MgO, CaO, FeO) compositional variations for ankerite against stratigraphy. See text for more details.

Table 6. Averaged siderite microprobe analyses for 29 ERIN drillcore samples for all major elemental oxides (MgO, MnO, FeO, CaO). Totals calculated by the sum of major element concentrations only. Highlighted samples are those with singular point data.

		Major-oxide concentrations (wt%)						
Sample	Height(m)	MgO	MnO	FeO	CaO	SiO_2	Totals	# Averaged samples
E1	645,7	5,12	0,98	53,12	0,32	2,12	61,67	5
E2	643,7	4,98	1,03	52,60	0,78	2,09	61,48	8
E5	627,5	7,12	0,46	50,54	1,13	1,17	60,42	4
E18	575,4	8,15	2,40	47,16	0,71	0,88	59,29	5
E24	555,3	7,06	0,20	51,15	0,74	1,61	60,75	2
E30	528,3	7,67	1,47	48,93	0,65	0,94	59,65	9
E31	525,9	7,38	0,88	50,55	0,65	1,83	61,29	6
E32	523,8	8,21	0,85	49,69	0,40	0,84	60,00	4
E33	520,5	7,29	1,03	50,12	0,79	0,64	59,86	8
E34	518,4	6,40	1,47	49,70	1,59	1,06	60,22	1
E36	512,3	6,49	1,43	50,24	1,30	0,04	59,51	5
E44	481,6	6,72	2,62	49,75	0,79	0,54	60,44	6
E47	473,3	7,72	1,71	48,20	0,55	0,36	58,53	8
E50	464,6	6,31	1,74	50,19	1,41	1,78	61,42	2
E51	461,4	6,61	2,11	49,27	0,68	1,15	59,82	10
E52	458,9	6,93	4,61	47,12	0,68	1,32	60,66	4
E54	452,2	6,11	2,16	50,56	0,68	1,07	60,58	5
E57	432,3	6,65	2,12	50,87	1,21	0,11	60,96	1
E59	424	6,69	4,08	47,36	1,66	1,17	60,96	3
E60	407,6	8,53	1,91	48,90	0,43	0,41	60,18	5
E66	388,6	6,12	5,44	46,93	1,90	0,30	60,68	2
E70	376,5	6,80	4,77	46,44	0,90	0,76	59,67	6

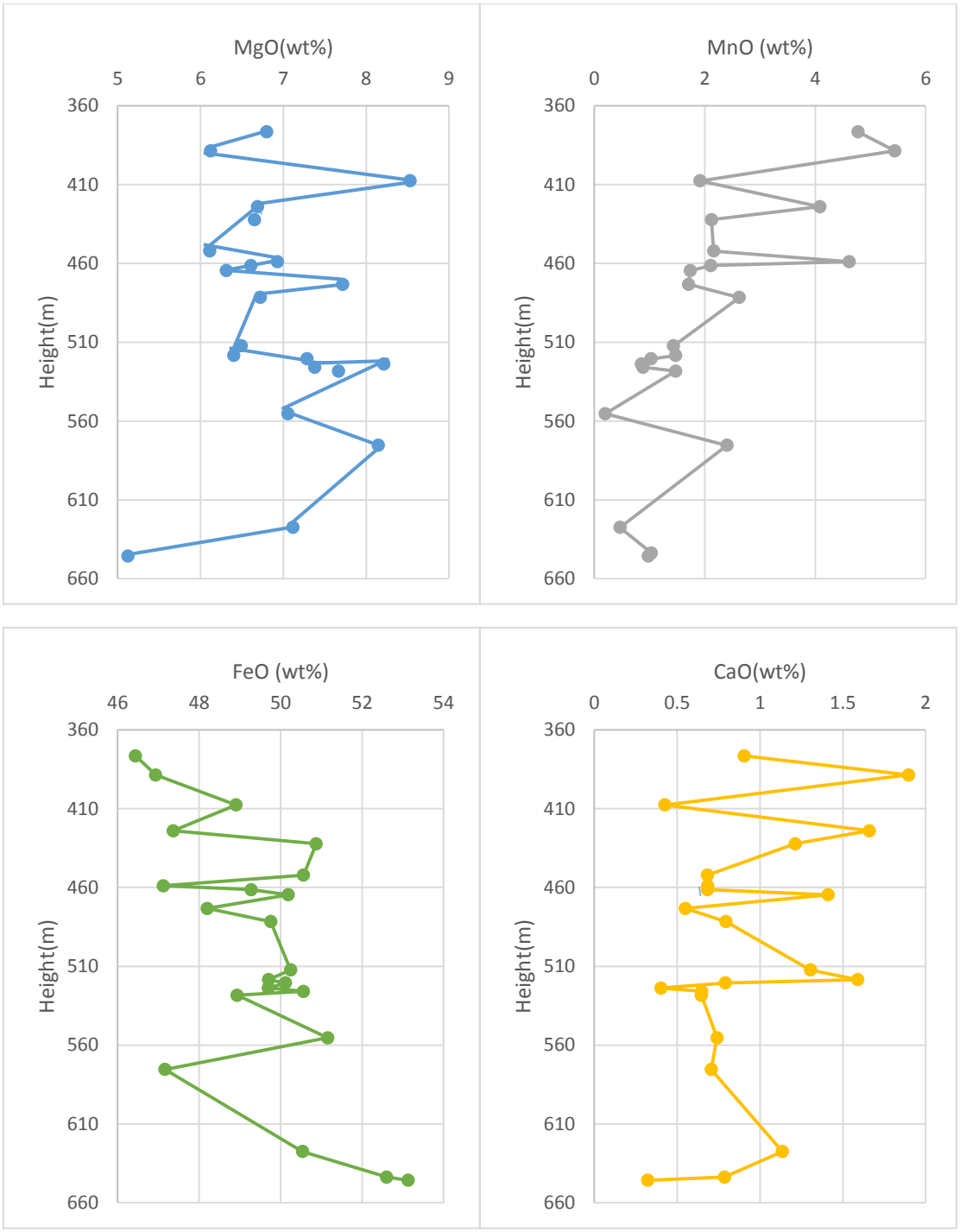

Figure 15. EPMA siderite major oxide (MnO, MgO, CaO, FeO) compositional variations against stratigraphy. See text for further details

4.4. Ratio relationships

The speciation data presented earlier, provide a relatively simple means of assessing the stratigraphic behaviour of Mn in the studied intersection of the Griquatown and upper Kuruman BIFs. The fact that Mn appears to be solely contained in the carbonate fraction of the rocks, implies that analysis of that fraction alone can provide a meaningful record of Mn distribution in the examined sequence of BIF. The application of microprobe application on individual carbonates minerals (ankerite and siderite), lends further support to the speciation results on a mineral-specific level. However, in order to view all these data (i.e. speciation and mineral-chemical) in the same context and assess them holistically, one needs to construct ratio diagrams depicting relative abundances for Fe and Mn contained in siderite, ankerite, and bulk carbonate. This becomes particularly apparent in light of the broadly antithetic behaviour between Fe and Mn in both ankerite and siderite, as illustrated in the respective binary plots of Figure 16. Such ratio diagrams are illustrated in the stratigraphic ratio profiles of Fig. 17.

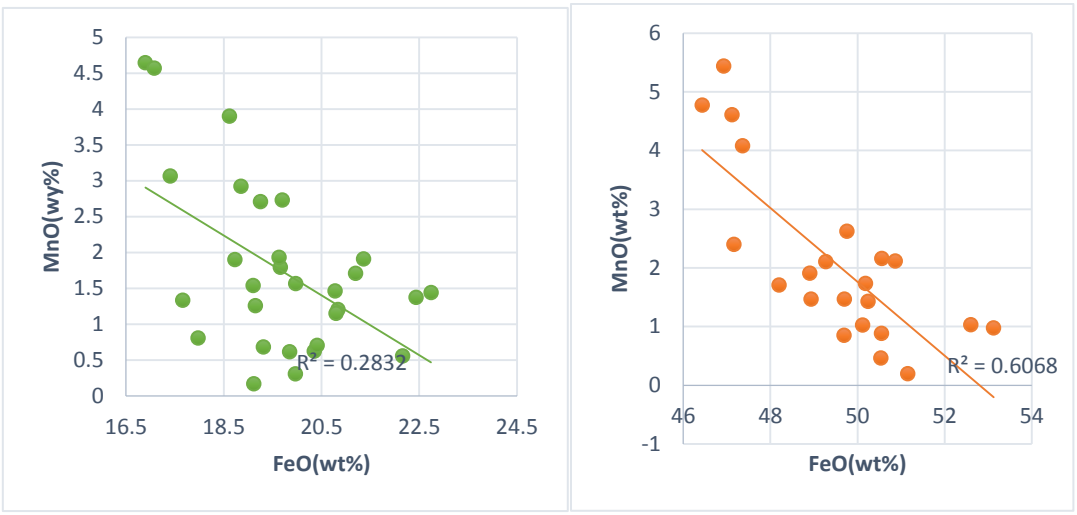

Figure 16. FeO *versus* MnO relationships for ankerite (left) and siderite (right)

Figure 17 below illustrates a striking resemblance in the Mn/Fe ratio profiles against stratigraphic height for both ankerite and siderite. This is an crucial relationship, as it appears to suggest that both carbonates record the same stratigraphic signal with respect to the partitioning of Mn relative to Fe in carbonate, and could be tentatively interpreted to imply either co-genesis of the two carbonates, or conservative behaviour with respect to Mn in the case of apparent replacement of one by the other. Moreover, the close similarity in the mineral-specific stratigraphic Mn/Fe pattern with that of bulk carbonate from the

speciation data, particularly with respect to the observed two-pronged MnO maxima at the base and top of the examined intersection, lends further support to the above notion that the two carbonates may well share a common origin.

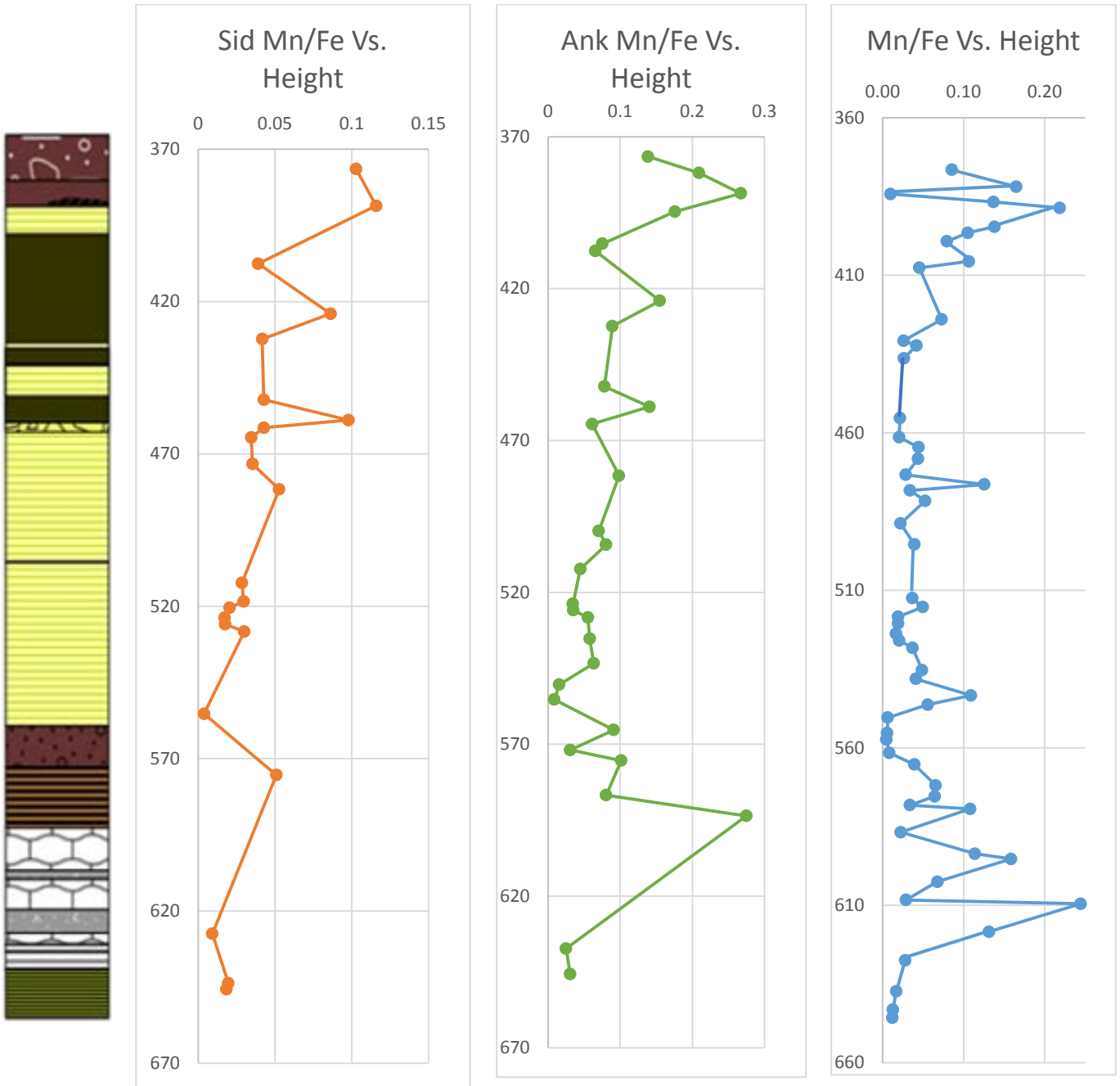

Figure 17. Juxtaposition of siderite and ankerite Mn:Fe ratio profiles against stratigraphic height (orange and green, left), and relative to bulk Mn:Fe vs. height (blue,right) from speciation analyses. Note the close similarity between the three profile, and specifically the two Mn/Fe maxima separated by one plateau minimum in the Griquatown BIF, and the very low Mn/Fe at the base of the profile, coinciding with the uppermost Kuruman BIF.

4.5. Summary

On the basis of the combined speciation and microprobe analytical data for the carbonate fraction of the BIF samples examined here, a number of preliminary conclusions can be drawn:

- Speciation data for the carbonate-extractable fraction of the BIF samples under investigation, point to bulk carbonate Mn/Fe ratio across the entire studied section between 0.01 and 0.25. Highest values of that ratio in the upper Griquatown BIF in conjunction with high modal abundance of carbonate in selected samples, results in percentage levels Mn in the rocks which is in itself an unusual feature in the context of BIF geochemistry worldwide (see review by Klein, 2005, for more information).
- Speciation analyses point to an evident increase in absolute bulk carbonate-hosted MnO stratigraphically upwards in the examined section, which is further characterized by two maxima at *ca*. 395 and 475 m below surface, separated by a plateau of relatively low values.
- On a mineral-specific level, both ankerite and siderite display a progressive increase in Mn relative to Fe stratigraphically upwards; this is also mimicked by the Mn/Fe speciation profile for bulk carbonate.
- There is a broadly antithetic relationship between the stratigraphic behavior of FeO and MnO in the two iron carbonate minerals ankerite and siderite: that is, the higher the Mn, the lower the Fe in both species.
- Relatively high Mn to Fe ratios are seen at two stratigraphic levels at the base and top of the examined section, in the form of two distinct spikes. These are recorded in mineral-specific as well as speciation data.
- The lowest MnO values and Mn/Fe ratios are observed at the base of the examined section and coincide with the uppermost portion of the microbanded Kuruman BIF.

The key preliminary conclusion that can be tentatively deduced from the above geochemical parameters is the distinct possibility that ankerite and siderite in the Griquatown and Kuruman BIF may share a common origin, at least with respect to their Mn contents and Mn/Fe ratio relationships. This point will be dealt with further in the next chapter, where carbon isotope applications are also introduced in the considerations.

Chapter 5: Carbon Isotopes

5.1. Introduction

Stable Isotope geochemistry has been at the centre of much interest for scholars throughout the past few decades, having being applied effectively in iron formations all around the globe. This has been done as part and parcel of efforts to elucidate many pertinent questions about BIF formation, including the rise of oxygen in the early Earth; source/s of Fe and Si for BIF; causes and controls of the strikingly banded nature of BIF; oceanic-atmosphere interactions and ocean stratification during BIF genesis and deposition; isotopic compositions of depositional waters; biological (microbial) *versus* abiotic processes that might have affected the primary sediment prior to and post-diagenesis; as well as possible isotopic changes that might have affected the BIF well after sedimentation and solidification, such as during prograde metamorphic, hydrothermal and/or meteoric-fluid rock interactions (Becker & Clayton, 1972; Baur et al, 1985; Gregory et al., 1990; Kaufman et al., 1990; Winter and Knauth, 1992; Beukes et al., 1990a,b; Beukes and Klein, 1990; Becker & Clayton, 1976; Perry & Tan, 1973; Perry et al., 1973; Dimroth & Kimberley, 1976; Kaufman et al., 1990; Tsikos et al., 2003, 2010; Heimann et al, 2010; Craddock & Dauphas 2011; Fischer et al., 2009; Planavsky et al., 2011, 2012; Lyons et al, 2014).

Mineral phases in iron formations that typically constitute candidates for light stable-isotope studies include Fe-carbonate minerals such as ankerite and siderite, along with coexisting calcite/dolomite where applicable; and silicate-oxide pairs such as quartz-magnetite/hematite pairs (e.g. Tsikos et al., 2003). This chapter focus only on isotopic applications on the carbonate fraction of the samples.

Conventional representation of carbon isotope variations are reported as $\delta^{13}C$ values, defined by the following equation:

$$\delta^{13}C_{mineral} = [(^{13}C/^{12}C)_{mineral}-(^{13}C/^{12}C)_{PDB}]/(^{13}C/^{12}C)_{PDB} * 1000,$$

where PDB is the acronym for *Pee Dee Belemnite* (Hoefs, 1987).

5.2. Background

A number of iron formation occurrences of Neoarchaean to Palaeoproterozoic age have been investigated using C and O isotopes. The contained carbonates in these iron formations all exhibit a pronounced depletion in their C-isotope composition relative to typical marine carbonates (Becker and Clayton, 1972; Baur et al., 1985; Beukes & Klein 1990; Kaufmann et al., 1990; Tsikos et al., 2003), with $\delta^{13}C$ values ranging typically between -4 and -14‰. Interpretations of such low carbon isotope values can be divided into two prevailing schools of thought, namely those who advocate an early diagenetic origin for the carbonates involving coupled organic carbon oxidation and Fe^{3+} reduction (e.g., Kaufmann et al., 1990; Tsikos et al., 2003); or precipitation of the carbonates directly from a stratified sea-water column with respect to C isotopes (e.g. Beukes and Klein, 1990; Winter & Knauth, 1992). The diagenetic model further implies that the carbonate $\delta^{13}C$ record of BIF would be a direct measure of a substantial contribution of organic-derived carbon to the precursor sediment. A number of both experimental and case studies have focused on evidence for carbonate diagenesis in BIF, and specifically on the role of Fe as key electron acceptor for organic carbon cycling, and have used carbonate as well as iron isotope data at bulk and mineral-specific level in direct support of diagenetic models (e.g. Fischer et al., 2009, Heimann et al., 2010; Posth et al., 2013).

The Asbestos Hills iron formation has been studied previously with respect to its carbon isotope composition. Beukes et al. (1990) investigated the transition from the Campbellrand carbonates to the overlying Kuruman iron-formation in terms of carbonate petrography, kerogen distribution and carbon-oxygen isotopic variations. They demonstrated that the carbonates in oxide-rich Kuruman iron-formation are more depleted in isotopically heavy carbon than those in the siderite-rich Griquatown iron-formation, whereas the kerogen in oxide banded iron-formations (BIF) is isotopically more enriched. They came to the conclusion that the ocean system was stratified with regard to dissolved carbonate, with the deeper water from which siderite-rich iron-formation formed being relatively more depleted in $\delta^{13}C$. The latter isotopic depletion was causally linked to hydrothermal activity, due to the very low organic matter supply suggested by the low kerogen content in the deeper-water siderite-facies BIFs.

Beukes and Klein (1990) also investigated the transition from the Kuruman microbanded iron formation and the conformably overlying clastic-textured Griquatown BIF in terms of sedimentology and geochemistry, including major, trace, REE element analyses and bulk carbon isotopes. They concluded that the carbonates in the iron-formation are depleted in ^{13}C, indicating involvement of organic matter during diagenetic alteration of the iron-formations. In addition, they also demonstrated that there are indications that total dissolved carbon dioxide in deeper water was more depleted in $\delta^{13}C$ than in shallower water.

More recent work by Fischer et al., (2009) investigated the Campbellrand carbonates in conjunction with the conformably overlying Kuruman iron formation in terms of $\delta^{13}C$ isotopes, and came to a somewhat different conclusion than that of Beukes and Klein (1990). Fisher et al. (2009) specifically demonstrated that the Campbellrand carbonates (both shallow and deeper water facies) consistently showed $\delta^{13}C$ values around -0.5 per mil, thus establishing that the $\delta^{13}C$ of the palaeo-water column DIC (dissolved inorganic carbon) was largely uniform. In contrast, the low $\delta^{13}C$ values for the iron formation carbonates (e.g. siderite) would have resulted from diagenetic remineralization of organic matter within the precursor iron-rich sediments. Horstmann & Halbich (1995) also investigated the Kuruman iron formation isotopically and came to a similar conclusion to the subsequent work of Fisher et al. (2009), but they also added that such depletions occur in addition to an already isotopically depleted carbon isotope signature inherited from a water mass containing a certain degree of hydrothermal input.

Finally, in the most recent pertinent study of the origin of iron formation carbonates, Johnson et al. (2013) combine existing carbon isotope data with radiogenic isotopes from BIF samples of the Kuruman iron formation. They argue that iron formation carbonates cannot reflect seawater compositions, but instead record closed system microbial Fe cycling in the initial soft precursor sediment, i.e. prior to lithification.

In this chapter, all relevant literature information and proposed models for the origin of the carbon isotope depletion of carbonates in BIF will be further assessed in light of stratigraphically well-controlled carbon isotope data from the ERIN and adjacent drillcores. The key objective will be to test whether systematic stratigraphic variation in carbon isotope

ratios exists in the bulk carbonate fraction of the examined BIFs; assess the causes and controls of such variation in view of petrographic and

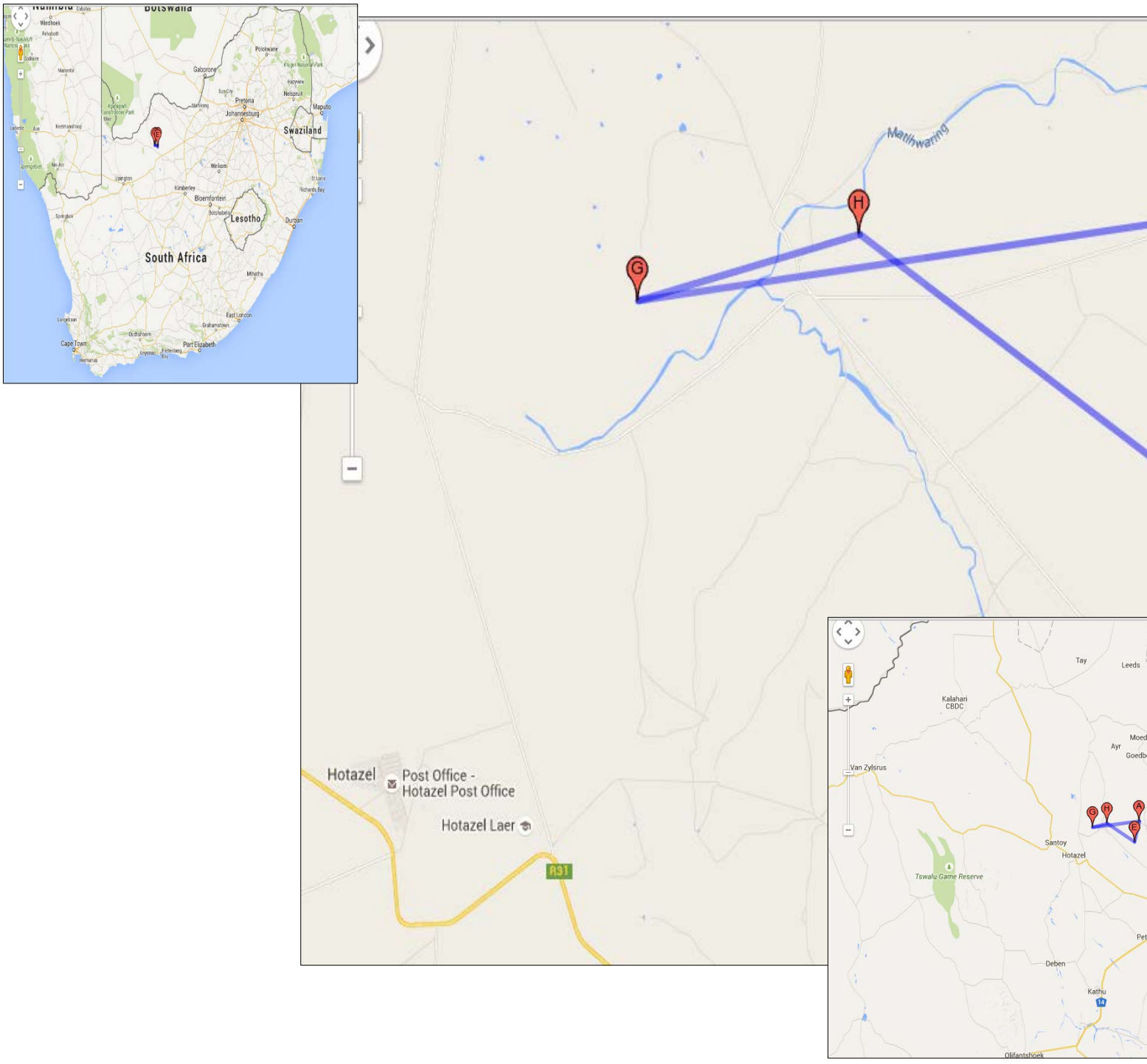

Figure 18. Google maps of the location of the different drillcores north-east of the Hotazel area, Northern Cape, South Africa, used in carbon isotope considerations of this chapter. The insert box at the top left shows the location of samples in Northern Cape South Africa (red flags). The lower right corner inset represents the Kuruman Manganese Field and the area of concern is zoomed at to show

the location of boreholes (centre image). G = GAS, H = HEX, A = ARPAN, E = ERIN. For scale reference, the geographical distance between GAS (G) and ARPAN (A) localities is ~20kms

5.2.1. Bulk carbon isotope considerations

5.2.1.1. Stratigraphic profile of ERIN core

Bulk carbonate-carbon isotope analyses were performed on the same 62 samples which were studied for their petrography, mineral chemistry and speciation geochemistry in earlier chapters. The isotopic results are presented in Table 8. The data reveal a general depletion in the $\delta^{13}C$ isotopic composition for the sampled upper Kuruman and Griquatown iron formations, relative to the typical marine bicarbonate isotopic signature assumed to have been approximately 0‰. The latter is thought to represent the isotopic composition of typical marine carbonates that would have formed via direct precipitation from the ancient water column (Baur et al., 1985, Carrigan & Cameron, 1991), thus reflecting the inferred Palaeoproterozoic $\delta^{13}C$ seawater isotopic composition.

The low $\delta^{13}C$ isotopic values for the sampled ERIN iron formation are in good agreement to those published for the same rocks previously (Beukes and Klein, 1990; Beukes et al, 1990; Horstmann & Halbich, 1995) as well as with other Palaeoproterozic iron formation occurrences elsewhere in the world (Becker and Clayton, 1972; Baur et al., 1985; Kaufman et al., 1990; Carrigan & Cameron, 1991; Winter and Knauth, 1992). In terms of absolute $\delta^{13}C$ values, these range from as low as -13.1 to as high as -5.5, with an overall average of ~-9.4‰ (Figure 19). Stratigraphically, the ERIN drillcore intersection examined can be conceptually subdivided into four portions of largely invariant isotopic signature:

- A basal, low-$\delta^{13}C$ interval (-10.0 to -11.5‰, samples E1-E3) which corresponds to the upper Kuruman BIF;
- An ~80m-thick, relatively high-$\delta^{13}C$ plateau (samples E5 to E27, mean -7.3‰) which straddles the transition from the upper Kuruman to the Griquatown BIF;
- An ~125m-thick, relatively low-$\delta^{13}C$ plateau (samples E28 to L3, mean -11.1‰) which characterizes the largest part of the Griquatown BIF; and,
- A ~30m-thick, relatively high-$\delta^{13}C$ section (samples E61 to E70, mean -8.0‰) at the topmost part of the Griquatown BIF up to the contact with the overlying Makganyene diamictite.

In spite of the above evident peaks and troughs in the stratigraphic variation of the bulk carbonate carbon isotope ratio across the examined section, the $\delta^{13}C$ signal appears to be relatively smooth, with gradual transitions from low to high values and back throughout the section. This is a rather curious feature for isotopic data that are purported to be controlled entirely via diagenetic processes: a closer look at the data of the acetate fractions of the speciation analyses reported in the previous chapter, permits the estimation of the variation in modal carbonate across the section. Estimated modal bulk carbonate concentrations in the samples on the basis of quantitative data from the total oxide yields of the dissolved acetate fractions (Appendix II), suggests that modal carbonate in the upper Kuruman and particularly Griquatown BIF fluctuates considerably from one sample to the next, from as low as 3.3% (sample E4) to as high as 67.2% by mass (sample E68), with a mean at ~33%, and with a generally gradual increase in modal bulk carbonate stratigraphically upwards. Against such variable modal carbonate abundances, it becomes problematic to explain the remarkable constancy in $\delta^{13}C$ data across thick sections of BIF as indicated in the foregoing, via diagenetic cycling processes alone. Therefore, the next step in interrogating that stratigraphic pattern in carbon isotope variation will be to examine its possible reproducibility across lateral space, and this is done in the section that follows.

Table 7. Depth and $\delta^{13}C$ of bulk carbonates of the Erin core

sample	depth	$\delta^{13}C$ carb
E70	376,5	-8,8
E69	381,9	-9,1
L4	383,6	-7,9
E68	384,2	-7,6
E67	386,7	-8,6
E66	388,6	-7,0
E65	390,2	-8,0
E64	394,6	-8,1
E63	396,5	-8,6
E62	399,2	-7,3
E61	405,2	-8,0
L3	405,6	-10,6
E60	407,6	-9,5
E59	424,0	-10,9
E58	430,8	-10,5
E57	432,3	-12,4
E56	436,4	-11,1
L2	449,8	-10,0
E53	455,3	-8,5
E51	461,4	-9,2
E50	464,6	-11,4
E49	467,6	-10,3
E48	468,2	-10,5
E47	473,3	-10,5
E46	476,4	-10,3
E45	478,3	-10,3
E44	481,6	-10,9
E42	488,8	-11,3
E40-b	495,4	-10,6
E40-a	498,8	-11,4
E37	509,8	-12,0

sample	depth	$\delta^{13}C$ carb
E36	512,5	-12,2
E35	515,3	-11,6
E34	518,4	-12,1
E33	520,5	-12,7
E32	523,8	-12,8
E31	525,9	-13,1
E30	528,3	-12,6
E29	535,3	-11,5
E28	538,1	-11,8
E27	543,4	-7,2
E26	546,3	-6,7
E25	550,4	-8,6
E24	555,3	-9,0
E23	557,4	-9,3
E22	561,6	-8,9
E21	565,3	-7,0
E19	571,9	-5,9
E18	575,4	-5,7
E17	578,2	-5,5
E16	579,4	-11,0
E14	586,8	-6,0
E13	593,6	-6,3
E12	595,3	-5,8
E10	602,5	-7,5
E9-b	608,3	-8,1
E8	609,5	-7,0
E7	618,4	-5,9
E5	627,5	-7,3
E3	637,3	-11,5
E2	643,1	-11,0
E1	645,7	-10,0

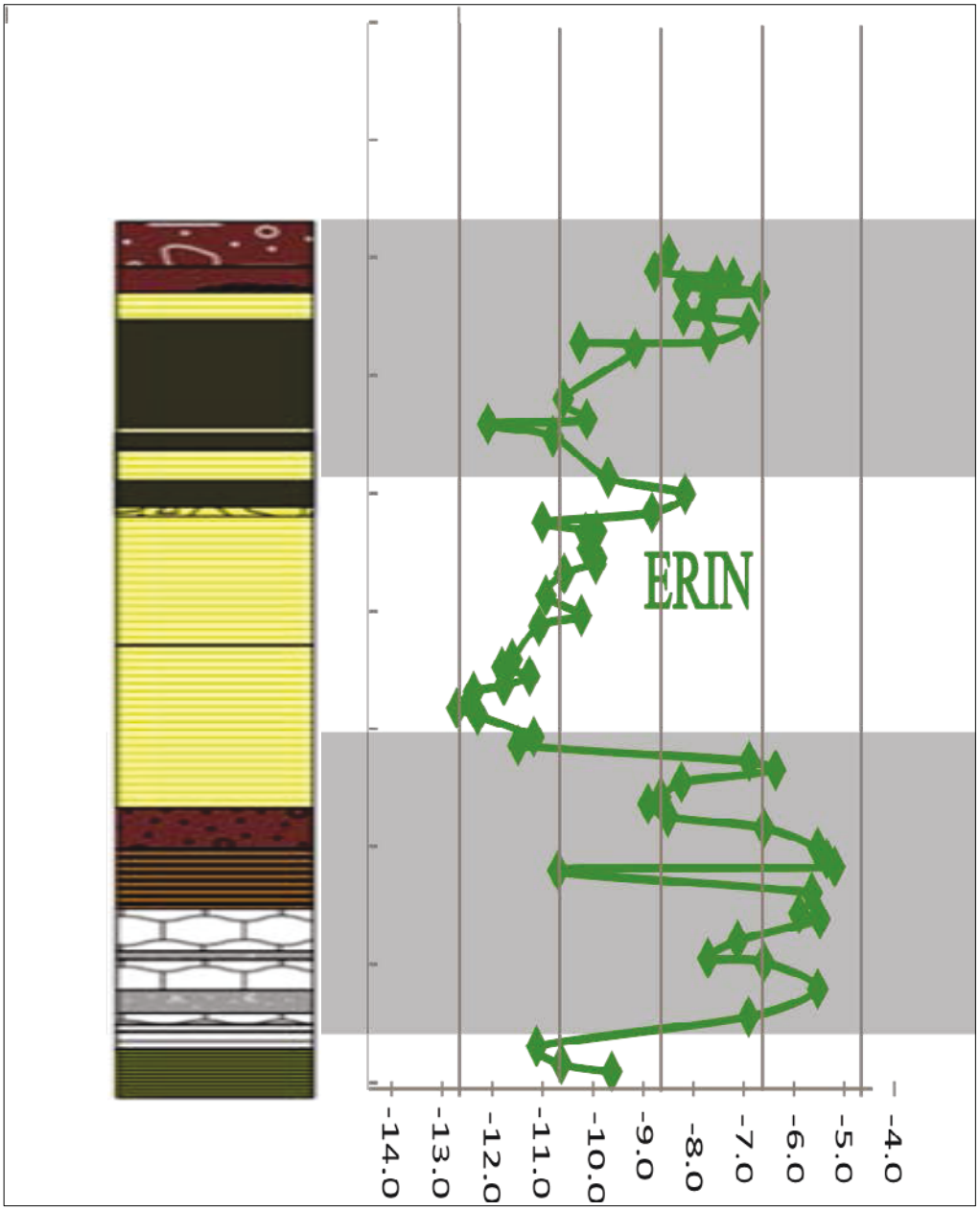

Figure 19. Bulk carbonate $\delta^{13}C$ stratigraphic profile juxtaposed next to the ERIN drillcore intersection, with shaded and unshaded areas respectively characterizing the peaks and troughs in bulk $\delta^{13}C$ as referred to in the text.

5.2.1.2. Comparative regional carbon isotope stratigraphy

Previous and ongoing studies (e.g. Fryer, 2015, submitted; Oonk, 2014, ongoing) have permitted the collection of further drillcore material from sections comparable to ERIN, across a region up to 20km between individual drillcore localities (Fig. 18). These additional drillcores, namely GAS, HEX and ARPAN, collectively capture the entire stratigraphy of the Kuruman and Griquatown BIFs, and thus allow the construction of similar bulk carbon isotope profiles like the one for the ERIN drillcore studied here. Sampling of the HEX, GAS and ARPAN cores was carried out by other researchers and made available to the author at comparatively lower resolution, i.e. approximately one sample every 10-15m, resulting in 28 samples for the GAS and HEX cores respectively, and 25 samples for the ARPAN core. All these additional samples were analysed for their bulk carbonate carbon $\delta^{13}C$ values along with those for the ERIN intersection, at the same laboratory (SUERC, Scotland) and using the same analytical protocol with the ERIN analyses. The only other stratigraphic profile of bulk carbon isotope data that could be added to the present ones from the literature, is the one of Beukes and Klein (1990) from the *ca*. 60m-thick Kuruman-Griquatown BIF transition as captured in the drillcore CORETSI, with a total of 30 samples collected in a fairly high sampling resolution. The beauty of the sampling technique utilized in this study is that the samples in question were collected at random intervals across the different boreholes and thus cannot in effect represent the same laterally extensive 'diagenetic horizon' in a paleao-basin statistically speaking.

Bulk carbonate-carbon isotope profiles for all five intersections as mentioned in the foregoing (i.e. ERIN, GAS, HEX, ARPAN and CORETSI) have been juxtaposed against each other in order to provide a more coherent view of stratigraphic $\delta^{13}C$ variation and its possible reproducibility on a larger geographical scale, and help assess its causes and implications. The profiles are compiled in Figure 20 against the same vertical scale. The BIF stratigraphy has been calibrated largely through the use of log information, and particularly via the recognition of the Kuruman-Griquatown BIF transition in drillcores ERIN, HEX and GAS (demarcated in Figure 20 by the two horizontal solid lines), and by the relatively invariant thickness of the Griquatown BIF from one section to the next, as confined in its upper part by the contact with the overlying Makganyene diamictite in cores HEX, ERIN and ARPAN.

The profiles of Figure 20 reveal a remarkable reproducibility in the carbonate-carbon isotope stratigraphy of the Kuruman and Griquatown BIFs, both in terms of absolute ranges in $\delta^{13}C$ values, but particularly with respect to the distinct isotopic sub-sections as defined in the profile of drillcore ERIN. The lateral correlation between individual profiles appears to be possible even on a finer resolution, as the latter is accomplished between the profiles for drillcore CORETSI (Beukes and Klein, 1990) and the corresponding section in drillcore ERIN (this study). Clearly, the application of carbon isotope stratigraphy as a correlative tool across different lithostratigraphic portions of the Kuruman and Griquatown BIFs seems to be working, calling for explanation as to the exact controls for this otherwise puzzling feature.

Before the significance of the below isotopic signals (fig. 20) are further evaluated and discussed, it is important to test further whether the bulk carbon isotope stratigraphy recorded in the Griquatown and Kuruman BIF may contain an artefact of mineralogical control in carbon isotope distribution, as it is known from previous sections that the carbonate component in many of the examined samples contains multiple species (ankerite, siderite and sometimes calcite as well). This is done in the section that follows.

5.2.1.3. Sequential carbonate-carbon isotope analyses

In order to establish whether bulk $\delta^{13}C$ data faithfully reflect the carbon isotope composition of individual carbonate species, a further test was performed at a different isotope laboratory (Department of Geosciences, University of Cape Town) on 8 samples selected from the ERIN section. These samples represent the entire carbon isotope stratigraphy of the studied ERIN profile in terms of both absolute range in $\delta^{13}C$ values, and of the four isotopically contrasting stratigraphic sub-sections as defined earlier in this chapter. Crucially, they are samples that contain both siderite and ankerite in modal abundances sufficiently high to permit sequential CO_2 extraction at different reaction temperatures with phosphoric acid, and subsequent isotopic measurements corresponding to the ankerite and siderite-fractions only.

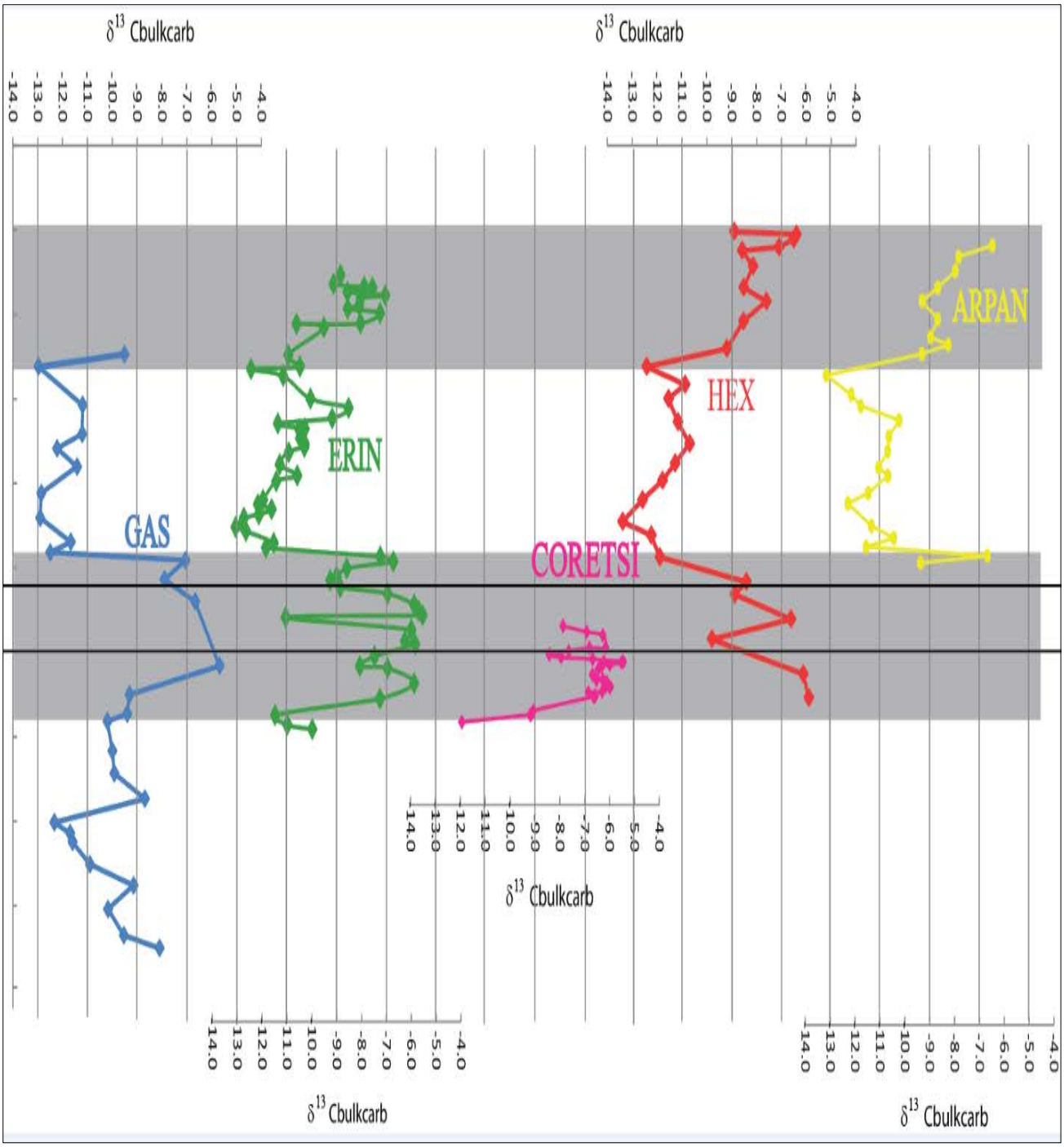

Figure 20. Comparison between the different drillcores from past and ongoing studies kms apart from one another. ERIN (green, present study), GAS (blue), HEX (red), ARPAN (yellow). Note the consistency in systematic variations of $\delta^{13}C$ between the different cores separated by 10s of kms. The two lines are the proposed transition between the microbanded Kuruman to the more clastic and granular textured Griquatown iron formation (isotopic data for drillcores GAS, HEX & ARPAN are available upon request).

The data for the 8 selected samples are shown in Table 8 and graphically illustrated in Figure 21 below. The bulk $\delta^{13}C$ for the selected sample subset covers essentially the entire range of values recorded in the ERIN section, from -5.7 to -12.8‰. For all samples analysed for their species-specific carbon isotope compositions, the corresponding data for ankerite and siderite appear to compare closely with and tightly "bracket" the bulk $\delta^{13}C$ values, as they differ by only about 1 per mil in all but one instances. Therefore, to all intends and purposes, the bulk carbonate-carbon isotope profile constructed for the selected samples mimics very closely the species-specific $\delta^{13}C$ profiles for ankerite and siderite. This is an important conclusion that adds further validity to the bulk carbon isotope stratigraphic re-construction that was carried out in the preceding sections, and removes the need to produce mineral-specific $\delta^{13}C$ data for every single sample.

The relative constant difference in $\delta^{13}C$ values between ankerite and co-existing siderite by approximately 1-1.5‰, could conceivably be interpreted as a consequence of equilibrium-related isotopic exchange between the two species in their environment of formation. However, it has to be noted here that the bulk data represent powdered core-sections of rock of a length up to 5cm, and therefore correspond to mixtures of a large number of individual carbonate grains that are not necessarily in textural equilibrium with one-another. Therefore, the use of these carbon isotope data as a palaeothermometer based on published fractionation equations would probably compromise paleo-temperature estimations and lead to spurious results. The demonstrable similarities in the different datasets, however, still suggests a likely co-genetic origin for the two carbonates, which is also supported by their mineral chemistry and especially their sympathetic variation in contained Mn as demonstrated in the previous chapter.

Table 8. $\delta^{13}C$ values for bulk carbonate, ankerite and coexisting siderite, for 8 selected BIF samples across drillcore ERIN

Sample	Depth (m)	Bulk $\delta^{13}C$	Ank $\delta^{13}C$	Sid $\delta^{13}C$
E61	405,2	-8	-8,55	-8,01
E49	467,6	-10,3	-10,37	-11,09
E46	476,6	-10,3	-9,54	-10,28
E32	523,8	-12,8	-11,68	-12,93
E24	555,3	-9	-7,88	-8,91
E19	571,9	-5,9	-5,55	-6,55
E18	575,4	-5,7	-5,17	-8,17
E1	645,7	-10	-8,51	-9,56

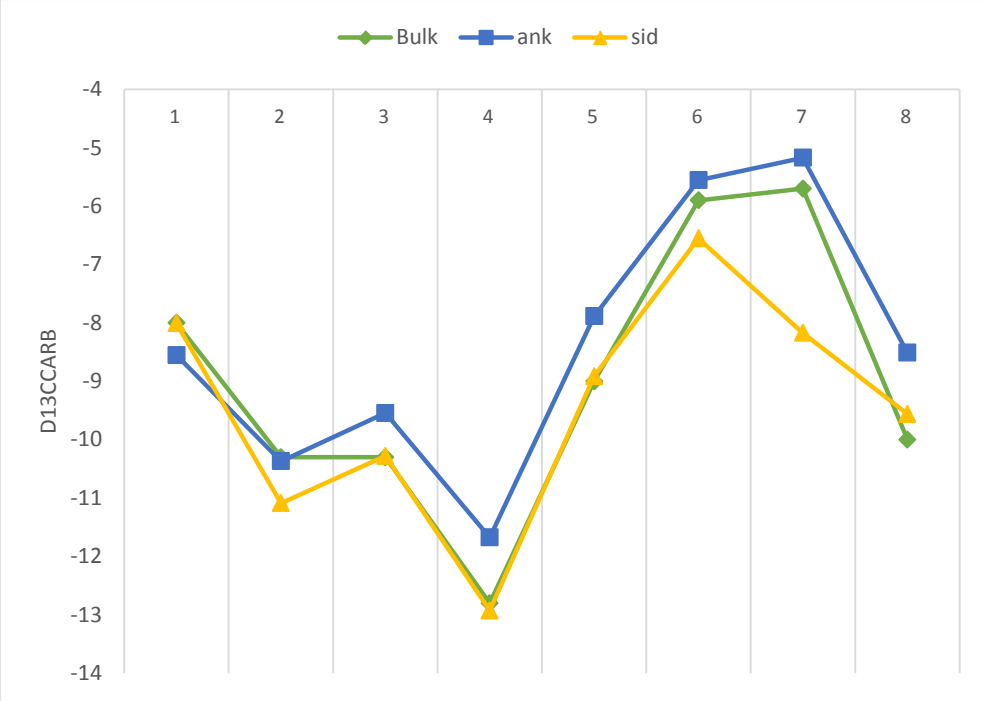

Figure 21. Bulk carbonate (green), ankerite (blue), and siderite (yellow) $\delta^{13}C$ isotopic profiles for 8 selected samples across the ERIN drillcore. Note the very close correspondence of the bulk *versus* species-specific $\delta^{13}C$ profiles, suggesting that the two carbonates are likely cogenetic, and that the bulk carbon isotope records are not affected by variations in modal carbonate mineralogy.

5.3. Summary: diagenesis *versus* primary carbonate deposition

Salient points concerning the carbon isotope results presented in this chapter are summarized below, and some preliminary conclusions are drawn with respect to the likely origin of the carbonate fraction of the examined BIFs.

- Bulk carbonate $\delta^{13}C$ values in the upper Kuruman and Griquatown BIFs are directly comparable to other classic iron formations of South Africa and globally, exhibiting a range of values between -5.5 and -13 ‰, with a mean around -9 ‰;
- The bulk carbonate-carbon isotope profile across the examined ERIN drillcore intersection, displays a smooth pattern of fluctuating $\delta^{13}C$ values across stratigraphy, which can be subdivided into alternating segments of high and low $\delta^{13}C$ (approximately -7.5 and -11 per mil on average respectively);
- Speciation analyses indicate that modal bulk carbonate in the BIF samples analyzed isotopically varies widely, from as low as 3% to as high as 66%;
- Ankerite and siderite $\delta^{13}C$ co-vary with bulk $\delta^{13}C$ as well as between them, with the difference in their absolute values generally being around 1-1.5 per mil;

- Bulk carbon isotope profiles across the entire Kuruman-Griquatown BIF stratigraphy examined, exhibit remarkable reproducibility across 10s of Km, suggesting an unexpected applicability of such records as a chemo-stratigraphic correlation tool.

The significance of the isotopic data in conjunction with the geochemical and petrographic data presented in preceding chapters, will be discussed at more length in the "Discussion" chapter that follows. At this point, it is important to point out that the records produced here do not appear to readily support a diagenetic origin for the BIF carbonates. Diagenetic models for BIF traditionally require that carbonate formation will take place through microbially-mediated redox reactions involving organic matter and primary ferric precursor species, and may also involve high-valence Mn precursors as electron acceptors when these are available in measurable concentrations in the primary sediment (see Heimann et al., 2010, for a comprehensive treatise). The carbon isotope signatures of such processes, and the chemical composition of the ensuing carbonates, will therefore be a function of a multitude of parameters, such as the relative rates of primary Fe, Mn and organic C precipitation; chemical (e.g. Ca/Mg ratio) and isotopic composition of pore-fluid/s involved; a well as the degree to which the diagenetic processes take place in a closed *versus* open system with respect to the overlying water column, at least for re-mineralized organic carbon and $Mn(II)_{aq}$. Considering the obvious complexity of the diagenetic process, the possibility of a largely invariant bulk $\delta^{13}C$ signature of BIF carbonate recorded across stratigraphically thick expanses of BIF, intuitively becomes remote at best and requires careful and holistic re-assessment of all geochemical and sedimentological information available.

Chapter 6: Discussion

6.1. BIF genesis: general

Genetic modelling of Paleoproterozoic BIF formation has traditionally involved a large variety of diverse processes and attendant major evolutionary changes in the early Earth's atmospheric and oceanic composition, from an early anoxic atmosphere dominated by CO_2 and methane, to the natural environment we enjoy today, characterized by sufficient oxygen levels to support highly sophisticated multi-cellular life forms (see Lyons et al., 2014, for a comprehensive review). With this in mind, it is likely that BIF deposition through time may have reflected different formation mechanisms which would have been primarily dependent on the prevailing oxygenation mechanism at the time of their formation. Should the preponderance of BIF deposition during the Neoarchean and Paleoproterozic suggest abundant Fe sequestration through oxidation by photosynthetically produced oxygen, it would rightfully render BIFs as a key and very effective oxygen sink on a global-scale. Therefore, peaks in BIF formation may well have coincided with times when Fe availability was outcompeting oxygen production in the surface ocean. Consequently, only after most of that dissolved ferrous Fe was depleted from the global marine reservoir would oxygen have been able to diffuse readily into the atmosphere, as governed by steep physico-chemical gradients across the ocean-atmosphere interface.

The ca. 2.4Ga old Kuruman and Griquatown BIFs of the Transvaal Supergroup are a typical example of BIFs that would have formed in a pre-GOE, anoxic ocean-atmosphere system. With the postulated lack of free oxygen at the time, it is apposite that an alternative oxidation mechanism must have been responsible for the deposition of initial precipitates of iron required to form these very large deposits. Looking at BIF mineralogy alone presents evidence that some form of Fe(II) oxidation was necessary for primary BIF formation, but the dominant processes responsible are still a matter of contention and debate, although increasing evidence points to photoferrotrophy as a most plausible primary oxidative mechanism (Crowe et al., 2008; Posth et al, 2010a).

Abiotic and biotic mechanisms for the deposition of BIF have been put forth throughout the years. Cloud (1968) was the first to propose a potential role of microorganisms in BIF formation, in an attempt to present a plausible alternative at the time to abiotic models

solely being held accountable for BIF deposition (Brown et al., 1995). Following this earlier work, new or refined existing models are continuously proposed in the literature for the genesis of BIF, approaching the problem through a myriad of possible angles such as the source of Fe and Si, the rhythmic banding of BIFs, geotectonic setting of formation, and biotic *versus* abiotic influence in BIF deposition, amongst others (see also Bekker et al., 2010). Beukes and Klein (1992) observed and pointed out the virtual lack of organic carbon in BIF (< than 0.1 wt% in the great majority of cases), which makes the interpretation of possible contributions of microbial process to genesis difficult on the basis of geochemical and petrographic studies alone. Despite the plethora of proposed models, three fundamental distinctions can be drawn between the various schools of thought; these are briefly discussed in the following section.

6.1.1. Oxygenic Photosynthesis

Cloud (1968) postulated a working model of BIF deposition which proposed that Fe(II) was abiotically oxidized by photosynthetically produced O_2. Subsequently, Klein and Beukes (1989) proposed that biotic oxidation by chemolithotrophic bacteria i.e. aerobic Fe(II)-oxidisers, would have been potential candidates for the precipitation of ferrous Fe in the photic zone. These models envisaged that O_2 could have been confined to local oxygen oases associated with cyanobacterial/chemolithotrophic blooms in coastal settings under an anoxic atmosphere, and thus an indirect biogenic precipitation of ferric hydroxide was deemed to have been possible. Essentially this model proposes that the Paleoproterozoic BIF deposition would have taken place in essentially stratified, relatively shallow-water, shelf-type basins, where photosynthetic O_2 production must have been occurring in the photic zone whilst the atmosphere and deeper part of the water column remained completely anoxic. During periods of maximum Fe precipitation, bottom anoxic waters would have transported ferrous Fe in solution produced by hydrothermal activity to shallower levels via some kind of (seasonal?) upwelling mechanism, which drove mixing and oxidation of the dissolved ferrous Fe and ultimately its delivery as particulate Fe-oxide to the basin floor, probably in the form of ferric oxy-hydroxide precursors.

Early work by Cloud (1973) proposes that due to the embryonic nature of such primitive O_2-producing microorganisms, they lacked advanced oxygen-mediating enzymes and thus required ferrous iron to detoxify oxygen. This meant the flourishing of such microorganisms

in relation to Fe(II) and nutrient supply, which would have episodically been made available. It is clear that such model entail the presence of free molecular oxygen in the Precambrian ocean, thus supporting the presence of oxygenic photosynthesis early in Earth's history (Koehler et al, 2010). The latter poses the obvious question of the timing that photosynthetic oxygen first appeared in the surface milieu of the Early earth and became relevant for Fe(II) oxidation. Questionable evidence for a cyanobacterial origin has been proposed for the 3.45Ga Apex chert of Warrawoona in Australia (Schopf, 1993, Brasier et al., 2002), 2.7Ga Stromatolitic assemblages of Tumbiana Formation in Western Australia (Buick, 1992), and the ~2.5Ga Marra Mamba iron formation and Mount Mcrae shale of the Hamersley Group, Western Australia (Brocks et al, 1999, Summons et al, 1999). Particularly with respect to the latter, the primary origin of indicative biomarkers contained in the said rocks has been brought into question, due to post-depositionary contamination (Rasmussen et al., 2009) and/or presence of such organic material also being detected in anoxygenic phototrophs (Rashby et al., 2007). All current available evidence therefore for the onset and character of oxygenic photosynthesis, remains inconclusive (Koehler et al, 2010).

The occurrence of mass-independent fractionation (MIF) of sulphur isotopes in rocks older than 2.4Ga, and by extension, the loss of it in rocks younger than 2.4Ga, has been used as a strong signal directly attributed to dramatic changes in concentration of atmospheric oxygen heralding the GOE. It is widely established that the loss of MIF represents a shift from anoxic photochemical reactions to an atmosphere with increasing abundances of free oxygen ($>10^{-5}$ PAL) progressively taking over the oxidation of reduced sulphur compounds (Farquhar et al, 2000, Moizsis, 2003, Pavlov and Kasting, 2002). Additionally, geological evidence such as hematite-rich paleosols, red beds, and surficial sedimentary deposits rich in detrital uraninite and pyrite (Rasmussen and Buick 1999), as well as selected non-traditional stable isotopes of redox-sensitive metals such as Cr (Frei et al, 2009), and Mo (Anbar et al, 2007) have provided additional evidence for the timing of the rise of oxygen in the oceans and atmosphere.

6.1.2. UV photo-oxidation

This model bases its hypothesis mainly on the fact that during formation and deposition of BIFs in the Paleoaproterozoic and Neoarchaen, and although the sun was 70-80% as luminous as it is nowadays (the so called "faint young sun paradox" discussed by Sagan &

Mullen, 1972), the early Earth was subjected to high levels of ultraviolet radiation due to the lack of an ozone layer during that time. The formation of ferric oxides may thus have been facilitated without the necessary aid of oxygen involved, through photo-oxidation of ferrous iron by UV radiation forming ferric iron (Cairns Smith, 1978). Under conditions of anoxia, augmented UV radiation, and high dissolved Fe(II) concentrations in the water column, dissolved ferrous iron species such as Fe^{2+} absorb radiation in the 200-400nm range, and then hydrolyse to form ferric hydroxides at circum-neutral pH (Braterman et al., 1983). This theory has however lost favour with a lot of scholars of recent: Konhausser et al. (2007) for example, rule out this mechanism in explaining the formation of Fe oxide minerals in BIF prior to 2.7Ga. Their arguments are based upon experimental observations carried out in a complex solution simulating disequilibrium Precambrian ocean chemistry, in which Fe(II)-rich hydrothermal waters react with Si-saturated seawater containing high HCO_3^- concentrations. Konhauser et al. (2007) demonstrated that the precipitation of amorphous ferrous silicates and carbonates would have occurred faster than photochemical oxidation, and argued that an alternative, anaerobic depositional mechanism must have been in operation instead.

6.1.3. Anoxygenic, phototrophic Fe(II)-oxidation

Oxidative BIF deposition via phototrophic Fe(II)-oxidizing bacteria is a relatively new topic in the BIF literature. The first discovery of these microorganisms occurred a few decades ago, and have recently been widely suggested as a plausible alternative hypothesis to the formation of BIFs in anaerobic conditions present in the Paleaoproterozoic ocean-atmosphere system (Widdel et al., 1993, Heising et al, 1999). The earliest suggestion of anoxygenic photosynthesis as a plausible mechanism for BIF deposition was made by Garrels et al., (1973) followed by Hartman (1984). These authors proposed that light, rather than free oxygen produced by eukaryotes and/or cyanobacteria in the photic zone, may have been responsible for coupling the carbon and iron cycles via photosynthesis that exploited Fe(II) as the preferred electron donor, ultimately producing Fe(III) rather than O_2. The phototrophic model thus comprises light energy fuelling CO_2 fixation coupled to microbial oxidation of ferrous iron by bacteria within the photic zone of the palaeo-environment of deposition (Konhausser et al., 2002). Support for such models is provided by experimental studies (e.g. Kappler et al., 2005) which demonstrate that the bacteria

responsible would have been adept to oxidising appreciable amounts of ferrous Fe to account for the large expansion of these deposits as seen in Superior type formations. Furthermore, Kappler et al. (2005) showed through growth experiments that such phototrophs can effectively oxidize Fe(II) up to a few 100m's of water depth.

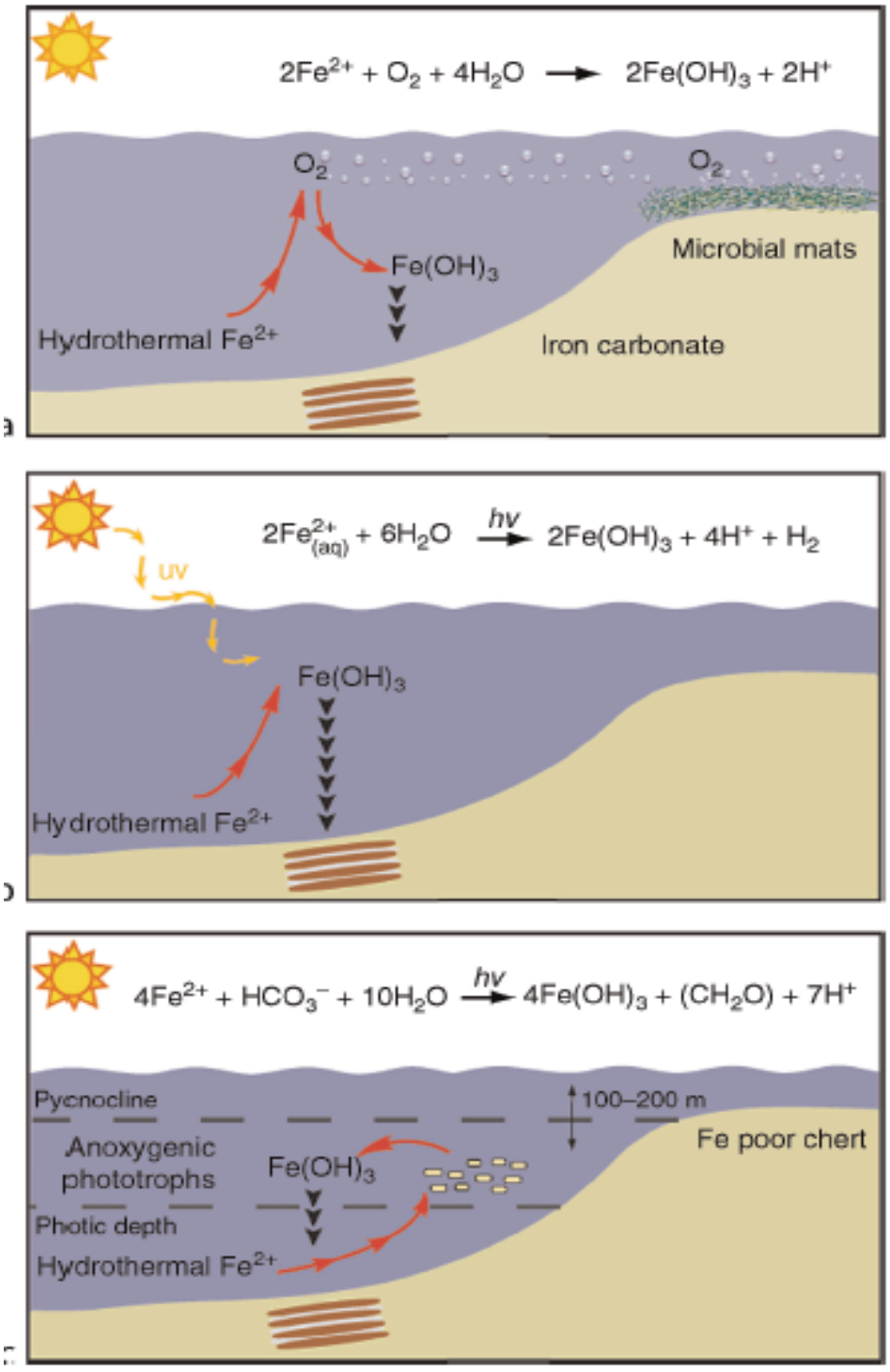

Figure 22. Models of banded iron formation deposition. A) Traditional model of BIF deposition involving production of oxygen by cyanobacteria, which is released into the water column to

chemically react with hydrothermally-derived dissolved Fe(II) (a). The two proposed mechanisms of deposition in an anoxic ocean water column are the abiotic Fe(II) photooxidation by UV light, which has recently been discounted (Konhauser et al., 2007) (b), and direct microbial Fe(II) oxidation via anoxygenic Fe(II)-oxidizing phototrophy (c) (Adapted from Posth et al., 2010a).

6.2. Genesis of the Transvaal BIF: diagenesis *versus* water-column processes

6.2.1. Anaerobic diagenesis: Organic carbon oxidation – ferric iron reduction (DIR)

A great number of studies have concentrated on the importance of microbially-driven organic carbon cycling during diagenesis of modern pelagic sediments characterised by anoxia (e.g. Froelich et al., 1979). Oxidation of organic matter in such environments is induced by the consumption of a series of suitable electron acceptors. The propagation of this process is governed by a series of reactions where organic matter is oxidized first by a coupled reduction with the oxidant yielding the greatest energy change per mole of organic carbon oxidised. The sequence of electron acceptors in order of the thermodynamically most efficient oxidant to the least, are: nitrate (HNO_3^-), manganese oxide/s (MnOOH, MnO_2), iron oxide/s ($Fe(OH)_3$, Fe_2O_3) and finally sulphate (SO_4^{2-}).

Bacterially-mediated reactions utilising a ferric phase as the most suitable electron acceptor for organic carbon re-mineralisation, are driven by chemoautolithotrophic bacteria through a process designated as 'Dissimilatory Iron Reduction' (DIR) (Lovley and Phillips, 1987). DIR is variously envisaged to have been the dominant process in the formation of Fe carbonates in BIFs (see Johnson et al., 2008, and references therein). The added prerequisite for DIR to have been the prevailing process of organic carbon cycling in BIF diagenetic environments, is the absence of other potential oxidants of higher thermodynamic preference for chemo-autotrophic bacteria to cycle organic carbon, such as nitrate or manganese oxy-hydroxides. Indeed, this is supported by the mineralogy and geochemistry of BIFs, which are renowned for their virtual lack of contained Mn (see, however, parts of the Griquatown BIF from this study) and no direct evidence whatsoever for the existence of nitrate in the primary environment of deposition.

Diagenetic iron carbonate formation (e.g. as siderite) would then be the consequential reflection of active DIR in the diagenetic environment, and its isotopic composition ought to also record at least partial evidence for organic carbon oxidation and incorporation into the carbonate structure, as isotopically light carbon. According to the simplified reactions (I) and (II) below, diagenetic siderite containing a mixture of DIR-cycled, oxidised organic matter of

an average $\delta^{13}C$ composition of *ca*. -28 ‰; along with some inorganic pore-fluid bicarbonate of a gross $\delta^{13}C$ value very close to 0‰, would be expected to carry an isotopically light signature as typically seen in BIF:

$$CH_2O + 8H^+ + 4Fe(OH)_3 \rightarrow 4Fe^{2+} + CO_2 + 11H_2O \quad (I)$$

$$Fe^{2+} + CO_2 + H_2O \rightarrow FeCO_3 + 2H^+ \quad (II)$$

It is readily evident that the above reactions require the supply of both organic matter and ferric precursors to the sediment from the overlying water column, irrespective of the exact oxidative mechanism for the Fe. Equation (I) above also indicates that for every 1 mole of organic carbon, four moles of ferric iron hydroxide will be reduced; therefore, the mineralogy of BIF and its final ferrous to ferric ratio will be a function – to a great degree – of the relative supply of the two reactants to the initial sediment through time. It is important to note here though, that BIFs are notoriously devoid of organic matter (e.g. see Beukes and Klein, 1990 for the Kuruman and Griquatown BIFs), suggesting that the extent of DIR would have been limited by the availability of organic matter in the original sediment and not by that of primary ferric species, unless much of the original organic carbon cycled during DIR was "leaked out" of the initial sediment into the supernatant marine waters, in an open-system process.

6.2.2. Organic carbon oxidation – dissimilatory manganese reduction (DMR)

Although BIFs are variously known to be very Mn-lean, the results presented earlier in this thesis with respect to the Griquatown BIF suggest that manganese must have occupied at least a transient redox role in the palaeoenvironment of deposition and diagenesis of the Griquatown and upper Kuruman BIF strata. The fact that the Mn contained in the Griquatown (and Kuruman) BIFs is almost solely carbonate-hosted, brings Mn into the fore as a potential electron acceptor for organic matter re-mineralisation in its own right, on the proviso that the Griquatown BIF carbonates are predominantly diagenetic in origin.

In a similar fashion to DIR, Lovley and Phillips (1987) and Lovley (1991) suggested that organic carbon oxidation coupled with dissimilatory manganese reduction (DMR) i.e. reduction of higher Mn-oxide, is bound to produce a Mn-rich carbonate species. This process involves, like with Fe, a complete reduction of high valence Mn oxide or oxy-

hydroxide (such as MnO_2), leading to the formation of a mixed Mn-Ca carbonate phase (commonly kutnahorite) in equilibrium with a diagenetic fluid. The presence of Mn in the Griquatown BIF suggests that a similar process like the one described above, would have been operative for the formation of the Mn-bearing carbonates observed, and that increased oxidation of manganese – relative to iron – from the divalent to the trivalent and/or tetravalent states may have been transiently possible. From an isotopic point of view, the intermediate $\delta^{13}C$ values for the Mn-bearing ankerite and siderite in the Griquatown strata would be explained in exactly the same fashion as interpreted in the foregoing section, i.e. it would reflect mixtures of isotopically light, recycled organic matter and relatively "heavy" pore-fluid bicarbonate. The only difference here would be that the initial Mn (hydro-)oxides would be involved as electron acceptors in diagenetic organic carbon cycling, and in fact would be expected to be the preferred ones on thermodynamic grounds, by comparison to co-existing primary ferric oxy-hydroxides (Tsikos et al., 2010). The chemical reactions involved for Mn-reduction alone, would simplistically be as follows:

$$CH_2O + 4H^+ + 2MnO_2 \rightarrow 2Mn^{2+} + CO_{2\,(org)} + 3H_2O \qquad \text{(III)}$$

$$Mn^{2+} + CO_{2(org)} + H_2O \rightarrow MnCO_3 + 2H^+ \qquad \text{(IV)}$$

The resultant mixed carbonate phase would require the combination of reactions (III) and (IV) with the equations (I) and (II) as shown for Fe earlier.

6.2.3. Accommodating the new isotopic and mineral chemical data.

If the Griquatown BIF carbonates examined in this thesis petrographically, chemically and isotopically, are entirely diagenetic in origin, then the preceding sections could be perceived to adequately explain their mode of origin, mineral-chemical variations and carbon isotope signatures. However, the presence of elevated manganese in the Griquatown BIF and specifically in its carbonate fraction is an atypical feature of BIF in the context of broadly coeval, similar occurrences worldwide, and requires a plausible explanation. Tsikos et al. (2010) proposed that the general dearth of manganese in BIF may be due to effective recycling of transient Mn oxides/hydroxides by ferrous iron within the upper parts of the primary water column, or to no oxidation of Mn at all and its resultant progressive

enrichment in solution relative to iron. Either process would have led to the development of a distinct spike of high Mn/Fe(aq) in the water column.

If the diagenetic model is indeed correct, then it could be argued that primary oxidation of at least some Mn(II), must have been at least transiently possible. The first question that emerges from that is: "what was the primary oxidative mechanism for Mn, and why was it temporarily more efficient, resulting in distinct Mn spikes in the Griquatown BIF stratigraphy at least twice (see geochemistry section)" That is, was Mn oxidized due to episodic increases in the oxidation potential of the primary water column, in the form of biologically-produced oxygen whiffs? Or, was such oxidation the result of an anaerobic biological mechanism that largely utilised Fe(II) (photoferrotrophy) but may have switched to Mn(II) in response to some sort of episodic environmental change (e.g. a rise in seawater temperature or alkalinity)? Constraining which of the above two mechanisms was more likely to have occurred is not possible through the results of this study alone; the end result, however, is that increased Mn relative to Fe must have become episodically available in the precursor BIF sediment. Subsequently, that Mn would have become implicated in organic carbon cycling as an electron acceptor, and ultimately sequestered (perhaps quantitatively) in the rock as diagenetic, Mn-bearing ankerite and/or siderite, with the required contributions in $Mg_{(aq)}$ and $Ca_{(aq)}$ derived from the pore-fluid/s involved.

Here is where the carbon isotope data for the Griquatown BIF carbonates can shed some additional light to the foregoing arguments. It was shown in chapter 5, that the carbon isotope composition of bulk carbonate and its stratigraphic variation, are remarkably reproducible laterally from one section to the next, and record smooth vertical variation in the form of distinct highs and lows in $\delta^{13}C$. This is despite the fact that the modal variation in the carbonate fraction of the samples is large, and ranges from a few percent up to two-thirds of the total mass of individual samples (see also chapter 5 for more details). In a given isotopic plateau such as the low $\delta^{13}C$ one corresponding to the ca. 125m-thick section of the Griquatown BIF in drillcore ERIN (see section 5.2.1.3. for details) fluctuations in modal carbonate are indeed significant across individual samples (consider for example samples E44 and E50 in appendices I, table A.2.4 where the total bulk carbonate for one sample is 1.39 wt% as compared to the bulk carbonate of the other sample which is 22.81wt%) but

the carbonate carbon isotope data over the same section are by comparison relative invariant. This is to say that, irrespective of how much carbonate has formed in a given sub-section of rock, the relative ratio of organic and inorganic carbon across the entire stratigraphic section considered remains effectively invariant. This then raises the next obvious question of what process exactly controls that relative isotopic constancy.

The diagenetic model for the origin of BIF carbonates predicts a dual, mixed source for the contained carbon, i.e. a mixture of inorganic (pore fluid-sourced) and recycled organic matter. Simple mixing of those two end-members would result in the intermediate $\delta^{13}C$ values observed in BIF carbonates. However, for those values to remain effectively constant across different samples regardless of modal carbonate abundance, requires that the relative ratio between organic-derived *versus* inorganic carbon must remain essentially constant, provided that their respective end-member carbon isotope signatures did not vary considerably through time (as a matter of fact, if the latter had varied, it would make the relative constancy in the carbon isotope data even harder to explain). To this curious circumstance, one must add the requirement that diagenetic carbonate formation in BIF is an inherently complex process that also involves the interplay of a number of other variables and chemical sources through time. These include, but are not limited to, periodic changes in the rate of primary organic supply to the initial sediment; fluctuating rates of Fe and Mn oxy-hydroxide precipitation in response to processes that operated in the upper water-column; the probability that diagenetic carbon cycling is accompanied by at least partial open-system loss of respired CO_2 from the sediment pile into supernatant marine waters; variations in pore-fluid chemistry through time, particularly with respect to aqueous species of Mg and Ca; and/or changes in various physico-chemical parameters such as temperature, alkalinity or pH, in response to variations in the palaeoenvironment of deposition. If anything, the isotopic composition of diagenetic carbonates would be expected to be highly variable on a variety of scales, in response to one or more of the aforementioned factors.

6.3. A chemically homogenous source for carbonate deposition?

The foregoing discussion leads to the obvious need to introduce an alternative mechanism that can more plausibly explain the isotopic and chemical characteristics of the carbonate

fraction in the examined Griquatown and upper Kuruman BIF samples. The isotopic data as presented in chapter 5, in combination with the speciation and mineral chemical data for ankerite and siderite of chapter 4, can be more readily accounted for by precipitation of precursor iron carbonate particles directly from a chemically and isotopically homogeneous aqueous reservoir, and subsequent re-crystallisation of such particles during diagenesis, with limited accompanying chemical and isotopic change. In simple words, a model of primary carbonate precipitation directly out of the original water-column, is proposed instead for the BIF carbonates.

In order for a primary precipitation model to account for the chemical and isotopic characteristics of the observed carbonates, an active long-term process of redox cycling of organic carbon and high valence species of Fe and Mn, must have been operative within the water column itself (Fig, 23). In other words, it is proposed that DIR, and possibly DMR as well, be transferred into the water column as efficient carbon and metal cycling mechanisms. The result of such processes would be the development of strong gradients in the relative abundances of Mn(II) and Fe(II) with depth, and in the isotopic signature of marine bicarbonate. Against such a strongly stratified water column, primary carbonate particles with contrasting isotopic and mineral-chemical signatures with respect to Mn/Fe ratio may have formed at variable water depths, and their precipitation would have faithfully transferred the chemical and isotopic signal of the corresponding parcel of water column in which they initially formed, to the sediment pile below.

Should the primary model for BIF carbonate precipitation hold true, it will hold important implications with regard to the origin of BIF in general. Active biological redox cycling of carbon and Fe and/or Mn within the water column via requires the constant supply of organic matter and high valence Fe (and possibly also Mn) from the photic zone, lending support to biological models for BIF genesis. The whole process would have been akin to an ancient equivalent of a biological pump, albeit with Fe oxy-hydroxide being the key electron acceptor. The primary precipitation of iron-rich carbonate would also result in the eventual net transfer of much of the organic-derived carbon into BIF, albeit in the form of isotopically light carbonate species. The deposition of BIF may therefore be thought as being one of the earliest significant events of (indirect) “organic” carbon burial in Earth history, on an ocean-

wide scale. Finally, BIF carbonates may indeed constitute faithful records of water column processes with respect to the long-term redox behaviour of Mn during BIF genesis, particularly with regard to the postulated progressive enrichment of Mn in solution and its eventual precipitation in voluminous amounts around the GOE (Hotazel Formation).

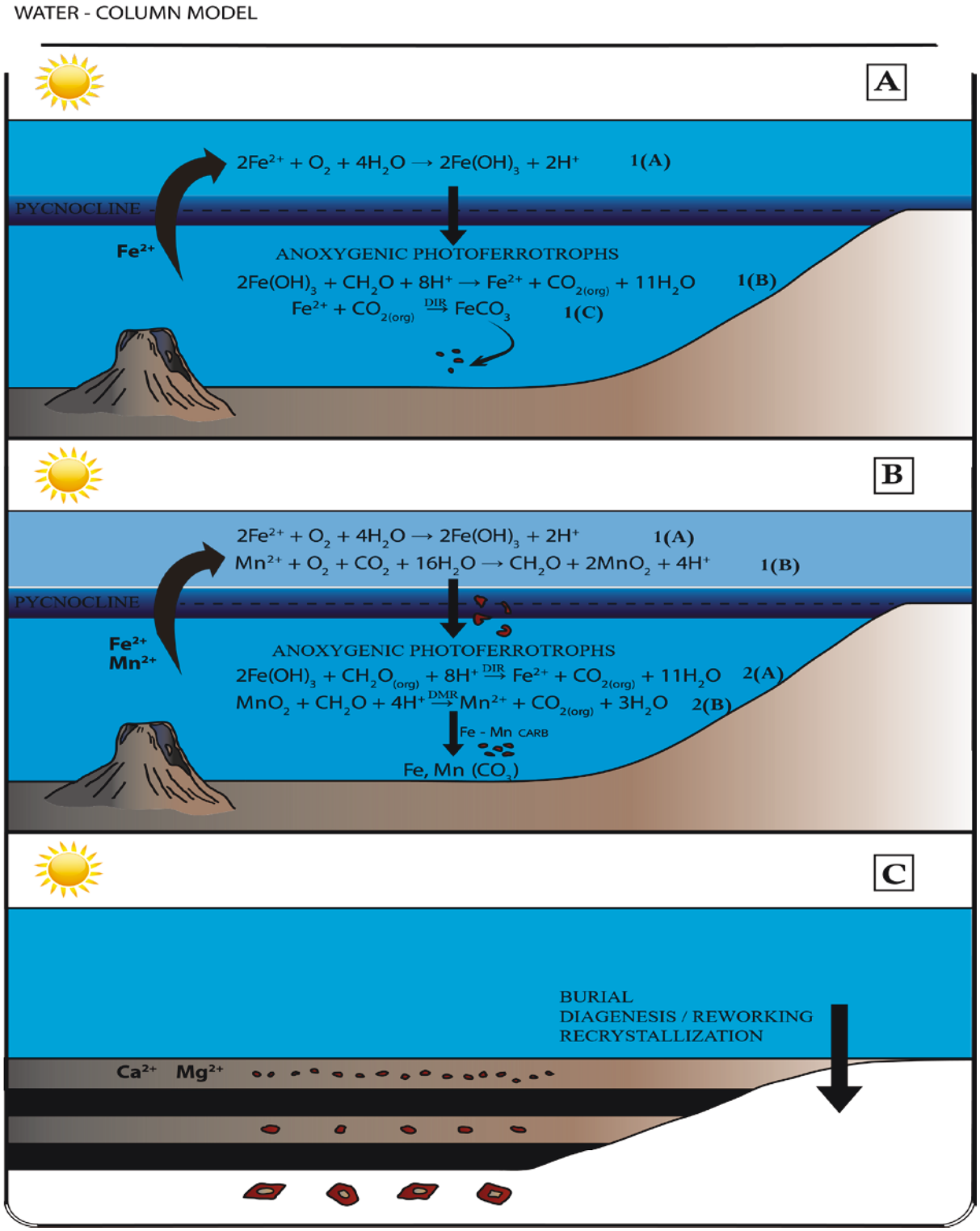

Figure 23. Water column model. Fe-hydroxide formation in the photic zone and transfer of the formed precursor sediment below the pynocline. DIR through organic carbon oxidation and ferrous

iron reduction forming particulates of Fe carbonates which settle into the sediment below. B) Progressive manganese increase in the water column and uptake of the latter in the crystal lattice of initial Fe carbonates forming Mn-rich carbonates as seen by the gradual increase in manganese seen in the Asbeshuewels iron formation. C) Burial-diagenesis-reworking and recrystallization of the sediment forming the observed mineral assemblages and diagenetic textures.

Chapter 7: Concluding remarks

7.1. Implications of the present work

The conclusion reached in the foregoing sections with respect to the origin of carbonates in the Griquatown and uppermost Kuruman BIFs sampled in this study, is that their isotopic and mineral-chemical characteristics appear to be at odds with widely-proposed diagenetic models of carbonate formation within the precursor BIF sediment that involved redox cycling of organic carbon by higher oxides of Fe and possibly Mn too. Although petrographic textures of coexisting iron carbonates (siderite and/or ankerite) as subhedral, neomorphic grains overgrowing seemingly earlier textures, indeed point to diagenetic crystallisation during diagenesis, this is by no means taken to imply here that the chemical and isotopic signals of these carbonates are also exclusively derived via diagenetic growth. It is the contention of the author that the Fe carbonates examined in this thesis, and possibly those in other BIFs of the world, inherited their chemical and isotopic signals in large part during primary precipitation out of a well-stratified water column, which was characterised by strong depth gradients in the isotopic composition of dissolved bicarbonate and in the dissolved $Mn/Fe_{(aq)}$ ratio. Such gradients would have developed through long-term redox cycling within the water-column via processes such as DIR and/or DMR, and carbonate particles forming in the water column would faithfully transfer and record the corresponding chemical and isotopic signatures of their depth of formation into the underlying sediment.

The increase of Mn in percentage levels with stratigraphic height in the carbonate fraction of the Griquatown BIFs, suggests that manganese may well have played its own important role in the cycling of organic carbon within the water column, provided that it was transiently oxidised by biological and/or abiotic mechanisms. Alternatively, its progressive enrichment relative to Fe with time may have ensued passively, i.e. without the major involvement of transient oxidised precursor species in water-column processes, and its eventual episodic sequestration in the form of Mn-rich Fe carbonate may simply reflect the

development of a strong $Mn_{(aq)}$ gradient in the water column with time. It is therefore plausible that Mn did become progressively enriched in the Palaeoproterozoic Ocean largely through simple Rayleigh distillation processes during BIF formation, and it appears that the carbonate fraction of BIF would have faithfully tracked that specific chemical evolution.

Possibly the farthest-reaching and arguably ambitious implication of the above findings in the context of the evolution of the early oceans and atmosphere across the GOE, is the possibility that the organic-derived carbon that ultimately became incorporated into isotopically light ferrous carbonates (i.e. siderite and ankerite) during BIF genesis, would have conceivably resulted in a progressive unidirectional positive shift in the carbon isotope composition of dissolved bicarbonate of the Palaeoproterozoic ocean with time. One could therefore cautiously argue that the large Lomagundi positive carbon isotope excursion expressed in several carbonate deposits of the world at around 2.2 Ga (Lyons et al., 2014), may be a direct record of that isotopic shift. In other words, the large volumes of Palaeoproterozoic BIFs may constitute the missing isotopically light carbon reservoir that the Lomagundi carbonate positive excursion requires in the context of global carbon mass balance in the Paleoproterozoic.

7.2. Proposed future Research

The author sees essentially one main way in which the findings of this study can be further assessed critically, and this is through experimental studies under controlled conditions in the laboratory that replicate the pre-GOE Palaeoproterozic Ocean on two specific fronts. Specifically, it is proposed that one set of experimental tests be undertaken that involves primary carbonate precipitation in simulated anoxic conditions, out of a water column that is enriched in dissolved iron as well as manganese. The primary purpose of such tests would be to elucidate the controls of the relative partitioning of Mn *versus* Fe in carbonates precipitating out of an anoxic water column, and whether or not the signatures read in the carbonate record of the Griquatown BIF can be replicated in the laboratory. The other set of experiments would involve the reaction of Fe and Mn oxyhydroxides <u>together</u> in the presence of isotopically labelled organic material, under simulated diagenetic conditions in the absence of free oxygen. Again, the key objective of such experiments would be to examine the partitioning of Mn *versus* iron in the ensuing products of the reaction, as well

as the carbon isotopic signature with respect to carbonate phases forming as a direct product of the process.

8. Reference List

Altermann, W., (1997) - Sedimentological evaluation of Pb–Zn exploration potential of the Precambrian Griquatown fault zone in the Northern Cape Province, South Africa. Mineral. Deposita 32, 382–391.

Altermann,W., Nelson, D.R., (1998) - Sedimentation rates, basin analysis and regional correlations of three Neoarchaean and Paleoproterozoic sub-basins of the Kaapvaal craton as inferred from precise U–Pb zircon ages from volcaniclastic sediments. Sediment. Geol. 120, 225–256.

Anbar AD, Duan Y, Lyons TW, Arnold GL, Kendall B, Creaser RA, Kaufman AJ (2007) - A whiff of oxygen before the great oxidation event? Science 317:1903–1906.

Bau M, Hohndorf A, Dulski P, Beukes NJ (1997) - Sources of rare-earth elements and iron in Paleoproterozoic iron-formations from the Transvaal Supergroup, South Africa: evidence from neodymium isotopes. J Geol 105:121–129.

Bau, M., Romer, R.L.,Luders, V., Beukes N.J., (1999) - Pb, O, and C isotopes in silicified Mooidraai dolomite (Transvaal Supergroup, South Africa): implications for the composition of Paleoproterozoic seawater and `dating' the increase of oxygen in the Precambrian atmosphere. EPSL., v.174. pp 43-57.

Baur, M.E., Hayes, J.M., Studley, S.A., Walter, M.R., (1985) - Millimeter-scale variations of stable isotope abundances in carbonates from banded iron-formations in the Hamersley Group ofWestern Australia. Econ. Geol. 80, 270‑282.

Becker, R.H. & Clayton, R.N., (1976) – Oxygen isotope study of a Precambrian iron-formation, Hamersley Range, Western Australia. Geochem. Cosmochim. Acta, 40:1153-1165.

Becker, R.H. and Clayton, R.N., (1972) - Carbon isotopic evidence for the origin of banded iron formation in Western Australia. Geochim. Cosmochim. Acta, 36: 577-595.

Becker, R.H., Clayton, R.N., (1972) - Carbon isotopic evidence for the origin of a banded iron-formation in Western Australia. Geochim. Cosmochim. Acta 36, 577‑595.

Beukes N.J. (1973) – Precambrian iron-formations of Southern Africa. Econ. Geol., 68:960-1005.

Beukes N.J. (1980a) – Lithofacies and stratigraphy of the Kuruman and Griquatown Iron Formations, Northern Cape Province, South Africa. Trans. Geol. Soc. S. Afr., 83:69-86.

Beukes N.J. (1983) – Palaeoenvironmental setting of iron-formations in the depositional basin of the Transvaal Supergroup, South Africa, in: Iron-Formations: facts and problems, eds., Trendall, A.F., and Morris, R.C. : developments in Precambrian Geology 6, Elsevier Sci. Pbl., p. 131-209.

Beukes N.J., (1980b) – Suggestions towards a classification of and nomenclature of iron formation. Trans. Geol. Soc. S. Afr., 83:285-290.

Beukes, N.J., and Gutzmer, J., (2008) - Origin and paleoenvironmental significance of major iron formations at the Archean-Paleoproterozoic boundary: in Hagemann S., et al., eds., Banded iron formation-related high-grade iron ore: Society of Economic Geologists Reviews in Economic Geology 15, p. 5–47.

Beukes, N.J., and Klein, C., (1990) – Geochemistry and sedimentology of a facies transition-from microbanded to granular iron-formation-in the Early Proterozoic Transvaal Supergroup, South Africa: Prec. Res., v. 47, p. 99-139.

Beukes. N.J., (1984) – Sedimentology of the Kuruman and Griquatown iron-formations, Transvaal Supergroup, Griqualand West, South Africa: Prec. Res., v.24, p. 47-84.

Brasier MD, Green OR, Jephcoat AP, Kleppe AK, Van Kranendonk MJ, Lindsay JF, Steele A, Grassineau NV (2002) - Questioning the evidence for Earth's oldest fossils. Nature 416:76–81.

Braterman PS, Cairns-Smith AG, Sloper RW (1983) - Photo-oxidation of hydrated Fe2+ – significance for banded iron formations. Nature 303:163–164.

Braterman, P. S., Cairns-Smith, A. G., and Sloper, R. W., (1983) - Photo-oxidation of hydrated Fe2 + – significance for banded iron formations. Nature, 303, 163–164.

Brocks JJ, Logan GA, Buick R, Summons RE (1999) - Archean molecular fossils and the early rise of eukaryotes. Science 285:1033–1036.

Brown, A. D., Gross, G. A., and Sawicki, J. A., (1995) - A review of the microbial geochemistry of banded iron formations. The Canadian Mineralogist, 33, 1321–1333.

Buick R (1992) - The antiquity of oxygenic photosynthesis: evidence for stromatolites in sulphate deficient Archaean lakes. Science 255:74–77

Burchell, W.J., (1822) – Travels in South Africa. Vol. I. 359pp.

Button, A., (1976a) - Transvaal and Hamersley basins – review of basin development and mineral deposits. Miner. Sci. Eng., 8: 262-293.

Button, A., (1976b) – Iron Formation as an end-member in carbonate sedimentary cycles in the Transvaal Supergroup, South Africa. Econ. Geol., 71: 193-201.

Cairns-Smith AG (1978) - Precambrian solution photochemistry, inverse segregation, and banded iron formations. Nature 276:807–808.

Carrigan W, .J., and Cameron E, .M., (1991) – Petrological & stable isotope studies of carbonate and sulphide minerals from the Gunflint Iron-formation, Ontario: Evidence for origin of Early Proterozoic Iron-Formation. Precambrian Research, 52, p. 347-380.

Cheney, E.S., (1995) - Sequence stratigraphy and plate tectonic significance of the Transvaal succession of southern Africa and its equivalent in Western Australia. Elsevier, v. 79., pp. 3-24.

Cilliers, J.J. le R., & Genis, J.H., (1964) – Crocidolite asbestos in the Cape Province. In: S.H. Haughton The Geology of some Ore Deposits of Southern Africa, Vol. II. Geol. Soc. S.Afr., Johannesburg, pp. 544-570.

Cloud, P., (1973) – Palaeoecological significance of the banded iron formation: Econ. Geol., v. 68, pp. 1135-1143.

Cornell, D.H., Schutte, S.S., & Englington (1996) – The Ongeluk basaltic andesite formation in Griqualand West, South Africa: Submarine alteration in a 2222 Ma Proterozoic sea: Precambrian Research, v. 79, p. 101-124.

Craddock, P., & Dauphas N., (2011) - Fe and C Isotope evidence for microbial Fe respiration throughout the Archean. EPSL., v. 303, pp. 121-132

Crowe, S.A., Jones, C.A., Katsev, S., Magen, C., O'Neill, A.H., Sturm, A., Canfield, D.E., Haffner, G.D., Mucci, A., Sundby, B., Fowle, D.A., (2008) - Photoferrotrophs thrive in an Archaean Ocean analogue, Proceedings from the National Academy of Sciences, v.. 105, pp. 15938-15943.

Cullen, D.J., (1963) – Tectonic implications of banded ironstone formations. J. Sediment. Petrol., 33: 387-392.

Dasgupta, D.R. (1965) – The transformation of ankerite during thermal treatment. Geological Survey of India, 29 Chowringhee, Calcutta 16, pp 1-6.

De Villiers, J., (1960) – The manganese deposits of the Union of South Africa: S. Afr. Geol. Surv., Handbook 2, 280p.

Dimroth, E. & Kimberley, M.M., (1976) – Precambrian atmospheric oxygen: evidence in the sedimentary distributions of carbon, sulphur, uranium, and iron: Can. Jour. Of Earth Sci., v. 13. No.9, pp. 1161-1185.

Dimroth, E. and Chauvel, J.J., (1973) – Petrography of the Sokoman Iron Formation in part of the central Labrador Trough, Quebec, Canada.Geol. Soc. Am. Bull., 84:111-134.

Du Toit A.L., (1945) – The origin of the amphibole asbestos deposits of South Africa. Geol. Soc. S. Afr., 48: 161-206.

Dymek, R.F., & Klein, C., (1988) – Chemistry, petrology and origin of banded iron-formation lithologies from the 3800 ma Isua Supracrustal Belt, West Greenland: Prec. Res., v.39, pp. 247-302.

Engelbrecht, L.N.J., (1962) – Markers in the Lower Griquatown Stage near Kuruman. Ann. Geol. Surv. S. Afr., 1: 71-75.

Ewers, W.E., & Morris, R.C., (1981) – Studies of the Dales Gorge Member of the Brockman iron-formation, Western Australia: Econ. Geol., v.76, pp 1929-1953.

Fairey ., (2010) – Petrography and geochemistry of the Hotazel-Mooidraai BIF-carbonate transition, Kalahari Manganese Field, Northern Cape Province. M.Sc. Thesis. Rhodes University, Grahamstown, South Africa,

Farquhar J, Bao H, Thiemens M (2000) - Atmospheric influence of Earth's earliest sulfur cycle. Science 289:756–758.

Fischer, W.W., Schroeder, S., Lacassie, J.P., Beukes, N.J., Goldberg, T., Strauss, H., Horstmann, U.E., Schrag, D.P., and Knoll, A.H., (2009) - Isotopic constraints on the Late Archean carbon cycle from the Transvaal Supergroup along the western margin of the Kaapvaal craton, South Africa: Precambrian Research, v. 169, pp 15-27.

Floran, R.J. & Papike, J.J.(1978) – Mineralogy and petrology of the Gunflint Iron Formation, Minnesota-Ontario: Correlation of compositional and assemblage variations at low to moderate grade. J. Petrol., 19:215-288.

Fockema, P.D., (1967) – Crocidolite and Associated Rocks of the Kuruman Area in the Northern Cape. Ph.D., Thesis, Univ. Witwatersrand, Johannesburg, 189pp. (unpubl.).

Frei R, Gaucher C, Poulton SW, Canfield DE (2009) - Fluctuations in Precambrian atmospheric oxygenation recorded by chromium isotopes. Nature 461:250–253.

French, B.M., (1968) – Progressive contact metamorphism of the Biwabik Iron Formation, Mesabi Range, Minnesota. Minn., Geol. Surv. Bull., 45, 103pp.

French, B.M., (1973) – Mineral assemblages in diagenetic and low-grade metamorphic iron formations. Econ. Geol., 68: 1063-1075.

Froelich, G.P., et al., (1979) - Early oxidation of organic matter in pelagic sediments of the eastern equatorial Atlantic: suboxic diagenesis. Geochimica et Cosmochimica Acta 43, 1075–1090.

Fryer, B.J. (1983) – Rare-earth elements in iron formations, in: Iron-Formations: in Precambrian Geology 6, Els. Sci, Pbl., 558p.

Fryer, B.J., (1977a) – Trace element geochemistry of the Sokoman iron-formation: Can. J. Earth Sci., v. 14, pp. 1598-1610.

Fryer, B.J., (1977b) – Rare earth evidence in iron-formations for changing Precambrian oxidation states: Geoch.et Cosm.Acta, v.41, pp. 361-367.

Fryer, B.J., 1977. Trace element geochemistry of the Sokorean Iron Formation. Can. J. Earth Sci., 14: 1598-1610.

Fryer, L., (2015) – Controls on the distribution of manganese in banded iron-formations of the Palaeoproterozoic Transvaal Supergroup, Northern Cape Province. M.Sc. Thesis Unpublished. Rhodes University, Grahamstown, South Africa, 115pp.

Garrels, R. M., Perry, E. A., and MacKenzie, F. T., (1973) - Genesis of Precambrian iron-formations and the development of atmospheric oxygen. Economic Geology, 68, 1173–1179.

Gole, M.J. (1980a) – Mineralogy and petrology of the very low metamorphic grade Archean banded iron formations, Weld Range, Western Australia. Am. Mineral., 65: 8-25.

Gole, M.J. (1981) – Archean banded iron-formations, Yilgarn Block, Western Australia. Econ. Geol., 76: 1954-1975.

Gole, M.J. and Klein, C., (1981) - Banded iron-formations through much of Precambrian time. J. Geol., 89: 169-183.

Gross, G.A., & McLeod, C.R., (1980) – A preliminary assessment of the chemical composition of iron formations in Canada: Can. Miner., v. 18, pp. 223-229.

Gross, G.A., (1965) – Geology of iron deposits in Canada: general geology and evaluation of iron deposits, v. 1: Dep. Of mines and Tech. Surveys, Econ. Geol. Rep. No.22, 173pp.

Gross, G.A., (1972) - Primary features in cherty iron formations. Sediment. Geol., 7: 241-261.

Gruner, J.W., (1936) - The structure and composition of greenalite. American Mineralogist 21, 449–455.

Gruner, J.W., (1944) - The composition and structure of minnesotaite, a common iron silicate in iron formation. American Mineralogist 29, 363–372.

Harington, J.S. & Cilliers, J.J. Le R., (1963) – A possible origin of the primitive oils and amino acids isolated from amphibole asbestos and banded ironstone. Geochim. Cozmochim. Acta, 27: 411-418.

Harington, J.S., (1962) – Occurrence of oils containing 3 : 4-benzpyrene and related substances in asbestos. Nature, 193: 43-45.

Hartman, H., (1984) - The evolution of photosynthesis and microbial mats: a speculation on banded iron formations: In Cohen, Y.,Castenholz, R.W., and Halvorson, H.O. (eds.), Microbial Mats: Stromatolites. New York: Alan Liss, pp. 451–453.

Heimann, A., Johnson, C.M., Beard, B.L., Valley, J.W., Roden, E.E., Spicuzza, M.J., and Beukes, N.J., (2010) - Fe, C, and O isotope compositions of banded iron formation carbonates demonstrate a major role for dissimilatory iron reduction in ~2.5 Ga marine environments: Earth and Planetary Science Letters, v. 294, p. 8–18,

Heising S, Richter L, Ludwig W, Schink B (1999) Chlorobium ferrooxidans sp. nov., a phototrophic green sulfur bacterium that oxidizes ferrous iron in coculture with a Geospirillum sp. strain. Arch Microbiol 172:116–124.

Hoefs, J., (1987) - Stable Isotope Geochemistry. Springer,Berlin, 241 pp.

Holland, H. D. (2002) - Volcanic gases, black smokers, and the great oxidation event. Geochim. Cosmochim. Acta 66, 3811–3826.

Holland, H. D. (2006) - The oxygenation of the atmosphere and oceans: Phil. Trans. R. Soc. v. 361, pp. 903–915.

Horstmann, U.E., & Halbich, I.W., (1995) – Chemical composition of banded iron-formations of the Griqualand West Sequence, Northern Cape Province, South Africa, in comparison with other Precambrian iron-formations: Prec. Res, v.72, p. 109-145.

Jacobsen, S.B., Pimentel-Klose, M.R., (1988) - A Nd isotopic study of the Hamersley and Michipicoten banded iron formations: the source of REE and Fe in Archean oceans. Earth Planet. Sci. Lett. 87, 29 44.

James, H.L., & Trendall, A.F., (1982) – Banded iron-formation: distribution in time and palaeoenvironmental significance, in: Mineral Deposits and the Evolution of the Biosphere, eds., H.D. Holland and M. Schidlowski: Springer-Verlag, pp. 199-218.

James, H.L., (1954) – Sedimentary facies of iron formation. Econ. Geol., 49: 235-293.

Johnson CM, Beard BL, Beukes NJ, Klein C, O'Leary JM (2003) - Ancient geochemical cycling in the Earth as inferred from Fe isotope studies of banded iron formations from the Transvaal craton. Contrib Mineral Petrol 144:523–547.

Johnson, C.M., Ludois, J.M., Beard, B.L., Beukes, N.J., Heimann, A., (2013) - Iron formation carbonates: Paleoceanographic proxy or recorder of microbial diagenesis? Geology, v. 41; no. 11; p. 1147–1150.

Johnson, J.E., Web, S.M., Thomas, K., Ono, S., Kirschvink, J.L., Fischer, W.W., (2013) - Manganese-oxidising photosynthesis before the rise of cyanobacteria: PNAS (in press), pp 1-6.

Jolliffe, F. (1935) - A study of greenalite. Am. Mineral., Vol. 20, 405-425pp.

Kappler A, Pasquero C, Konhauser KO, Newman DK (2005) - Deposition of banded iron formations by anoxygenic phototrophic Fe(II)-oxidizing bacteria. Geology 33:865–868.

Karhu, J.A., Holland, H.D., (1996) - Carbon isotopes and the rise of atmospheric oxygen. Geology 24, 867–870.

Kasting, J.F. (1993) - Earth's early atmosphere. Science, v. 259, pp. 920–926.

Kaufman AJ., Hayes J.M., Klein C. (1990) - Primary and Diagenetic Controls of Isotopic Compositions of lron-Formation Carbonates- Geochimica Cosmochimica Acta (54),3461-3473.

Kaufmann, A.J., Hayes, J.M., and Klein, C., (1990) – Primary and diagenetic controls of isotopic compositions of iron-formation carbonates: Geoch.Cosm.Acta, v. 54, pp. 3461-3473.

Kimberley, M.M., (1978) – Palaeoenvironmental classification of iron formations: Econ. Geol., v. 73, pp. 215-229.

Kimberley, M.M., (1989a) – Nomenclature for iron formations: Ore Geology Reviews, v. 5, pp. 1-12.

Kirschvink, J.L., Gaidos, E.J., Bertani, L.E., Beukes, N.J., Gutzmer, J.,Maepa, L.N., Steinberger, R.E., (2000) - Paleoproterozoic Snowball Earth: extreme climatic and geochemical change and its biological consequences. PNAS 97, 1400–1405.

Klein C (2005) - Some Precambrian Banded Iron Formations (BIFs) from around the world: their age, geologic setting, mineralogy, metamorphism, geochemistry, and origin. Am Mineral. 90:1473–1499.

Klein C, Beukes NJ (1992) - Proterozoic iron-formations. In: Condie KC (ed) Proterozoic crustal evolution. Elsevier, Amsterdam,pp 383–418.

Klein C. and Beukes N.J. (1992) - Models for Iron-Formation Deposition- In The Proterozoic Biosphere, a Multidisciplinary Study, SchopfJ.W. and Klein C., Cambridge UniversityPress,147-152.

Klein C. and Beukes N.J. (1993) - Sedimentology and Geochemistry of the Glaciogenic Late Proterozoic Rapitan Iron-Formation in Canada- Economic Geology (88),542-565.

Klein, C. & Bricker, O.P., (1977) – Some aspects of the sedimentary and diagenetic environment of Proterozoic banded iron-formation. Econ. Geol., 72: 1457-1470.

Klein, C. & Fink, R.P., (1976) – Petrology of the Sokoman Iron Formation in the Howells River area, at the western edge of the Labrador Trough. Econ. Geol., 71: 453-487.

Klein, C. & Gole, M.J., (1981) – Mineralogy and petrology of parts of the Marra Mamba Iron Formation, Hamersley Basin, Western Australia. Am. Mineral., 66: 507-525.

Klein, C. and Beukes, N.J., (1992) - Time distribution, stratigraphy and sedimentologic setting and geochemistry of Precambrian ironformations. In: J.W. Schopf and C. Klein (Editors), The Proterozoic Biosphere: A Multidisciplinary Study. Cambridge University Press, New York, pp. 140-146.

Klein, C., (1974) – Greenalite, stilpnomelane, minnesotaite, crocidolite and carbonates in a very low-grade metamorphic Precambrian iron formation. Can. Mineral., 12: 475-498.

Klein, C., (1978) - Regional metamorphism of Proterozoic iron-formation, Labrador Trough, Canada. Am. Mineral., 63:898-912.

Klein, C., (1983) - Diagenesis and metamorphism of Precambrian banded iron formations. In: Trendall, A.F., Morris, R.C. (Eds.), Iron-formation: Facts and Problems. Elsevier, Amsterdam.

Klein, C., Beukes, N.J., (1989) - Geochemistry and sedimentology of a facies transition from limestone to iron-formation deposition in the Early Proterozoic Transvaal Supergroup, South Africa. Econ. Geol. 84, 1733–1774.

Klemm, D.D., (1979) – A biogenetic model of the formation of the banded iron formation in the Transvaal Supergroup, South Africa. Miner. Deposita, 14: 381-385.

Konhauser KO, Hamade T, Raiswell R, Morris RC, Ferris FG, Southam G, Canfield DE (2002) - Could bacteria have formed the Precambrian banded iron formations? Geology 30:1079–1082.

Konhauser, K.O.,Hamade, T.,Raiswell, R.,Morris, R.C., Ferris, F.G., Southam,G., Canfield, D.E., (2002) - Could bacteria have formed the Precambrian banded iron formations? Geology. 30, 1079–1082.

Krapez, B., Barley, M.E., Pickard, A.L., (2003) - Hydrothermal and resedimented origins of the precursor sediments to banded iron-formation: sedimentological evidence fromthe Early Palaeoproterozoic Brockman Supersequence ofWestern Australia. Sedimentology 50, 979–1011.

La Berge, G.L., (1966) – Pyroclastic rocks in South African iron-formations. Econ. Geol., 61:572-581.

Lesher, C.M. (1978) – Mineralogy and petrology of the Sokoman Iron Formation near Arda Lake, Quebec. Can. J. Earth Sci., 15: 480-500.

Li, Y. (2014) - Micro- and nanobands in late Archean and Palaeoproterozoic banded-iron formations as possible mineral records of annual and diurnal depositions. Earth and Planetary Science Letters 391: 160-170

Lovley DR (1991) - Dissimilatory Fe(III) and Mn(IV) reduction. Microbiol Rev 55:259–287

Lyons, T.W., Reinhard C.T., Planavsky N.J., (2014) – The rise of oxygen in the Earth's Early Ocean and atmosphere. Nature, v. 406, pp. 307-315.

Malherbe, S.J., (1970) – Flat-pebble conglomerates in the Dolomite Series in the Northern Cape Province. Ann. Geol. Surv. A.Afr., 8: 89-94.

Maynard, B., (1982) - Extension of Berner's "New geochemical classification of sedimentary environments" to ancient sediments: Journal of Sedimentary Petrology, v. 52, p. 1325–1331.

McConchie D (1987) - The geology and geochemistry of the Joffre and Whaleback Shale members of the Brockman iron formation, Western Australia. In: Appel PWU, LaBerge GL (eds) Precambrian iron-formations. Theophrastus, Athens.

McSwiggen, P.L., & Morey, G.B., (2007) - Overview of the mineralogy of the Biwabik Iron Formation, Mesabi Iron Range, northern Minnesota. Regulatory Toxicology and Pharmacology. Elsevier, Vol 52. S11–S25.

Mel'nik, Yu.P., (1982) – Precambrian Bandedn Iron-formations: Physiochemical Conditions of Formation. Elsevier, Amsterdam, 310pp.

Moffat, R., (1858) – Report of a survey of a portion of the Orange River eastward of Little Namaqualand. Parliamentary Report G1 – 1858, Cape Town.

Mojzsis, S.J., (2003) - Probing early atmospheres. Nature. v. 425: pp. 249–251.

Moore, J.M., Tsikos, H., Polteau, S., (2001) - Deconstructing the Transvaal Supergroup. South Africa: implications for Paleoproterozoic paleoclimate models. J. Afr. Earth Sci. 33, 437–444.

Morey, G.B., (2003) - Paleoproterozoic Animekie Group related rocks and associated iron ore deposits in the Virginia Horn. In: M.A. Jirsa, G.B. Morey (Eds.), Contributions to the Geology of the Virginia Horn Area, St. Louis County, Minnesota. Minnesota Geological Survey Report of Investigation 53, 74–102.

Oonk, P., (ongoing) – Species-specific trace element and stable isotope geochemistry across the BIF stratigraphy of the Transvaal Supergroup in Griqualand West, South Africa and implications for the history of atmospheric oxygen. PhD. Thesis Ongoing. Rhodes University, Grahamstown, South Africa, -pp.

Passchier E.W. & Trouw R.A.J., (1996) – Microtectonics Vol. 1., Rio De Janeiro, Springer Science & Business Media, pp. 366.

Pavlov, A.A., Kasting J.F., (2002) - Mass-independent fractionation of sulfur isotopes in Archean sediments: strong evidence for an anoxic Archean atmosphere. Astrobiology 2:27–41.

Perry, E.C. Jr., & Tan, F.C., (1973) – Significance of carbon isotope variations in carbonates from the Biwabik iron-formation, Minnesota, in: Genesis of Precambrian Iron and Manganese deposits: Proc. Klev Symp. 1970, UNESCO Paris, 382 p.

Pickard, A.L., (2003) - SHRIMP U–Pb zircons ages for the Palaeoproterozoic Kuruman iron formation, Northern Cape Province. South Africa: evidence for simultaneous BIF deposition of the Kaapvaal and Pilbara cratons. Precambrian Res. 125, 275–315.

Pickard, A.L., Barley, M.E., Krapeˇz, B., (2004) - Deep-marine depositional setting of banded ironformation: sedimentological evidence from interbeddedclastic sedimentary rocks in the early Paleoproterozoic Dales Gorge Member of Western Australia. Sedimentary Geol. 170, 37‑62.

Planavsky, N. J. et al (2011) - Widespread iron-rich conditions in the mid-Proterozoic ocean. Nature 477, 448–451.

Planavsky, N. J., Bekker, A., Hofmann, A., Owens, J. D. & Lyons, T. W. (2012) - Sulfur record of rising and falling marine oxygen and sulfate levels during the Lomagundi event. Proc. Natl Acad. Sci. USA 109, 18300–18305.

Planavsky, N.J., Rouxel, O.J., Bekker, A., Hofmann, A., Little, C.T.S., and Lyons, T.W., (2012) - Iron isotope composition of some Archean and Proterozoic iron formations: Geochimica et Cosmochimica Acta, v. 80, p. 158–169

Polteau, S., (2000) - Stratigraphy and geochemistry of the Makganyene Formation, Transvaal Supergroup, South Africa. Unpublished M.Sc. Thesis. Rhodes University, Grahamstown, South Africa, p.146.

Polteau, S., Moore, J.M., Tsikos H., (2005) - The geology and geochemistry of the Palaeoproterozoic Makganyene diamictite: Elsevier, v. 146, p. 257–274.

Posth NR, Konhauser KO, Kappler A (2010a) - Microbiological processes in BIF deposition. In: Glenn C, Jarvis I (eds) Authigenic minerals: sedimentology, geochemistry, origins, distribution and applications. Journal of Sedimentology IAS Special Publication Series.

Rashby, S. E., Sessions, A. L., Summons, R. E., and Newman, D. K., (2007) - Biosynthesis of 2-methylbacteriohopanepolyols by an anoxygenic phototroph. Proceedings of National Academy of Sciences of the United States of America, 104(38), 15099–15104.

Rasmussen B, and Buick R., (1999) - Redox state of the Archean atmosphere: evidence from detrital heavy metals in ca. 3250–2750 Ma sandstones from the Pilbara Craton. Aust Geol 27:115–118.

Rogers A.W. and Du Toit, A.L., (1909a) – Report on the geology of parts of Prieska, Hay, Britstown, Carnavon and Victoria West, Annu. Rep. 1908, Geol. Comn. Cape of Good Hope, pp. 9-110.

Rogers, A.W., (1907) – Geological survey of parts of Bechuuanaland and Griqualand West. Annu. Rep. 1906. Geol. Comn. Cape of Good Hope, pp. 7-86.

Rogers, A.W., (1937) – The pioneers in South African geology and their work. Trans. Geol. Soc. S. Afr., Annexure to Vol. 39,130pp.

Roy, S., (1997) - Genetic diversity of manganese deposition in the terrestrial geological record. In: Nicholson, K., Hein, J., Bühn, B., Dasgupta, S. (Eds.), Manganese Mineralisation: Geochemistry and Mineralogy of Terrestrial and Marine Deposits. Special Publication—Geological Society of London, vol. 119, pp. 5–27.

Sagan, C. & Mullen, G. (1972) - Earth and Mars: evolution of atmospheres and surface temperatures. Science 177, 52–56.

Schopf, J.W., (1993) - Microfossils of the early Archean Apex Chert: new evidence of the antiquity of life. Science 260:640–646.

Simonson, B.M., (1985) - Sedimentological constraints on the origins of Precambrian iron-formations. Bull. Geol. Soc. Am., 96: 244-252.

Simonson, B.M., and Hassler, S.W., (1996) - Was the deposition of large Prebambrian iron formation linked to major marine transgression?: Journal of Geology, v. 104, p. 665–676.

Stow, G.W., (1874) – Geological notes upon Griqualand West. Q.J. Geol. Soc. London, 30: 581-680.

Summons RE, Jahnke LL, Hope JM, Logan GA (1999) - 2-Methylhopanoids as biomarkers for cyanobacterial oxygenic photosynthesis. Nature 400:554–557.

Trendall, A.F. & Blockey, J.G., (1970) – The iron-formations of the Precambrian Hamersley Group, Western Australia, with special refer to the associated Crocidolite: West. Austr. Geol. Surv. Bull. V. 119, 366pp.

Trendall, A.F., (1965) - Progress report on the Brockman Iron Formation in the Wittnoom-Yampire area. Geol. Surv. West. Aust., Annu. Rep., 1965: 55-65.

Trendall, A.F., (1968) – Three great basins of Precambrian banded iron-formation deposition: a systematic comparison: Geol. Soc. Amer. Bull., v. 79, pp. 1527-1544.

Trendall, A.F., (1983) - The Hamersley Basin. In: A.F. Trendall and R,C. Morris (Editors), Iron-Formation: Facts And Problems. Developments in Precambrian Geology, 6, Elsevier, Amsterdam, pp. 69-129.

Trendall, A.F., Compston,W.,Williams, I.S., Armstrong, R.A., Arndt, N.T., McNaughton, N.J., Nelson, D.R., Barley, M.E., Beukes, N.J.,De Laeter, J.R., Retief, E.A., Thorne, A.M., (1990) - Precise zircon U–Pb chronological comparison of the volcano-sedimentary sequences of the Kaapvaal and Pilbara Cratons between about 3.1 and 2.4 Ga. In: Glover, J.E., Ho, S.E. (Eds.), Proceedings of the Third International Archaean Symposium. Perth. Geoconferences (W.A.) Inc., Perth, pp. 81–83 (extended abstracts).

Tsikos H, Matthews A, Erel Y & Moore JM (2010) - Iron isotopes constrain biogeochemical cycling of Fe and Mn in a Palaeoproterozoic stratified basin. Earth & Planetary Science Letters 298, 125–134.

Tsikos, H., (1994) - The minerology and geochemistry of the Voelwater banded iron-formation, Northern Cape Province. M.Sc. Thesis Unpublished. Rhodes University, Grahamstown, South Africa, 127pp.

Tsikos, H., (1999) - Petrographic and geochemical constraints on the origin and post-depositional history of the Hotazel iron-manganese deposits, Kalahari Manganese Field,

South Africa. Ph.D. Thesis Unpublished. Rhodes University, Grahamstown, South Africa, 217pp.

Tsikos, H., Beukes, N.J., Moore, J.M., Harris, C., (2003) - Deposition, diagenesis, and secondary enrichment of metals in the Paleoproterozoic Hotazel iron-formation, Kalahari Manganese Field, South Africa. Econ. Geol. 98, 1449–1462.

Tsikos, H., Moore, J.M., Harris, C., (2001) - Geochemistry of the Palæoproterozoic Mooidraai Formation: Fe-rich limestone as end member of iron formation deposition, Kalahari Manganese Field, Transvaal Supergroup, South Africa. J. Afr. Earth Sci. 32, 19–27.

Van Niekerk, C.B. & Burger, A.J., (1978) – A new age for the Ventersdorp acidic lavas. Trans. Geol. Soc. S. Afr., 81: 155-163.

Von Backstrom, J.W., (1963) - Septarian concretions in the Lower Griquatown Stage of the Pretoria Series near Kuruman, Cape Province. Ann. Geol. Surv. S. Afr., 2: 78--88.

Webb, A.D., Dickens, G.R., Oliver, N.H.S., (2003) - From banded iron-formation to iron ore: geochemical and mineralogical constraints from across the Hamersley Province, Western Australia. Chem. Geol. 197, 215‑251.

Widdel F, Schnell S, Heising S, Ehrenreich A, Assmus B, Schink B (1993) - Ferrous iron oxidation by anoxygenic phototrophic bacteria. Nature 362:834–836.

Winter, B.L. and Knauth, L.P., (1992) - Stable isotope geochemistry of cherts and carbonates from the 2.0 Ga Gunflint Iron Formation: implications for the depositional setting, and the effects of diagenesis and metamorphism. Precambrian Res., 59: 283-313.

Appendices

A.1. Analytical Methods

A.1.1. EPMA

EPMA analyses were conducted on carbon-coated, polished thin sections containing siderite and ankerite grains as observed under the microscope. The main objective was to acquire measurements for 5 major element oxide compositions namely, SiO_2, CaO, MgO, MnO and FeO. EPMA data acquisition was performed at the University of Cape Town, Department of Geological Sciences, on a JEOL JXA 8320 Superprobe, using 4 wave-dispersive spectrometres. Analytical conditions employed were: acceleration voltage 15kv, probe current 20nA, counting time 10sec on peak and 5 sec on background, and beam spot size less than 1 micron. Natural standards were used for measuring the characteristic X-rays. ZAF matrix correction method was employed for quantification. Totals for all major oxides analysed that ranged between 57 – 60% (i.e. excluding CO_2 which cannot be analysed for) suggested optimum carbonate analyses on the basis of ideal compositions for ankerite and siderite from the literature. Averaged concentrations of the analysed oxides were also used for individual samples as presented below in EPMA data tables.

A.1.2. X-Ray Powder Diffraction Analysis

X-Ray powder diffraction analyses were performed on all samples, with main aim to detect and identify relative carbonate abundances of ankerite and siderite against stratigraphy up-section, in order to guide the microprobe analytical and stable isotope analyses on selected samples containing both carbonate species. Measurements were carried out using a HR-XRD Scan diffractometer with a X'Celerator detector at the University of Cape Town. Samples were prepared as back-loaded pellets in plastic sample holders. Analyses of the XRD patterns were done on Crystal Sleuth. The measurements were done using the following diffractometer settings:

GenKVmA:	10,10
Omega:	19.45000
Two Theta:	38.9000
Scan Type:	Step

Scan Axis:	2 Theta/Omega
First Angle:	24.00000
Last Angle:	54.00000
Scan Range:	29.80000
Step Width:	0.02000

A.1.3. Bulk acetate-dithionite-oxalate sequential extraction

The technique used for the speciation analyses of this study is routinely employed at the University of California at Riverside, and is the same as that quoted by Reinhard et al. (2009). The latter performed extractions of carbonates and oxides using the sequential extraction technique of Poulton and Canfield (2005), which measures the iron present as carbonates by extraction with Na acetate at pH 4.5 for 48 h at 50^{O}C (Fe_{carb}), as ferric oxides by extraction with dithionite at pH 4.8 for 2 h at room temperature (Fe_{ox}) and as magnetite by extraction with oxalate at pH 3.2 for 6 h at room temperature (Fe_{mag}). The data used in this thesis are restricted to those obtained via the acetate extraction step. All data, however, are reported in the data tables that follow.

A.1.4. Bulk δ^{13}C isotope analyses

Fractions of all powdered samples of BIF from the ERIN, GAS, HEX and ARPAN drillcores were reacted at 100^{o}C in 100% phosphoric acid overnight, or at 75^{o}C over 72 hours, in order to yield CO_2 gas for coexisting siderite and ankerite together. The analyses were carried out at the stable isotope laboratory of SUERC in East Kilbride, Scotland, under the supervision of Dr Adrian Boyce. Tests done in-house SUERC have confirmed that the δ^{13}C data for siderite-ankerite mixtures are closely reproducible regardless which exact reaction time/temperature method is employed. The resultant CO_2 gas was subsequently extracted and sealed in glass vials and then analysed for C and O-isotope ratios (the latter were neither used nor reported) on a DeltaXP mass spectrometer in dual inlet mode. Reported δ values were normalized to Pee-Dee Belemnite (PDB).

A.1.5. Sequential dissolution of ankerite and siderite and resultant δ^{13}C measurements

Stable isotope geochemical analyses were also conducted on siderite and ankerite pairs in 8 pre-selected samples, in order to test and evaluate the relationship between bulk and species-specific carbonate-carbon isotope signals. Selection of the latter was done on the basis of coexistence of carbonate species (ankerite and siderite) as revealed by XRD analyses and petrographically, and in order to cover all major first-order variations in bulk δ^{13}C across stratigraphy of the ERIN core as recorded by the data obtained at SUERC. Sample processing and isotopic analyses was done at the Department of Geology, University of Cape Town.

Sample powders and 100% phosphoric acid were mixed in evacuated and sealed glass sample holders and were then allowed to react at a temperature of 50^{o}C for extracting CO_2 from ankerite (together with that from little calcite in a few samples) at this first step. The next step involved reacting the now ankerite-free powders at 100^{o}C for the extraction of

siderite-hosted CO_2 extraction overnight. The resultant gas was subsequently sealed in glass vials and then analysed for carbon and oxygen (not reported or used) isotopes on a DeltaXP mass spectrometer in dual inlet mode. Reported δ values were normalized to Pee-Dee Belemnite (PDB)

A.2. Tabulated speciation data

A.2.1. Major Element oxide concentrations from the acetate fraction

Sample	MgO	CaO	MnO	FeO
E71	2,716418	4,626333	0,735519	23,00166
E70	1,88806	3,879531	1,721673	20,199
E69	1,84918	9,69555	1,297348	7,881603
E68	3,440169	2,198127	0,334294	33,84543
E67	2,866593	13,08679	1,42011	10,4001
E66	2,157143	11,66667	2,007042	9,204586
E64	2,169468	9,334477	0,997516	7,236135
E63	2,481633	5,971459	1,129217	10,7526
E62	1,638627	5,413243	2,003143	25,25513
L3	3,201563	9,341518	1,708272	16,09896
E60	3,35142	8,452456	0,83582	18,43767
E59	0,743351	3,853078	0,634871	8,718417
E58	1,952416	2,391397	0,594573	22,98224
E57	0,396085	5,303343	0,233536	5,61513
E56	1,336774	0,059447	0,432594	16,51039
E53	2,199623	3,16707	0,440153	20,4729
E51	0,718229	1,747496	0,126321	6,214022
E50	0,222473	0,008174	0,094449	2,132562
E48	2,34166	12,63082	0,571219	13,03604
E47	2,53345	1,986775	0,582766	20,33964
E46	1,780619	5,254174	2,109721	16,83472
E45	2,032392	1,028894	0,619623	18,38041
E44	2,976434	8,326531	1,42527	27,19499
E42	3,069556	0,758425	0,502176	22,6763
E40-b	2,762044	5,77633	1,043091	26,68289
E39	1,068027	6,131195	0,329728	7,528345
E38	1,619687	7,402354	0,494274	9,089097
E36	2,427038	7,080375	0,64847	17,76011
E35	0,914046	5,763702	0,31447	6,355462
E34	1,114048	1,315077	0,169175	8,89504
E33	1,181181	1,012108	0,245636	12,87048
E32	0,832519	0,710919	0,171095	10,36685
E31	0,640302	1,719137	0,111686	5,437317
E30	0,945947	4,131225	0,26092	7,052557
E29	2,257996	12,53628	0,499958	10,27456
E28	2,194418	8,52193	0,455533	11,11496
E27	0,164328	24,23805	0,256036	2,350065
E26	1,061818	1,557129	0,908891	16,29942
E25	2,619048	6,207483	0,117694	18,73016

E24	2,230588	4,882353	0,07497	13,14858
E23	0,90961	0,192579	0,034686	7,255411
E22	1,241325	0,042119	0,106616	12,84081
E21	0,393878	0,256922	0,05005	1,279297
E19	2,829119	14,50903	0,785843	12,02895
E18	3,187565	13,13694	0,710932	11,04433
E17	2,481603	2,112412	0,51009	15,19045
E16	0,267879	0,830682	0,292077	2,710438
E14	2,576495	2,596171	0,490315	21,80985
E13	0,888664	3,037133	0,512374	4,503811
E12	0,848711	3,731429	0,415465	2,625185
E10	0,405877	3,220372	0,1451	2,152138
E9-b	1,651508	5,137357	0,299318	10,37956
E8	0,169043	13,52609	0,375762	1,53913
E7	0,147414	4,109566	0,21917	1,67237
E6	0,254561	0,305021	0,028086	3,042306
E5	1,009504	0,132381	0,328841	11,73637
E4	0,300644	0,022963	0,013918	1,609366
E3	0,842374	2,460283	0,137311	8,187546
E2	0,940084	0,035841	0,241487	18,8842
E1	1,141379	1,761761	0,237895	19,65517

A.2.2. Major Element oxide concentrations from the dithionite fraction

Sample	MgO	CaO	MnO	FeO
E1	0,095328	0,267488	0,013809	0,013833
E2	0,123561	0,216094	0,017585	0,017617
E3	0,057793	0,265432	0,003826	0,003833
E4	0,210576	0,183638	0,003361	0,003367
E5	0,184752	0,207766	0,013515	0,013538
E6	0,097339	0,123228	0,004236	0,004244
E7	0,0626	0,19823	0,008882	0,008898
E8	0,060574	0,415155	0,01275	0,012773
E9	0,122302	0,217265	0,013003	0,013026
E10	0,08409	0,307765	0,004112	0,00412
E12	0,091804	0,25619	0,014523	0,014548
E13	0,080231	0,215059	0,014148	0,014172
E14	0,12541	0,2757	0,024626	0,024669
E16	0,052773	0,251136	0,011628	0,011648
E17	0,1651	0,234504	0,025682	0,025728
E18	0,089257	0,436417	0,018206	0,018238
E19	0,1261	0,367816	0,01188	0,011901
E21	0,087553	0,357597	0,0253	0,025344
E22	0,141475	0,258089	0,00398	0,003987
E23	0,091567	0,178831	0,000553	0,000554
E24	0,110227	0,355294	0,003581	0,003587
E25	0,132111	0,536565	0,00503	0,005039
E26	0,081072	0,264279	0,042558	0,042633
E27	0,028927	0,601778	0,006812	0,006824
E28	0,09697	0,377506	0,014226	0,014251
E29	0,063747	0,294502	0,011874	0,011895
E30	0,086163	0,162175	0,008503	0,008518
E31	0,071245	0,181941	0,003367	0,003373
E33	0,092462	0,156325	0,010756	0,010775
E34	0,118478	0,255808	0,009527	0,009544
E35	0,081182	0,101887	0,014491	0,014517
E36	0,169861	0,397558	0,035793	0,035856
E38	0,065251	0,202532	0,009682	0,009699
E39	0,053823	0,173761	0,010809	0,010828
E40	0,148905	0,241032	0,028174	0,028224
E42	0,342456	0,244847	0,030823	0,030877
E44	0,171345	0,363057	0,088048	0,088203
E45	0,189077	0,191929	0,037766	0,037832
E46	0,071113	0,251406	0,060934	0,061041
E47	0,212681	0,175471	0,033013	0,033071
E48	0,081355	0,504802	0,017687	0,017718

E49	0,235758	0,169318	0,054231	0,054327
E50	0,007018	0,023	0,001325	0,001328
E51	0,242214	0,31107	0,109802	0,109996
E53	0,131872	0,217111	0,021724	0,021762
E56	0,143002	0,180793	0,017888	0,017919
E57	0,027711	0,203891	0,001746	0,001749
E58	0,135896	0,244238	0,045884	0,045964
E59	0,042453	0,264639	0,013292	0,013316
E60	0,149518	0,418387	0,043275	0,043351
E61	0,053462	0,241648	0,009825	0,009843
E62	0,118644	0,242428	0,07289	0,073019
E63	0,114526	0,246923	0,039115	0,039184
E64	0,08	0,26817	0,02904	0,029091
E65	0,165878	0,414927	0,099996	0,100172
E66	0,074032	0,429932	0,059912	0,060018
E67	0,105791	0,503134	0,039152	0,039221
E68	0,038732	0,192812	0,014606	0,014632
E69	0,064016	0,43911	0,033111	0,033169
E70	0,116045	0,277612	0,081167	0,08131
E71	0,17403	0,358689	0,153891	0,154163
L3	0,129391	0,425391	0,068022	0,068142

A.2.3. Major Element oxide concentrations from the oxalate fraction

Sample	MgO	CaO	MnO	FeO
E1	0,514138	0,738801	0,09533	9,464
E2	0,512911	0,744476	0,107415	12,090
E3	0,152949	0,722467	0,026854	2,915
E4	0,139817	0,736276	0,002926	0,807
E5	1,30065	0,730234	0,138256	13,596
E6	0,06569	0,762926	0,003657	0,541
E7	0,05272	0,787757	0,00442	8,600
E8	0,037339	0,720976	0,007089	3,250
E9	0,103478	0,727099	0,014129	8,647
E10	0,083056	0,752102	0,003628	10,125
E12	0,094667	0,757975	0,007491	10,906
E13	0,147148	0,756921	0,017762	3,103
E14	0,394392	0,747007	0,084762	8,378
E16	0,044152	0,735896	0,014073	0,896
E17	0,375373	0,731216	0,096701	24,562
E18	0,055599	0,733457	0,015816	11,810
E19	0,092276	0,720498	0,007141	11,205
E21	0,040213	0,732893	0,012152	18,802
E22	0,519912	0,75912	0,03232	7,488
E23	0,208485	0,721574	0,006186	15,357
E24	0,133882	0,736217	0,00567	14,044
E25	0,500794	0,751954	0,028468	14,092
E26	0,547368	0,726171	0,359175	8,705
E27	0,016866	0,719889	0,001605	5,535
E28	0,095215	0,745922	0,016925	16,305
E29	0,055831	0,720339	0,010338	14,216
E30	0,110419	0,735338	0,016967	17,111
E31	0,192906	0,741503	0,021112	28,277
E33	0,308018	0,732224	0,061307	27,458
E34	0,211211	0,768983	0,031087	20,069
E35	0,268763	0,732226	0,08504	5,025
E36	0,345129	0,746125	0,101751	13,042
E38	0,034119	0,74243	0,005868	0,456
E39	0,042844	0,735	0,008276	1,749
E40	0,419708	0,73278	0,123723	12,144
E42	0,9813	0,77895	0,185157	15,861
E44	1,182732	0,757289	0,685062	14,764
E45	0,711262	0,733448	0,231439	10,613
E46	0,194206	0,747343	0,295006	5,429
E47	0,930655	0,775002	0,234347	21,659
E48	0,082307	0,739793	0,021049	2,390

E49	0,505606	0,740091	0,210907	10,827
E50	0,001892	0,716538	0,00035	0,015
E51	1,567528	0,745642	0,700036	18,221
E53	0,643013	0,732063	0,145097	11,929
E56	0,967914	0,748512	0,224216	12,876
E57	0,027081	0,735498	0,004244	0,484
E58	0,536952	0,743124	0,194288	7,420
E59	0,02121	0,730008	0,013073	0,208
E60	0,257077	0,743444	0,090263	3,318
E61	0,017738	0,741988	0,004206	1,170
E62	0,198112	0,737183	0,178969	36,090
E63	0,336327	0,748915	0,175616	14,302
E64	0,161921	0,745315	0,064533	19,150
E65	0,174367	0,746847	0,127358	4,960
E66	0,042206	0,743016	0,04037	12,577
E67	0,058637	0,721409	0,025123	8,763
E68	0,075738	0,746664	0,086725	0,634
E69	0,026115	0,721136	0,015319	3,916
E70	0,240896	0,738558	0,194682	14,866
E71	0,497612	0,737541	0,523952	8,682
L3	0,235313	0,73037	0,160879	12,436

A.2.4. Table of two selected samples from the acetate fraction. Take note of the bulk carbonate column

Sample	MgO	CaO	MnO	FeO	Mg(CO2)	Ca(CO2)	Mn(CO2)	Fe(CO2)	Bulk CO2	Bulk C	Bulk carb
E44	2,976434	8,326531	1,42527	27,19499	2,046298	3,816327	0,497713	9,348279	15,70862	4,284168	55,63185
E50	0,222473	-0,00817	0,094449	2,132562	0,15295	-0,00375	0,032982	0,733068	0,915254	0,249615	3,356565

A.3. Tabulated raw microprobe data

A.3.1. Ankerite (n=118)

MgO (wt%)	MnO (wt%)	FeO (wt%)	SiO2 (wt%)	CaO (wt%)	Total	Sample comment	Height (m)
6,1	2,55	18,74	0,6459	29,61	57,6846	E70	376,5
6,18	2,77	20,88	0,2448	27,8	57,8748	E70 carb 2	376,5
5,73	2,87	19,12	0,2702	28,31	56,3176	E70 carb 3	376,5
6,95	2,66	19,51	3,85	24,84	57,81	E70 carb 4	376,5
6,27	2,52	18,76	5,27	27,1	59,92	E70 carb 5	376,5
5,68	3	21,16	0,6267	26,8	57,2668	E70 carb 6	376,5
7,17	3,59	19,08	0,1048	27,88	57,8489	E69 carb 1	381,9
7,7	3,93	17,74	0,0429	28,13	57,6398	E69 carb 10	381,9
7,22	3,64	16,81	0,0038	29,23	56,9098	E69 carb 11	381,9
7,4	3,82	17,05	0,0448	29,74	58,0549	E69 carb 12	381,9
7,22	3,83	19,02	0,0101	27,24	57,3443	E69 carb 2	381,9
7,26	3,53	19,12	0,0226	27,01	56,9608	E69 carb 3	381,9
7,87	3,75	17,66	0,0454	28,18	57,5175	E69 carb 4	381,9
7,05	4,04	18,34	0,0675	28,26	57,8036	E69 carb 5	381,9
4,97	4,61	20,7	0,0414	27,82	58,1599	E69 carb 6	381,9
7,84	3,97	16,15	3,93	27,96	59,8677	E69 carb 7	381,9
6,77	3,71	18,52	5,53	26,33	60,8837	E69 carb 8	381,9
6,13	4,18	19,1	0,1966	27,16	56,7667	E69 carb 9	381,9
6,71	4,25	17,32	0,1007	28,06	56,4407	E66 carb 1	388,6
7,27	4,74	18,37	0,0818	25,99	56,4701	E66 carb 4	388,6
7,08	4,53	16,26	0,0429	27,65	55,6097	E66 carb 5	388,6
6,76	5,4	45,6	0,1	2,83	60,69	E66 carb 6	388,6
9,72	4,27	43,49	0,0865	3,19	60,7565	E66 carb 7	388,6
6,8	4,71	15,55	0,0534	28,76	55,8735	E66 carb 8	388,6
9,24	3,94	41,7	0,0505	6,03	61,0929	E66 carb 9	388,6
7,67	2,91	17,71	2,46	27,73	58,5239	E64 carb 1	394,6
9,34	2,95	16,9	2,35	26,44	58,065	E64 carb 10	394,6
9,49	3,09	17	0,0609	28,76	58,4345	E64 carb 2	394,6
9,26	3,22	16,87	3,37	26,22	58,9401	E64 carb 3	394,6
9,59	3,12	16,38	0,1569	28,22	57,4669	E64 carb 4	394,6

9,12	2,9	16,5	2,37	26,92	57,81	E64 carb 5	394,6
8,36	3,23	17,02	0,4207	28,61	57,7073	E64 carb 6	394,6
8,88	3,2	17,24	1,2209	26,87	57,4109	E64 carb 7	394,6
8,81	3,04	19,58	1,3696	24,18	56,9796	E64 carb 8	394,6
9,32	3,12	17,78	1,5652	26,5	58,3403	E64 carb 9	394,6
9,24	1,44	18,74	0,0201	27	56,4402	E61 carb 1	405,2
9,45	1,44	15,82	0,0164	28,11	54,8425	E61 carb 10	405,2
0,12	1,39	18,77	1,6382	31,57	63,5004	E61 carb 11	405,2
0,2	1,38	15,86	1,288	28,92	57,678	E61 carb 12	405,2
8,82	1,1496	18,27	0,1834	27,66	56,083	E61 carb 2	405,2
9,53	1,44	17,78	0,0429	27,99	56,7829	E61 carb 3	405,2
9,56	1,253	16,19	0,3726	29,42	56,8289	E61 carb 5	405,2
9,18	1,32	17,97	0,4193	28,52	57,4094	E61 carb 6	405,2
9,64	1,35	16,89	0,0777	28,66	56,6177	E61 carb 7	405,2
8,58	1,1885	16,61	5,54	26,26	58,1786	E61 carb 8	405,2
9,69	1,47	17,75	0,1068	27,04	56,1306	E61 carb 9	405,2
8,85	1,3	19,07	0,0683	26,62	55,9638	E60 carb 10	407,6
8,95	1,2198	18,97	0,5246	27,82	57,4844	E60 carb 11	407,6
8,75	1,1705	18,99	1,8344	26,57	57,3204	E60 carb 8	407,6
9,15	1,34	19,56	0,085	26,46	56,595	E60 carb 9	407,6
6,63	4,89	43,37	1,5736	5,58	62,0437	E59 carb 1	424
6,02	3,16	18,8	0,1345	29,43	57,5502	E59 carb 11	424
6,4	2,97	18,52	0,0775	29,99	58,1188	E59 carb 2	424
5,68	4,63	47,27	1,6034	2,04	61,2302	E59 carb 3	424
6,31	4,85	42,38	0,1085	7,69	61,4235	E59 carb 4	424
6,28	2,71	19,31	0,0896	29,35	57,7453	E59 carb 5	424
6,31	2,81	18,98	0,015	30,43	58,545	E59 carb 6	424
6,25	2,88	17,48	3,37	28,53	58,5101	E59 carb 7	424
6,14	2,89	20,15	0,5049	27,81	57,4949	E59 carb 8	424
6,44	1,95	20,18	0,0368	27,85	56,4569	E57 carb 1	432,3
6,51	1,7	20,19	0,1747	28,53	57,1909	E57 carb 10	432,3
6	1,84	20,87	0,1473	28,85	57,7979	E57 carb 13	432,3
5,96	1,81	21,93	1,6604	27,03	58,4695	E57 carb 14	432,3
5,79	2,25	22,89	4,64	24,42	60,0265	E57 carb 2	432,3
7,69	1,76	19,88	2,0985	27,1	58,6676	E57 carb 3	432,3
5,14	2,09	22,15	0,8207	26,8	57,0007	E57 carb 4	432,3
5,72	1,77	22,13	0,317	27,33	57,3624	E57 carb 5	432,3
5,73	1,98	22,01	0,3966	28,22	58,36	E57 carb 9	432,3
6,17	1,65	19,45	0,2366	29,6	57,1067	E54 carb 1	452,2
6,2	1,78	19,85	0,0857	29,05	56,9657	E54 carb 2	452,2
5,82	1,56	22,13	0,0569	27,26	56,8469	E54 carb 3	452,2
6,53	1,2564	18,45	0,0182	30,19	56,4839	E54 carb 4	452,2
5,64	1,4	22,38	0,1069	26,14	55,7266	E54 carb 9	452,2
6,35	2,69	18,64	0,7772	28,64	57,2758	E52 carb 1	458,9
6,51	2,62	19,35	3,75	28,05	60,3075	E52 carb 2	458,9

7,04	2,7	18,6	0,1288	29,27	57,8113	E52 carb 4	458,9
6,54	2,73	20,52	0,2148	27,87	57,9593	E52 carb 6	458,9
5,99	1,38	21,48	2,97	26,7	58,6166	E50 carb 1	464,6
6,14	1,37	22,9	0,7295	26,9	58,0707	E50 carb 2	464,6
5,93	1,36	22,92	0,2788	27,66	58,1488	E50 carb 4	464,6
5,81	1,284	23,96	3,53	26,41	60,994	E50 carb 7	464,6
6,34	1,93	44,26	0,1946	8,19	60,9146	E50 carb 8	464,6
6,72	1,72	21,38	2,4	27,48	59,7779	E44 carb 4	481,6
6,87	1,68	21,29	2,37	27,03	59,2512	E44 carb 6	481,6
7,63	1,93	19,63	3,61	26,53	59,4018	E44 carb 7	481,6
8,78	0,9232	18,55	0,3064	29,62	58,1796	E39 Carb 1	499,8
6,61	1,0745	22,17	2,91	27,98	60,7445	E39 Carb 10	499,8
7,21	1,46	20,78	0,307	27,61	57,4255	E39 Carb 3	499,8
6,91	1,2443	20,86	0,7026	29,54	59,2744	E39 Carb 4	499,8
7,09	1,32	21,19	0,9706	28,84	59,5025	E39 Carb 5	499,8
6,88	1,1987	20,41	0,4808	29,65	58,6875	E39 Carb 6	499,8
7,02	1,36	20,75	2,51	27,72	59,3601	E39 Carb 8	499,8
7,11	1,46	20,27	1,657	26,98	57,5564	E38 Carb 1	504,3
7,91	1,31	19,04	0,1393	28,74	57,2281	E38 carb 1	504,3
9,99	2,24	15,18	0,0547	27	54,5093	E38 carb 10	504,3
0,41	1,54	15,15	0,7393	26,72	54,5593	E38 carb 11	504,3
7,45	2,48	18,67	0,0984	27,23	55,9409	E38 Carb 2	504,3
8,02	1,2709	19,01	0,231	28,75	57,2819	E38 carb 2	504,3
7,74	1,29	18,8	0,3509	28,31	56,5019	E38 carb 3	504,3
7,03	1,45	20,65	1,8327	26,44	57,4698	E38 Carb 4	504,3
8,2	1,36	18,68	0,3079	28,55	57,0979	E38 carb 4	504,3
7,28	1,6	20,77	2,78	25,66	58,09	E38 Carb 5	504,3
7,48	1,37	18,28	0,1199	29,05	56,3383	E38 carb 5	504,3
7,49	2,49	20,01	3,4	26,63	60,0531	E38 Carb 6	504,3
7,49	1,46	18,48	0,1917	28,07	55,736	E38 carb 6	504,3
7,2	1,64	20,47	1,0775	28,16	58,5476	E38 Carb 7	504,3
8,38	1,55	17,84	0,2242	28,23	56,2852	E38 carb 7	504,3
8,35	1,62	19,59	2,55	26,73	58,9011	E38 carb 8	504,3
8,29	1,77	18,24	2,17	26,24	56,7211	E38 carb 9	504,3
8,76	0,8947	17,89	1,9056	28,54	58,083	E36 carb 1	512,3
8,18	0,8346	18,15	0,0626	29,45	56,6772	E36 carb 2	512,3
8,41	0,6842	17,89	0,0328	30,09	57,1299	E36 carb 5	512,3
7,35	0,8956	20,5	4,27	26,88	59,9352	E36 carb 7	512,3
8,19	1,9	47,94	0,2996	2,71	61,0465	E36 carb 8	512,3
0,32	0,7554	17,84	0,7507	28,06	57,7383	E34 carb 1	518,4
8,79	0,6033	19,71	2,54	27,43	59,157	E33 carb 1	520,5
8,37	0,5948	19,52	0,6072	26,62	55,7497	E32 carb 1	523,8
7,53	0,761	20,97	1,524	26,18	57,0641	E32 carb 4	523,8
7,34	0,5113	18,26	2,84	23,78	52,7313	E32 carb 7	523,8
7,77	0,7458	20,75	0,5171	27,7	57,5437	E32 carb 8	523,8

8,35	0,541	20,01	3,01	26,71	58,6332	E31 carb 1	525,9
9,4	1,0572	18,82	1,7592	27,12	58,2509	E31 carb 13	525,9
7,61	1,1504	48,87	1,0151	2,67	61,3155	E31 carb 2	525,9
8,32	0,4348	19,11	4,95	25,08	57,9609	E31 carb 5	525,9
1,01	1,41	15,34	3,14	26,66	57,6259	E31 carb 7	525,9
8,86	0,7529	17,95	4,42	29,57	61,5822	E31 carb 8	525,9
7,57	1,1346	19,1	2,23	27,07	57,1236	E30 carb 10	528,3
8,16	1,066	19,22	3,9	27,34	59,6986	E30 carb 13	528,3
8,47	0,9065	33,01	0,5597	22,13	65,1314	E30 carb 3	528,3
8,72	1,2066	23,88	0,2766	23,75	57,8332	E30 carb 4	528,3
7,69	1,1027	19,42	0,4883	28,03	56,8159	E30 carb 7	528,3
7,86	1,0308	19,04	4,41	27,66	60,0009	E29 carb 1	535,3
7,19	1,0578	21,24	0,6833	28,64	58,8465	E29 carb 2	535,3
7,06	1,1528	20,34	2,24	25,23	56,0758	E29 carb 3	535,3
7,23	1,1559	20,78	0,3181	27,96	57,444	E29 carb 4	535,3
6,86	0,8915	22,3	0,6238	29,04	59,7811	E29 carb 5	535,3
7,27	1,2891	20,29	0,7797	27,62	57,2548	E29 carb 7	535,3
7,13	1,0873	21,4	0,5341	28,54	58,7562	E29 carb 8	535,3
6,65	1,1649	21,45	0,0728	27,88	57,3067	E29 carb 9	535,3
5,48	1,36	23,33	0,0327	27,7	57,9209	E27 carb 10	543,4
5,16	1,48	23,37	0,3202	28,06	58,4141	E27 carb 2	543,4
5,66	1,39	23,75	0,1434	25,52	56,4635	E27 carb 3	543,4
5,58	1,37	23,38	0,1841	27,62	58,1341	E27 carb 4	543,4
6,51	1,1986	21,81	1,5868	26,4	57,5055	E27 carb 5	543,4
5,69	1,37	22,83	0,0864	27,37	57,4428	E27 carb 6	543,4
5,66	1,67	22,82	0,3886	27,72	58,2586	E27 carb 7	543,4
5,5	1,66	22,28	0,473	27,88	57,793	E27 carb 8	543,4
5,91	0,9926	22,76	0,155	28,15	58,0867	E27 carb 8	543,4
9,02	0,6043	19,16	0,3353	28,58	57,6996	E27 carb 9	543,4
5,76	1,89	21,09	-	29,27	58,0101	E27 carb 9	543,4
9,14	0,3262	19,7	1,3273	27,14	57,7398	E25 carb 1	550,4
8,8	0,3023	20,5	1,0993	26,81	57,5355	E25 carb 2	550,4
9,25	0,26	19,56	0,4268	27,79	57,3368	E25 carb 3	550,4
8,97	0,2949	21,86	4,7	24,6	60,425	E25 carb 4	550,4
7,78	0,3291	20,1	1,1512	27,45	56,8582	E25 carb 5	550,4
9,4	0,3614	19,58	0,3949	28,53	58,373	E25 carb 6	550,4
8,61	0,262	18,93	0,5062	30,07	58,4184	E25 carb 7	550,4
8,73	0,1765	17,7	6,42	27,15	60,1765	E24 carb 10	555,3
9,58	0,2307	36,15	4,54	12,33	62,9307	E24 carb 11	555,3
7,48	0,1434	19,46	5,89	27,21	60,2507	E24 carb 3	555,3
8,83	0,1822	19,21	3,79	26,82	58,8448	E24 carb 4	555,3
7,53	0,1507	18,06	8,72	26,07	60,5308	E24 carb 6	555,3
8,06	0,1489	19,02	5,88	25,19	58,299	E24 carb 7	555,3
0,04	0,1871	21,82	6,26	22,05	60,4309	E24 carb 8	555,3
8,5	1,023	18,16	0,7527	29,84	58,3237	E21 carb 1	565,3

7,6	1,79	19,66	0,0937	28,24	57,3958	E21 carb 2	565,3
7,84	1,46	18,56	2,36	28,63	58,9844	E21 carb 4	565,3
7,38	1,77	17,97	0,0052	25,74	52,9485	E21 carb 5	565,3
8,72	0,4775	20,59	0,6634	28,57	59,021	E19 carb 1	571,9
8,49	0,5308	20,5	0,3762	27,54	57,4486	E19 carb 10	571,9
8,94	0,5738	20,37	0,5426	27,62	58,1697	E19 carb 2	571,9
8,98	0,569	20,4	0,0977	27,27	57,396	E19 carb 3	571,9
9,62	0,707	19,34	0,4225	27,33	57,4196	E19 carb 4	571,9
9,47	0,6184	19,73	0,4906	28,28	58,5891	E19 carb 5	571,9
8,9	0,6833	19,88	0,0889	28,62	58,2315	E19 carb 6	571,9
9,4	0,6587	19,63	1,0003	27,89	58,6796	E19 carb 7	571,9
0,07	0,6622	18,59	0,3176	27,91	57,5499	E19 carb 8	571,9
9,82	0,6369	19,15	0,8441	27,26	57,711	E19 carb 9	571,9
7,29	1,95	18,73	2,43	27,77	58,1762	E18 carb 1	575,4
6,63	2,37	18,26	4,94	26,83	59,0478	E18 carb 2	575,4
7,32	1,82	19,17	0,5506	27,86	56,7576	E18 carb 3	575,4
9,01	1,38	17,42	1,4395	26,29	55,5396	E18 carb 4	575,4
7,16	1,46	18,75	0,5349	29,03	56,9784	E18 carb 5	575,4
6,94	1,42	18,39	0,4151	28,97	56,2108	E18 carb 6	575,4
6,22	1,89	21,35	0,0317	27,29	56,8203	E14 carb 1	586,8
5,85	2,24	20,42	1,5215	27,49	57,5401	E14 carb 10	586,8
6,11	1,95	22,75	2,32	25,71	58,8848	E14 carb 2	586,8
6,09	1,52	20,9	0,9984	28,38	57,8884	E14 carb 3	586,8
5,99	1,33	22,34	0,0394	26,74	56,5111	E14 carb 4	586,8
6,42	1,88	20,25	0,055	26,66	55,2913	E14 carb 5	586,8
7,38	1,3	19,42	1,3965	26,72	56,2165	E14 carb 6	586,8
6,66	2,07	19,52	2,58	25,1	55,9604	E14 carb 7	586,8
6,54	2,08	19,64	0,117	27,24	55,6295	E14 carb 8	586,8
7,51	3,87	17,9	3,28	24,67	57,23	E13 carb 1	593,6
6,27	3,26	19,17	0,3383	29,29	58,3787	E13 carb 10	593,6
7,48	5,54	16,13	1,8704	27,65	58,719	E13 carb 11	593,6
8,15	4,71	16,43	2,66	26,76	58,71	E13 carb 2	593,6
7,26	5,35	15,72	1,0959	28,03	57,456	E13 carb 3	593,6
8,54	4,58	17,31	2,17	25,51	58,1101	E13 carb 4	593,6
7,81	5,27	16,07	0,9705	27,15	57,2947	E13 carb 5	593,6
9,04	4,09	15,33	4,09	26,81	59,4236	E13 carb 6	593,6
7,91	4,88	16,76	0,3008	27,58	57,4309	E13 carb 8	593,6
7,66	4,35	16,57	1,513	27,88	57,9787	E13 carb 9	593,6
0,2717	4,98	7,18	0,2089	43,43	56,0916	E7 carb 1	618,4
0,0326	1,9	16,91	0,4304	42,36	61,6331	E7 carb 13	618,4
0,304	3,56	13,01	0,2902	42,66	59,8242	E7 carb 3	618,4
0,2993	3,65	3,57	0,5962	46,46	54,5756	E7 carb 7	618,4
0,1813	3,89	18,69	0,5047	40,22	63,5457	E7 carb 8	618,4
6,9	0,5632	22,86	0,1346	27,65	58,145	E3 carb 4	637,3
7,11	0,577	21,6	1,2945	26,75	57,3377	E3 carb 5	637,3

7,05	0,5791	22,88	0,948	26,51	57,9672	E3 carb 6	637,3
6,99	0,6031	28,41	1,9898	21,81	59,8359	E3 carb 7	637,3
6,93	0,6973	22,79	0,12	28,24	58,7774	E3 carb 8	637,3
6,38	0,747	22,35	0,19	38,56	68,2595	E3 carb2	637,3
6,88	0,804	22,64	0,3332	27,98	58,6372	E3 carb2b	637,3
6,92	0,4985	21,3	1,4083	28,28	58,4068	E3 carb3	637,3
4,39	1,064	49,95	3,37	2,53	61,3188	E2 Carb 6	643,7
7,1	0,591	22,05	2,4	27,91	60,051	E1 carb 1	645,7
7,67	0,5988	19,59	2,0326	28,48	58,4555	E1 carb 3	645,7
7,36	0,6853	22,16	0,2597	29,08	59,545	E1 carb 5	645,7
6,75	0,8432	21,92	0,206	29,86	59,5903	E1 carb 6	645,7
7,78	0,6434	21,11	1,0205	27,68	58,234	E1 carb 8	645,7

A.3.2. Siderite (n=122)

MgO (wt%)	MnO (wt%)	FeO (wt%)	SiO2 (wt%)	CaO (wt%)	Total	Sample Comment	Height (m)
7,1	4,81	46,02	0,2247	0,7861	59,0053	E70 carb 10	376,5
6,89	4,94	46,49	0,1897	0,715	59,2822	E70 carb 11	376,5
6,9	4,76	46,64	0,9041	1,1181	60,3222	E70 carb 12	376,5
6,53	4,6	45,45	2,74	0,9998	60,3619	E70 carb 7	376,5
6,36	4,86	47,17	0,115	1,0518	59,5854	E70 carb 8	376,5
7	4,67	46,84	0,4054	0,7512	59,6667	E70 carb 9	376,5
5,48	5,48	48,26	0,4963	0,9617	60,678	E66 carb 2	388,6
7,43	6,97	44,86	0,4977	1,93	61,7248	E66 carb 3	388,6
0,3	2,02	48,21	0,0939	0,3184	60,9492	E60 carb 1	407,6
9,4	1,93	48,54	0,0144	0,3544	60,3136	E60 carb 14	407,6
8,13	2,02	49,59	0,0921	0,5951	60,4272	E60 carb 2	407,6
8,03	1,98	49,16	0,248	0,4743	59,8923	E60 carb 3	407,6
7,39	1,75	43,67	8,1	0,226	61,1941	E60 carb 4	407,6
8,13	1,78	49,62	0,7166	0,5198	60,8611	E60 carb 5	407,6
8,34	2	50,05	0,0956	0,5085	61,0484	E60 carb 6	407,6
8,96	1,85	47,61	0,9857	0,1845	59,6241	E60 carb 7	407,6
7,1	4,07	46,52	1,7786	1,5	61,0157	E59 carb 10	424
7,28	3,55	48,29	0,1268	1,44	60,7141	E59 carb 9	424
7,21	2,17	49,41	2,76	1,0007	62,5507	E57 carb 12	432,3
6,08	2,08	50,79	2,67	1,86	63,4801	E57 carb 6	432,3
6,65	2,12	50,87	0,0712	1,2125	60,9592	E57 carb 8	432,3
6,55	2,06	50,83	0,1113	0,8048	60,3944	E54 carb 10	452,2
5,95	2,1	50,71	0,1231	0,6417	59,6456	E54 carb 11	452,2
5,87	2,44	50,48	0,0399	0,6111	59,4787	E54 carb 12	452,2
6,13	2,04	49,89	0,1949	0,6406	58,9931	E54 carb 5	452,2
5,8	2,12	49,53	0,6439	0,6584	58,7685	E54 carb 6	452,2
3,98	1,1329	53,14	0,3453	0,3961	58,9943	E54 carb 7	452,2

6,06	2,16	50,88	0,0597	0,7123	59,8721	E54 carb 8	452,2
6,95	4,78	46,58	0,5392	0,9982	59,8475	E52 carb 10	458,9
7,03	4,26	47,1	2,24	0,5183	61,1483	E52 carb 7	458,9
6,58	4,15	48,2	1,147	0,5032	60,5802	E52 carb 8	458,9
7,16	5,26	46,59	0,3447	0,7133	60,0681	E52 carb 9	458,9
6,32	2,3	48,67	1,639	0,7948	59,7238	E51 carb 1	461,4
6,92	2,3	50,23	0,1914	0,7377	60,3862	E51 carb 10	461,4
6,71	2,13	49,38	1,2468	0,7064	60,1733	E51 carb 2	461,4
6,52	2,01	49,43	1,6079	0,4551	60,0898	E51 carb 3	461,4
6,61	2,14	49,11	1,6711	0,6712	60,2024	E51 carb 4	461,4
6,69	1,97	49,14	2,52	0,4092	60,7292	E51 carb 5	461,4
6,47	1,91	49,03	1,7498	0,5013	59,6612	E51 carb 6	461,4
6,58	2,3	49,01	0,2796	0,7819	58,9816	E51 carb 7	461,4
6,8	2,18	49,13	2,0188	0,464	60,6452	E51 carb 8	461,4
6,46	1,84	49,59	0,2585	1,3083	59,5699	E51 carb 9	461,4
6,34	1,87	50,17	0,0545	1,3725	59,8223	E50 carb 6	464,6
6,28	1,6	50,2	2,25	1,45	61,8595	E50 carb 9	464,6
7,58	1,89	46,83	0,4024	0,4495	57,2647	E47 carb 1	473,3
7,07	1,7	49,06	0,7368	0,4415	59,0597	E47 carb 2	473,3
7,43	1,65	47,89	2,91	0,5166	60,3967	E47 carb 3	473,3
7,73	1,69	47,2	2,32	1,316	60,2561	E47 carb 4	473,3
7,51	1,37	48,33	3,49	0,1598	60,8599	E47 carb 5	473,3
8,49	1,6	48,93	0,8079	0,1206	59,9486	E47 carb 6	473,3
7,85	1,98	47,81	1,245	0,6821	59,5671	E47 carb 7	473,3
7,75	2,08	47,07	1,9443	0,8139	59,6583	E47 carb 8	473,3
7,89	1,59	49,3	0,7733	0,3429	59,9037	E47 carb 9	473,3
7,64	2,88	48,56	0,1648	0,6725	60,0264	E44 carb 10	481,6
6,21	2,45	50,84	0,113	0,3713	59,9843	E44 carb 2	481,6
6,74	2,55	49,86	0,1137	1,53	60,8482	E44 carb 3	481,6
6,94	2,59	49,04	1,4864	0,7655	60,8219	E44 carb 5	481,6
6,76	2,52	50,03	0,1802	0,7455	60,2426	E44 carb 8	481,6
6,04	2,75	50,19	0,0937	0,6821	59,7558	E44 carb 9	481,6
6,76	2,06	49,17	0,0744	1,3848	59,4771	E36 carb 10	512,3
7,45	1,83	49,63	3,55	0,3938	62,881	E36 carb 11	512,3
6,65	2,07	48,88	0,2292	1,88	59,7093	E36 carb 3	512,3
6,86	1,62	49,24	1,8535	1,2194	60,7929	E36 carb 4	512,3
4,68	0,9169	52,93	0,1249	1,2759	59,9278	E36 carb 6	512,3
7,5	0,4933	50,99	0,4369	0,7591	60,2424	E36 carb 9	512,3
6,4	1,47	49,7	1,0337	1,59	60,2158	E34 carb 2	518,4
6,75	1,009	50,45	1,2677	1,0094	60,4861	E33 carb 10	520,5
7,04	0,9763	51,59	0,545	0,3159	60,4672	E33 carb 2	520,5
8,23	0,7749	48	1,5564	1,86	60,4213	E33 carb 3	520,5
6,78	1,54	49,3	2,63	0,3713	60,6819	E33 carb 4	520,5
8,86	0,6552	49,61	1,5171	0,354	61,0373	E33 carb 5	520,5
6,26	0,8671	51,78	0,21	0,6585	59,8919	E33 carb 7	520,5

6,59	1,1252	50,71	0,663	0,4308	59,5327	E33 carb 8	520,5
7,77	1,2716	49,49	0,1072	1,3236	59,9762	E33 carb 9	520,5
6,93	1,1274	51,12	0,3515	0,2683	59,7972	E32 carb 2	523,8
8,04	0,833	50,09	0,2277	0,2778	59,6137	E32 carb 3	523,8
8,37	0,5758	49,67	0,84	0,7223	60,1782	E32 carb 5	523,8
9,51	0,8638	47,89	1,1323	0,3421	59,7383	E32 carb 6	523,8
5,15	0,92	52,58	0,5618	1,3363	60,5481	E31 carb 11	525,9
8,61	1,5	49,06	0,8011	0,3745	60,3964	E31 carb 12	525,9
7,91	0,7078	50,42	0,6899	0,3464	60,0741	E31 carb 3	525,9
6,78	0,6239	51,61	0,1422	0,9081	60,0643	E31 carb 4	525,9
7,83	0,5915	49,78	1,3365	0,6296	60,2415	E31 carb 6	525,9
7,99	0,953	49,87	1,4998	0,2842	60,6483	E31 carb 9	525,9
5,24	1,0113	46,39	4,25	1,99	58,9039	E30 carb 1	528,3
9,29	1,67	47,83	0,7017	0,3158	59,8075	E30 carb 11	528,3
9,67	1,6	47,41	0,3748	0,3324	59,4582	E30 carb 12	528,3
7,56	1,67	49,34	0,9949	0,5548	60,1197	E30 carb 14	528,3
6,83	0,8084	51,19	0,2594	0,8346	59,9872	E30 carb 16	528,3
8,17	1,34	49,45	0,242	0,602	59,8286	E30 carb 17	528,3
7,18	1,55	48,43	5,05	0,5622	62,7722	E30 carb 2	528,3
7,49	1,94	48,78	3,31	0,5344	62,0545	E30 carb 5	528,3
7,32	1,43	46,71	5,27	0,8406	61,5706	E30 carb 6	528,3
1,98	0,8141	54,35	0,822	0,749	58,7151	E30 carb 8	528,3
5,48	1,2264	51,24	0,2882	1,2396	59,4743	E30 carb 9	528,3
7,32	0,1917	50,85	0,8277	0,5994	59,7888	E24 carb 1	555,3
6,79	0,2005	51,45	1,0442	0,8803	60,3651	E24 carb 2	555,3
6,37	0,2749	51,09	0,741	0,4622	58,9462	E24 carb 9	555,3
8,91	2,38	47,12	1,7459	0,5948	60,7507	E18 carb 10	575,4
7,25	2,46	47,8	2,0174	0,842	60,3694	E18 carb 11	575,4
9,34	2,34	44,89	1,6911	0,6749	58,9515	E18 carb 7	575,4
7,84	2,42	47,44	1,5482	0,7906	60,0388	E18 carb 8	575,4
7,39	2,4	48,55	1,0601	0,6241	60,048	E18 carb 9	575,4
7,3	0,3813	50,98	-	1,1442	59,8191	E5 carb 3	627,5
6,99	0,4073	50,85	0,0701	1,3362	59,7822	E5 carb 4	627,5
6,34	0,4555	50,84	0,0871	1,2486	58,9713	E5 carb 5	627,5
7,83	0,612	49,47	2,48	0,8085	61,2271	E5 carb 6	627,5
5,4	0,8571	52,61	1,0626	0,5821	60,557	E2 Carb 10	643,7
5,27	0,6686	53,53	0,2326	0,5827	60,2839	E2 Carb 11	643,7
4,79	1,1213	52,58	1,0908	0,5562	60,1384	E2 Carb 3	643,7
4,86	1,1244	52,49	2,57	0,4664	61,5418	E2 Carb 4	643,7
4,84	1,2236	53,35	0,6238	0,2861	60,3235	E2 Carb 5	643,7
5,17	1,1013	53,31	0,2717	0,7252	60,5783	E2 Carb 7	643,7
5,1	1,0917	52,96	0,1446	0,5505	59,8468	E2 Carb 8	643,7
5,21	1,217	52,06	0,1698	0,559	59,2158	E2 Carb 9	643,7
4,96	1,1154	53,93	2,22	0,3602	62,5926	E1 carb 10	645,7
5,29	0,8931	51,08	5,61	0,3073	63,2536	E1 carb 11	645,7

4,41	0,9888	53,64	1,6615	0,2605	60,9744	E1 carb 13	645,7
4,87	1,1085	53,83	0,896	0,2663	61,0596	E1 carb 14	645,7
7,24	0,9089	52,6	1,1894	0,5373	62,4756	E1 carb 2	645,7
6,09	0,7695	53,14	0,2185	0,4168	60,6348	E1 carb 4	645,7
6,18	1,0909	52,2	0,627	1,63	61,7724	E1 carb 7	645,7
4,14	0,9401	54,56	3,74	0,2567	63,6369	E1 carb 9	645,7